The Use of Shear Wave Elastography to Estimate the Mechanical Properties of the Soft Tissues Surrounding the Proximal Femur

by

Sukirat Kaur Bhullar

A thesis

presented to the University of Waterloo

in fulfillment of the

thesis requirement for the degree of

Master of Science

in

Kinesiology and Health Sciences

Waterloo, Ontario, Canada, 2023

Author's Declaration

I hereby declare that I am the sole author of this thesis. This is a true copy of the thesis, including any required final revisions, as accepted by my examiners.

I understand that my thesis may be made electronically available to the public.

Abstract

Introduction: Falls are the leading cause of injury, morbidity, and mortality amongst older adults nationally and worldwide, with 95% resulting in hip fractures. Previous studies have found that the soft tissues (subcutaneous adipose and muscle) surrounding the proximal femur influence the magnitude and distribution of the impact force transmitted to the underlying bone during an impact, and thus hip fracture risk. However, there is a gap in the literature since studies have not explored the role of the soft tissues' mechanical properties, particularly Young's modulus, on the impact force magnitudes and distribution during both resting and muscle contracted states. This gap can be addressed using shear wave elastography (SWE), an ultrasound imaging technique that quantifies soft tissues' shear wave velocity (SWV). SWV can be used to compute the Young's moduli of the tissues and gain a better understanding of the mechanical properties of the tissues. Investigating the SWV of the soft tissues would help improve the biofidelity of physical and computational hip models, which would allow us to better understand lateral fall impact dynamics and help to improve the design of hip fracture prevention technologies.

Objectives and Hypotheses: There were two main objectives of this thesis. The first objective was to evaluate the intra-rater reliability of the SWE protocol used to characterize the SWV of the soft tissues (subcutaneous adipose and muscle) in the lateral-hip region, and the potential influence of muscle contraction on intra-rater reliability. The second objective was to assess the influence of muscle contraction on the soft tissues' SWV. Based on the previous literature, it was hypothesized that: 1) the intra-rater reliability of the subcutaneous adipose and muscle SWV measurements taken with this protocol would range from good to excellent (ICC > 0.75), and would not be influenced by contraction state, and 2) there would be an interaction effect of muscle contraction on the SWV magnitudes of the soft tissues. It was expected that: a) the muscle SWV magnitude would be greater during the muscle contracted state compared to the resting state, while b) the subcutaneous adipose SWV magnitude would not change during the resting and muscle contracted states.

Methods: Twenty healthy, young adults between the ages of 18-35 years with a BMI ≤ 24.9 kg/m^2 were recruited. The elastography setting on the GE LOGIQ E10 commercial ultrasound machine and a linear probe were used to take 3 measurements of the muscle and subcutaneous adipose tissues from a marked location on the participants' left lateral hip region. Three measurements from each tissue were taken during the muscle relaxed and contracted states, resulting in 12 measurements being collected from each participant. A two-way mixed effects absolute agreement intraclass correlation (ICC) model was used to assess the intra-rater reliability of the measurements and the influence that muscle contraction had on it. A two-way repeated measures analysis of variance (ANOVA) was used to assess the potential interaction effect of muscle contraction on the SWV magnitudes of the soft tissues.

Results: As hypothesized the intra-rater reliability of the subcutaneous adipose and muscle tissues ranged from good to excellent ($0.81 < ICC < 0.95$) and was not influenced by contraction state. This aligned with previous literature and supported that the protocol was appropriate for examining the influence of muscle contraction on SWV (Objective 2). Two-way repeated measures ANOVA revealed a significant interaction effect of muscle contraction on the SWV magnitudes of the soft tissues ($p < 0.05$), which was particularly driven by the significant increase in the muscle's SWV from resting to contracted state ($p < 0.001$). In contrast, the subcutaneous adipose's SWV was not different during the two conditions ($p = 0.825$). These results aligned with the hypothesis and indicated that the moduli of the soft tissues in this region respond differently between relaxed and contracted states.

Discussion and Conclusion: The protocol used in this thesis had good to excellent intra-rater reliability and can be used to characterize the moduli of the soft tissues in additional locations in the hip region. Additionally, the influence of BMI and aging on the stiffness of the soft tissues in this region can also be investigated. Muscle contraction also influenced the SWV of the muscle, while the SWV of the subcutaneous adipose did not change. This finding indicates that the soft tissues in the hip have unique properties and respond differently to muscle contraction. Accordingly, it is worth exploring whether they should be modelled separately in biomechanical models of the hip and pelvis. Implementing this finding in physical and computational models that currently bulk together the properties of the soft tissues in the hip, should improve their biofidelity. Additionally, the protocol used in this thesis, along with the differences observed in the soft tissues' SWV, can potentially be used to assess muscle quality. Since alternative modes on the ultrasound, such as echo intensity, are currently used to assess changes in muscle quality, SWE may be an alternative technique that can be used.

Acknowledgements

To begin with, I'd like to thank my supervisor, Dr. Andrew Laing, for your endless support, patience, and guidance throughout this project. I have always wanted to work with you since taking your third-year Trauma Biomechanics class and am so grateful for this opportunity. Throughout this project, I encountered many difficult hurdles, which I could not have crossed without your support and encouragement. I will miss our weekly Tuesday morning meetings.

I am also thankful for my committee members, Dr. Marina Mourtzakis, Dr. Monica Maly, and Dr. Tyson Beach, for their assistance with the development of this project. Your input during my proposal and committee meetings not only challenged me as a student but also helped to sculpt this project. I appreciate you all for taking the time to help guide me through this journey and helping me improve as a researcher.

To my fellow IBAL lab members, thank you for your continued support and encouragement. A special shout out to Jordan Hobson for helping me pilot my protocol and with all my collections. I appreciate your help! I am also very grateful for all the amazing people who I had the opportunity to work with, I will cherish our friendships. Special shout-outs to Daphne Ho, Riggy Ho, Hefu Tao, Bryanna Oriuwa, Ryan Chhiba, Mai Wageh, Tom Hoshizaki, Sanjay Veerasammy, Gary Mangan, Tavleen Deol, Astha Patel, and Jashon Chouhan. This would not have been possible without your support.

This project would also not have been possible without the behind-the-scenes help of Jeff Rice and Alicia Nadon. You both played an instrumental role in the completion of this thesis, and I appreciate your help.

I would also like to thank my family for their unwavering support. Thank you to my mom, Darmant Bhullar, Harpal Mehmi, Sukhmeet Bhullar, and Bella Bhullar for motivating me throughout this journey and for having my back during the difficult times. I could not have done this without you, and I love you all so much!

Lastly, sincerest thanks to Arjun Cheema. Words cannot describe how much your support throughout this journey means to me. "ਮੈਂ ਤੈਨੂੰ ਬਹੁਤ ਪਿਆਰ ਕਰਦਾ ਹਾਂ "

Table of Contents

List of Figures

List of Tables

List of Abbreviations

BMD: Bone mineral density

BMI: Body mass index

CT: Computed tomography

E: Young's modulus

FE: Finite element

G: Shear modulus

GT: Greater trochanter

ICC: Intraclass correlation coefficient

LTC: Long-term care

MVC: Maximum voluntary contraction

ROI: Region of interest

SE: Strain elastography

SWE: Shear wave elastography

SWV: Shear wave velocity

TE: Transient elastography

TSTT: Trochanteric soft tissue thickness

US: Ultrasound

Chapter 1
Thesis Overview

Approximately 20-30% of older adults experience one or more falls each year in Canada, resulting in increased rates of injuries, morbidity, and mortality amongst this population (Government of Canada, 2021; World Health Organization, 2007). A common injury caused by falls is hip fractures, with approximately 28,000 annual cases in Canada and more than 95% of them being caused by falls (Scott et al., 2010). Hip fractures result in increased rates of mortality, disability, and medical costs compared to other fragility fractures (Auais et al., 2018). The older adult population is expected to increase (Statistics Canada, 2017), resulting in an increase in the incidence of hip fractures (Nikitovic et al., 2013), which already have direct attributable healthcare system costs of approximately $1.1 billion per year. These costs are expected to increase to $2.4 billion by 2041 (Schneider & Guralnik, 1990; Wiktorowicz et al., 2001).

Hip fracture risks are elevated with side-ways falls (Yang et al., 2020) and the characteristics of the underlying bone and soft tissues, including the femur's strength (Palanca et al., 2021) and bone mineral density (BMD) (Greenspan et al., 1994). A negative correlation exists between body mass index (BMI) and hip fracture risk (De Laet et al., 2005; Gonnelli et al., 2014; Hayes et al., 1993). However, it is difficult to gain a better understanding of hip fractures and the factors that influence their risk through in-vivo studies and ex-vivo, cadaveric studies, as living individuals cannot be exposed to high loads and cadaveric tissues do not directly represent the response of living tissues, respectively. Thus, physical and computational models have been developed to better understand hip fracture causations, the risk factors associated with them, and to design engineering-based interventions to help with their prevention. The majority of the finite element models incorporate the soft tissues around the pelvis (Fleps et al., 2018; Fleps et al., 2019; Galliker et al., 2022; Majumder et al., 2007; Majumder et al., 2008); however, they often bulk the soft tissues (subcutaneous adipose and muscle tissues) together.

Soft tissue properties, such as thickness and muscle contraction state, influence the total force distribution in the pelvis during an impact. Based on the current literature, individuals with a lower BMI experience peak pressures that are 55% greater than those with a higher BMI. BMI is also highly correlated with trochanteric soft tissue thickness (TSTT) (Maitland et al., 1993; Choi et al., 2010), which is known to influence peak impact forces and energy absorption during impacts to the hip (Robinovitch et al., 1995). Additionally, muscle contraction is known to influence the impact characteristics by increasing the total impact force experienced during lateral falls on the hip (Martel et al., 2018). It is also known to

increase pelvic stiffness in females (Martel et al., 2018) and may change the geometry of the skin surface, ultimately influencing the impact force distribution (Pretty et al., 2017). The properties of these soft tissues also influence the effectiveness of hip fracture prevention technologies, including hip protectors and compliant flooring (Bhan et al., 2013; Choi et al., 2010; Galliker et al., 2022; Laing et al., 2008a; Laing et al., 2008b; van Schoor et al., 2006). However, since the mechanical properties of these tissues and the influence of muscle contraction on these properties have not been previously explored, they cannot be included in hip models to increase their biofidelity and help to address the existing gaps in the literature.

As an initial step towards gaining a better understanding of hip fracture mechanisms, risk factors, and impact dynamics, the mechanical properties of the soft tissues (subcutaneous adipose and muscle) within this region should be assessed. Accordingly, this thesis aimed to use shear wave elastography (SWE), an ultrasound (US) imaging technique, to quantify the shear wave velocity (SWV) of the soft tissues in the lateral hip region. SWV can be used to compute Young's moduli of these tissues and gain a better understanding of their mechanical properties. The proposed thesis focused on 1) assessing the intra-rater reliability of the protocol that was used to 2) characterize the mechanical properties of the soft tissues (subcutaneous adipose and muscle) in the lateral hip region during relaxed and muscle contracted states. Figure 1 provides a visual framework of this thesis and section 2.7 contains more information regarding its research questions and hypotheses.

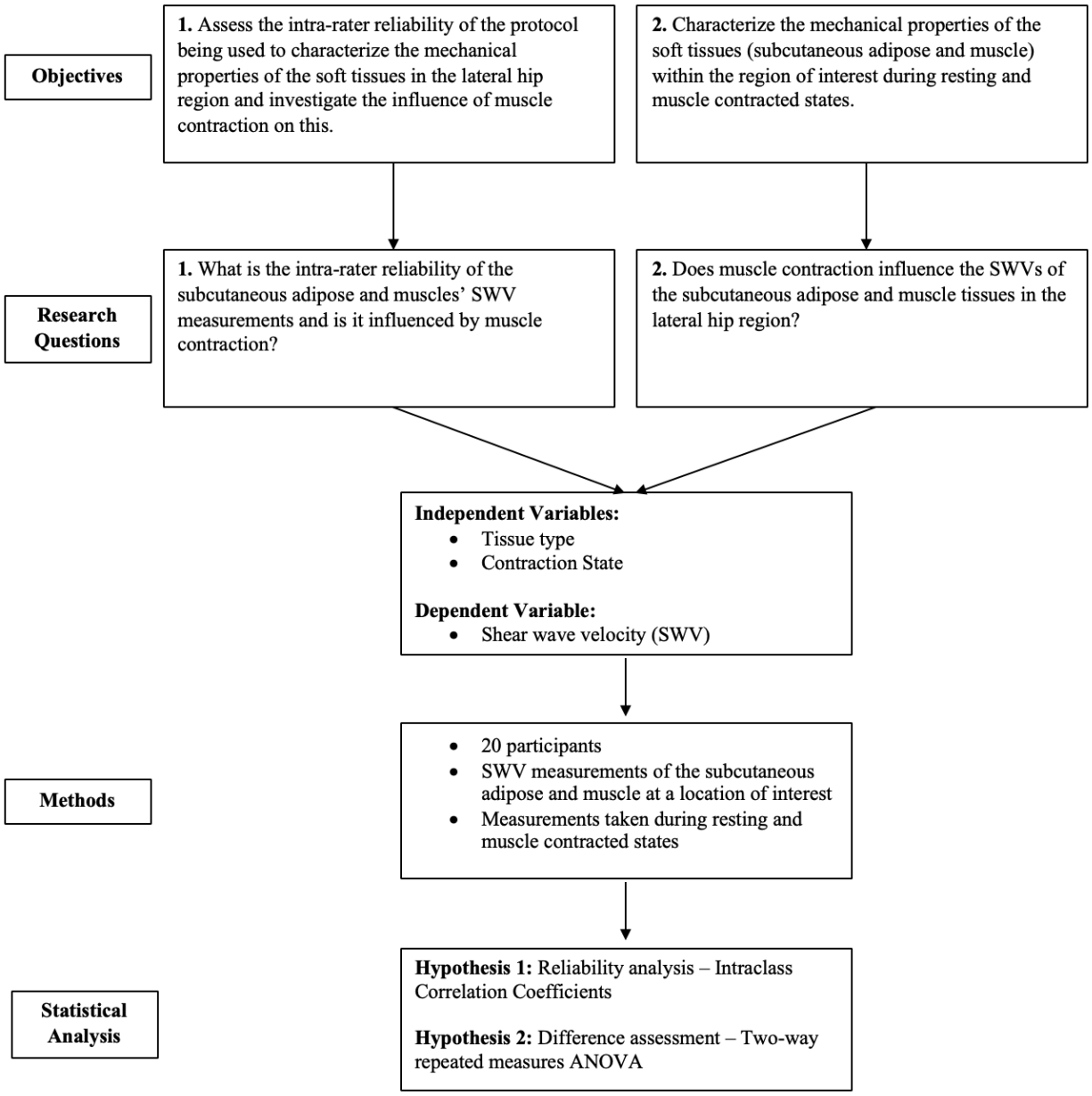

Figure 1: *Thesis Framework*

Chapter 2
Literature Review

2.1 Hip Fracture Epidemiology

2.1.1 Prevalence of Fall-Related Hip Fractures

Falls are the leading cause of injury, morbidity, and mortality amongst the older adult population both nationally and globally (Government of Canada, 2021; World Health Organization, 2007). There are approximately 28,000 annual cases of hip fractures in Canada, with more than 95% of them being caused by falls (Scott et al., 2010). Compared to other fragility fractures, including spine and wrist, hip fractures result in increased rates of mortality, disability, and medical costs (Auais et al., 2018). Approximately 25% of older adults who experience hip fractures die within a year (Nikitovic et al., 2013) and 50% experience difficulties performing daily activities and a decline in independence (Wolinsky et al., 1997). As life expectancy increases (Decady & Greenberg, 2014) and the baby-boomer cohort (people born between 1946 and 1965) ages, the older adult population is expected to increase (Statistics Canada, 2017), resulting in the incidence of hip fractures to continue increasing (Nikitovic et al., 2013).

2.1.2 Burden Caused by Fall-Related Hip Fractures

Based on the current literature, fall-related hip fractures have a large economic burden. In Canada, hip fractures have a direct attributable healthcare system cost of approximately $1.1 billion per year. This cost is expected to rise to $2.4 billion by 2041, as the older adult population continues to increase (Schneider & Guralnik, 1990; Wiktorowicz et al., 2001). In Ontario, the direct yearly costs are $282.1 million, with post-fracture costs being an additional $64.5 million in the second year of rehabilitation (Nikitovic et al., 2013). As mentioned above, older adults who have sustained a hip fracture tend to have difficulties performing daily activities, resulting in their transfer to long-term care (LTC) facilities. Wiktorowicz and colleagues (2001) found that approximately 15.5% of community-dwelling older adults were transferred to LTC facilities after sustaining a fracture, where their average yearly cost of living was $44,156. Their cost of living was greater compared to when they were residing in their communities ($21,385) and to the other LTC residents' cost of living ($33,729) (Wiktorowicz et al., 2001).

Along with the economic burden, fall-related hip fractures result in a social burden. These fractures are related to increases in morbidity, with 18-22% of patients requiring LTC (Jaglal et al., 1996) and two-thirds of community-dwelling patients requiring home-care services (Nikitovic et al., 2013). Death related to hip fractures within the first year is 13-23%, with 5.6% of patients who die within their

first 30 days of hospitalization (Nikitovic et al., 2013). Additionally, recovering patients have difficulties performing daily activities, such as taking medication (Magaziner et al., 2000; Dyer et al., 2017), dressing (Beaupre et al., 2007), and walking (Magaziner et al., 2000). Those residing in LTC have lower mobility recovery rates than those that continue to reside in their community, with only 21% being able to recover their mobility entirely (Neuman et al., 2014). Additionally, 53% of pre-fracture community-dwelling older adults, who continue to reside within their communities' post-fracture, require assistance to access places within walking distance (Magaziner et al., 2000). Individuals also experience a heightened fear of falling (Bower et al., 2016) which may also influence their recovery. The likelihood of them sustaining a second hip fracture also remains high as one in twenty (5.08%) patients are likely to experience a second hip fracture within their first year of recovery, and this rate increases to 8.11% within the second year (Lönnroos et al., 2007). Overall, older adults who sustain hip fractures endure hardships to their health, costs of living and in the social aspects of their lives, which greatly influences their independence and quality of life (Papaioannou et al., 2009). As the older adult population continues to increase, along with the incidence of hip fractures, it is important to understand the risk factors related to these hip fractures to improve the design of preventative technologies and rehabilitation programs.

2.2 Biomechanical Factors that Influence Fall-Related Impact Dynamics & Hip Fracture Risk

2.2.1 Risk Factors for Hip Fractures

Several fall factors increase the risk of hip fractures, including fall height (Yang et al., 2020), orientation (Pretty et al., 2021a; Yang et al., 2020), and landing configuration (Yang et al., 2020). With the majority of hip fractures resulting from falls initiated from standing heights. There is a 2.4-fold greater risk of hip fractures from falls initiated at standing heights compared to those initiated from lower heights (Norton et al., 1997). Specifically, Yang and colleagues (2020) found that the majority of hip fractures in LTC facilities were caused by falls from standing heights, while 38% of non-fractures occurred from falls from lower heights, such as falls succeeding sitting tasks. As a protective mechanism to prevent head impacts, approximately 38% of falls involve the rotation of the body during the descent phase to change the landing configuration (Yang et al., 2020). Forty-two percent of forward-directed falls involve the individual rotating to land side-ways and 41% of side-ways falls involve individuals rotating backwards (Yang et al., 2020), which decreases their risk of hip impact by 10-fold (Yang et al., 2016). The risk of hip fractures is increased by 5.5-fold during side-ways landing compared to forward fall landing

configurations (Yang et al., 2020). Thus, landing configuration is one of the strongest determinants of hip fractures and increases their risk by approximately 20-fold compared to other factors (Hayes et al., 1993). Additionally, impact forces directed towards the posterolateral aspect of the pelvis increase the likelihood of hip fractures by six times (Yang et al., 2020) because they result in greater contact forces on the proximal femur (Keyak, 2001; Yang et al., 2020). Having high contact forces in this region of the femur increases the likelihood of a hip fracture because the proximal femur has the lowest strength compared to the other regions (Yang et al., 2020). In summary, hip fracture risks are elevated based on the biomechanics of the fall.

Additionally, bone and soft tissue characteristics also influence the risk of hip fractures. The femur's strength, also known as fracture load, is influenced by its morphology, subcortical bone voids (Palanca et al., 2021), and bone mineral density (BMD) (Dragomir-Daescu et al., 2018). Greenspan and colleagues (1994) found that the BMD is not only lower in individuals who fractured their hips compared to individuals without hip fractures, but it is significantly lower at the femoral neck, intertrochanter, and trochanter. Studies have also reported a negative correlation between BMI and fracture risk (De Laet et al., 2005; Gonnelli et al., 2014; Hayes et al., 1993). A higher BMI has been found to act as a protective mechanism against hip fractures (Gonnelli et al., 2014) as the increased soft tissue in the hip region absorbs energy during a fall (Fleps et al., 2018). BMI is also highly correlated with trochanteric soft tissue thickness (TSTT) (Maitland et al., 1993; Choi et al., 2010). As expanded on in section 2.2.3, the soft tissues overlying the femur influence the total forces transmitted to the bone during an impact and thus, fracture risk. Further research should focus on understanding the influence that soft tissue characteristics have on lateral fall impact dynamics and hip fracture risk.

2.2.2 Force Distribution during Lateral Falls

The force distribution following a lateral fall is primarily influenced by the impact's magnitude and the type of lateral fall, which dictates the loading vector orientation and the primary point of impact on the pelvis. Pretty and colleagues (2021a) utilized three different fall simulations (Figure 2) to evaluate their impact vector magnitude, center of pressure, and direction. The fall simulations that they used were the pelvis, kneeling, and squat release falls which represented different fall types observed in older adults. The highly controlled pelvis release falls were initiated by the release of an electromagnet that caused the participant to impact their lateral hip directly. In contrast, during the kneeling release falls, the faller impacted the knee before impacting the hip laterally. While during the squat release falls, the faller flexed their knee, hip, and ankle during the descent phase, before rotating their bodies laterally to impact the hip.

During the pelvis release, the peak force loading vector was directed closest to the greater trochanter (GT). However, during the kneeling release, the force's loading vector was directed more medially, with respect to the femoral shaft, while during the squat release, it was directed more distally. In the anterior-posterior plane, both the kneeling and squat release falls impact force loading vector was directed more anteriorly, compared to the pelvis release falls. In all three releases, the mean location of the center of pressure was 0.1-1.1 cm posterior and 0.8-1.8 cm distal to the GT (Pretty et al., 2021b). The force distribution during these falls is dependent on the distribution and type of soft tissues underlying their primary points of contact. The pelvic soft tissues play a critical role in influencing the impact force distribution and are discussed in greater detail in section 2.2.3. Overall, during all three of these types of lateral falls, peak forces are initially directed distal and posterior to the GT (Pretty et al., 2021a; Pretty et al., 2021b).

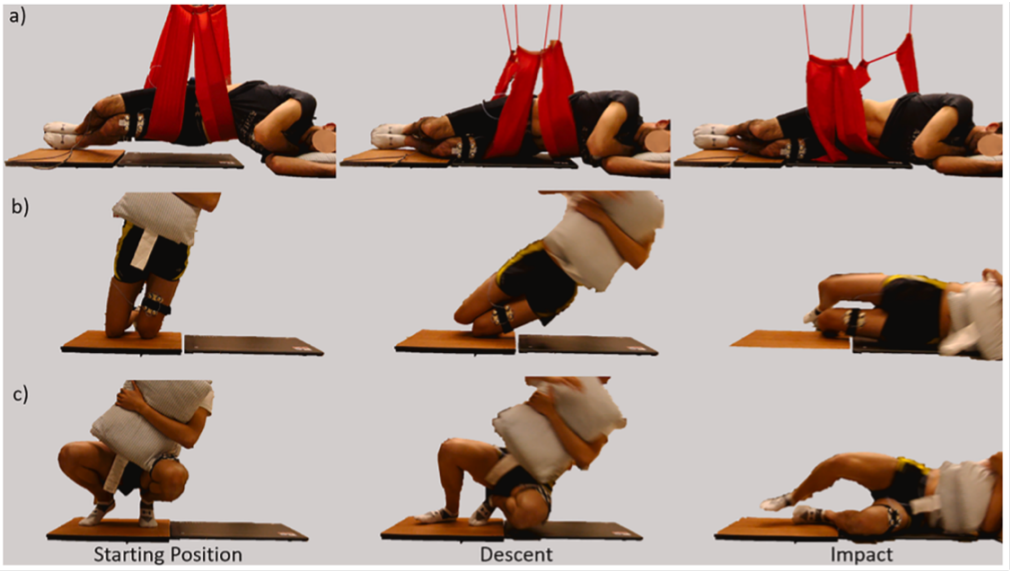

Figure 2: *Phases of a) Pelvis, b) Kneeling, and c) Squat Release Fall Simulation Protocols (Pretty et al., 2021b)*

2.2.3 Influence of Soft Tissues on Fall Impact Dynamics

Soft tissue properties, such as thickness and muscle contraction, influence the total force distribution in the pelvis during an impact. Based on the current literature, individuals with a lower BMI experience peak pressures that are 55% greater than those with a higher BMI. BMI is also highly correlated with trochanteric soft tissue thickness (TSTT) (Maitland et al., 1993; Choi et al., 2010), which

is known to influence peak impact forces and energy absorption during hip impacts (Robinovitch et al., 1995). Higher TSTT has been associated with decreased peak impact forces when the forces are normalized to the individual's body mass, as it shunts energy away from the femur (Pretty et al., 2021a; Pretty et al., 2021b). However, when these forces are not normalized to the individuals' body mass, taller and heavier individuals experience increased forces over their proximal femur than shorter and thinner individuals. Pretty and colleagues (2017) reported that males experience 47% greater local impact forces over the GT during a lateral fall than females, which is likely caused by differences in body mass. Body mass is directly related to the kinetic energy of an impact; therefore, individuals with increased mass, higher BMI, and TSTT, may experience increased impact forces than those who have a lower mass. However, there are some inconsistencies in the literature regarding the association between BMI and peak impact forces. Some studies have found that BMI does not influence peak forces (Pretty et al., 2017; Choi et al., 2010), while others have reported that individuals with higher BMI or TSTT experience increased peak forces (Levine et al., 2013; Pretty et al., 2021b). Although there are some inconsistencies regarding the association between BMI and peak impact forces, decreased BMI is associated with lower peak impact pressure (Choi et al., 2010; Pretty et al., 2017). Individuals with a low BMI may have a smaller pelvis with a decreased contact area during the fall, causing the majority of the force to be applied in a smaller area overlying the GT, compared to high BMI individuals where loads can be distributed to the outer regions of their pelvis (Pretty et al., 2017). Overall, soft tissues influence the impact force dissipation during a lateral fall. However, studies have not explored the role that these soft tissues' mechanical properties have on the impact force's magnitude and distribution.

Additionally, muscle contraction is known to influence the impact characteristics by increasing the total impact force experienced during lateral falls on the hip (Martel et al., 2018). Increased muscle activation has also been shown to increase the stiffness of the pelvic tissues in females (Martel et al., 2018) and may alter the geometry of the skin surface, ultimately influencing the impact force distribution (Pretty et al., 2017). Additionally, Pretty and colleagues (2017) found muscle activation during a fall increases peak impact forces and the skin's contact area, which leads to no differences in peak pressure during muscle-relaxed and contracted states. However, a limitation that may have influenced their results is that their muscle activation targets (20-30% MVC) were based on upper limb impact data from studies that simulated forward falls. There is currently a gap in the literature regarding the muscle activation patterns of muscles in the lower limbs during lateral falls. Pretty and colleagues (2017) also reported that gluteal muscle activation did not influence the TSTT overlying the GT and they did not assess its effects on the soft tissues' elastic moduli and skin-surface geometry in the surrounding trochanteric regions. Accordingly, there is a knowledge gap in the literature regarding the influence of muscle contraction on

the soft tissue properties that could potentially influence (and/or be incorporated into) computational models of hip impact dynamics.

2.2.4 Influence of Soft Tissues on Hip Injury Prevention Technology (Hip Protectors & Compliant Flooring)

As discussed in the previous sections, the pelvic soft tissues influence the total force distribution along the proximal femur during lateral hip falls. They also influence the effectiveness of hip fracture prevention technologies, including hip protectors and compliant flooring (Bhan et al., 2013; Choi et al., 2010; Galliker et al., 2022; Laing et al., 2008a; Laing et al., 2008b; van Schoor et al., 2006). Hip protectors and compliant flooring will be discussed in greater detail in the following sections.

2.2.4.1 Hip Protectors

Hip protectors are devices that consist of either soft- or hard-shell pads that are embedded in undergarments to cover the proximal femur (Laing et al., 2008a). They are known to reduce the risk of hip fractures amongst ambulatory older adults by 3-fold when worn at the time of a fall (Korall et al., 2019). They attenuate forces by absorbing the energy from the impact and/or shunting it away from the GT into the surrounding pelvic soft tissues (Kunnus et al., 2000; Laing et al., 2008a; Laing et al., 2008b).

The ability of hip protectors to attenuate impact forces is influenced by the underlying pelvic soft tissues (Choi et al., 2010; Galliker et al., 2022; Laing et al., 2008a; Laing et al., 2008b; van Schoor et al., 2006). In an impact testing simulation using surrogate femurs, van Schoor and colleagues (2006) reported that in combination with a thick (2.54-cm) soft tissue layer, hard-shell hip protectors reduced peak forces by 68-80% and soft-shell hip protectors reduced them by 42-62%. Both types of protectors reduced the peak impact forces below the average hip fracture threshold of 3100 N; however, hard-shell protectors reduced the impact forces significantly more. When the impact testing simulations were conducted with a thinner soft tissue layer (1.27-cm), only hard-shell hip protectors were able to reduce the peak impact forces below the fracture threshold. In this scenario, hard-shell protectors reduced peak forces by 67-86%, while soft-shell protectors reduced them by 19-46%. This suggests that soft tissue thickness influences the effectiveness of hip protectors and should be considered when designing these devices. Similarly, in a pelvis release experimental study with human volunteers, Laing and Robinovitch (2008a) found that as BMI increased, soft-shell hip protectors were able to attenuate less impact forces. Specifically, these hip protectors attenuated 15-35% of the peak impact force in individuals with a BMI of 19 kg/m^2, while they only attenuated 7.5-10% in individuals with a BMI of 27 kg/m^2. Similarly, Choi and colleagues (2010) reported that soft-shell hip protectors provided more than twice the reduction in peak pressure and

increased shunting of pressure away from the GT in low BMI participants, compared to high BMI participants. Building upon this work, Galliker and colleagues (2022) used an FE model to find that protectors attenuate the greatest forces over the GT and transfer them to the surrounding soft tissues in low BMI individuals. In contrast, for a high BMI individual, wearing the protector was found to increase the peak forces over the GT because it acted as a force concentrator, which elevated hip fracture risk.

Altogether, the findings from these studies suggest that the effectiveness of hip protectors is influenced by the characteristics of the underlying soft tissues. A large portion of the literature has focused on the influence that BMI and TSTT have on the force attenuation capabilities of these protectors. However, studies have not considered the effect that the soft tissues' mechanical properties have on the protector's effectiveness. Therefore, a greater understanding of these soft tissues' mechanical properties could lead to the improvement of wearable hip protectors.

2.2.4.2 Compliant Flooring

In addition to hip protectors, compliant flooring is another promising intervention for reducing fall-related injuries (Drahota et al., 2022). These floors attenuate the peak forces applied to the pelvis (by up to 11.7%) and increase the time to peak force (by up to 25.5%) (Bhan et al., 2013). They are designed to have decreased stiffness, compared to conventional flooring, which helps to reduce the magnitude and distribution of the impact force during side-ways falls (Laing et al., 2006; Laing & Robinovitch, 2009) similar to the native soft tissues (section 2.2.3) and wearable hip protectors (section 2.2.4.1). Additionally, BMI has been found to influence the force attenuation capability of this compliant flooring. Following lateral pelvic release experiments utilizing participants with a wide range of BMI, Bhan and colleagues (2013) found that the compliant flooring attenuated 18.4% of the peak forces in low BMI participants and only 0.3% in high BMI participants. Since BMI is highly correlated with TSTT (Maitland et al., 1993; Choi et al., 2010), the protective capacity of the flooring is influenced by the soft tissue thickness overlying the pelvic region. Although researchers have considered the influence that the pelvic soft tissues' thicknesses have on the effectiveness of this intervention, there are no studies that have explored the influence of their elastic moduli. Therefore, understanding the mechanical properties of these soft tissues would be the preliminary step towards better understanding their influence on the effectiveness of compliant flooring.

2.2.5 Take-Home Messages

There are several factors that influence the risk of fall-related hip fractures, including the soft tissues overlying the proximal femur. These tissues influence the magnitude and distribution of the impact forces transmitted to the underlying bone during an impact and the effectiveness of hip injury prevention technologies. Muscle contraction is also known to influence the skin-surface impact characteristics during lateral falls including increased pelvic stiffness and total impact force (Martel et al., 2018), and altered force distribution (Pretty et al., 2017). Although studies have explored the role that soft tissues have on the force distribution, impact dynamics, and effectiveness of preventative technologies, there is a large gap in the literature regarding their mechanical properties and the influence they have on fall-related impact dynamics and preventative technologies.

2.3 Finite Element Models of Pelvic Impact Dynamics & Soft Tissues

Finite element (FE) models of the hip allow us to simulate different lateral falls and understand the effect of their impact forces on the femur. This is especially beneficial when only low-magnitude impact forces can be applied to the femur during in vivo fall experiments. Table 1 provides a summary of the different FE models designed to simulate the hip region. The majority of the FE models incorporate the soft tissues around the pelvis (Fleps et al., 2018; Fleps et al., 2019; Galliker et al., 2022; Majumder et al., 2007; Majumder et al., 2008), except for a CT scan-based FE model presented by van der Zijden and colleagues (2015). Although these models do consider soft tissues, they often bulk them together, rather than including the individual properties of the subcutaneous adipose and muscle tissues in the pelvic region. They also fail to consider the damping effect of muscle activation during lateral falls, although muscle activation is known to affect total impact forces, soft tissue stiffness (Martel et al., 2018), and tissue level stresses (Choi et al., 2015). There is a gap in the literature regarding the mechanical properties of these tissues, and the influence that muscle activation has on them, preventing these details from being included in these models. Bridging this gap would increase the biofidelity of these models, allowing for more accurate outcomes to be extracted. This would ultimately lead to the improvement of engineering-based interventions, such as hip protectors and safety flooring.

Table 1: Description of Finite Element (FE) Models of the Hip*. This table provides a summary of all the different FE models of the hip that are currently being used, along with details regarding their methods, tissues modelled, stiffness values of the soft tissues modelled, and their limitations.*

Author/Year	**Methods**	**FE Model Skin Surface Geometry**	**Tissues Modelled**	**Soft Tissue Stiffness**	**Limitations**
Majumder et al. (2007) & (2008)	CT scan-based non-linear 3D FEM of human pelvis-femur-soft tissue complex modelled	Soft tissue geometry matched a 58-year-old male (77.47 kg)	Bone, ligaments, and bulk soft tissue	To consider the effect of large deformation, used the non-linear hyperelastic "Mooney-Rivlin material mode" to determine the stiffness of the soft tissue. Mooney-Pivlin Coefficients C10 and C01 (where C01 = C10/4) that determine the stiffness of soft tissue were selected as 85.5 kPa and 21.38 kPa, respectively.	Only a single participant modelled Bulked soft tissue modelled Muscle activation was not considered (damping effects of pelvic muscles and ligaments could not be incorporated in the model)
van der Zijden et al. (2015)	CT scan-based FEM of the femoral head and hemi-pelvis of one healthy male femur (81 years) and one osteoporotic female femur (81 years)	Bones modelled to match the two specimens	Bone	No soft tissues modelled	Oversimplification of model where no soft tissue (adipose and muscle) was not considered Only two specimens (1 healthy and 1 osteoporotic)
Fleps et al. (2018)	Dynamic linear and non-linear FEMs were constructed using CT scans for two participants (1 male and 1 female) to represent cadaveric pendulum-	Soft tissue geometry matched the subjects	Bone, ligaments, cartilage, femoral capsule & bulk TSTT	Effective pelvic stiffness, in the range of 300-1000 N, experimentally and FEM derived: Experiment = 50.7-80.3 N/mm FEM_linear = 47.4-77.3 N/mm FEM_nonlinear= 46.9-79.8 N/mm	Only two specimens were modelled Bulked soft tissues together (not representing the heterogeneity of the tissue) and used ballistics gel as a soft tissue surrogate

	based hip fractures				
Fleps et al. (2019)	Subject-specific explicit FEMs modelled 6 females and 5 males ages 54-94 years old (with an average age of 77.1(13.4) years	Soft tissue geometry matched subjects tested in an experimental study by Fleps et al. (2018)	Bone, ligaments, cartilage, femoral capsule & bulk TSTT	Effective pelvic stiffness ex vivo experimentally and FEM derived: Ex vivo = 58.5-492.0 N/mm FEM_nonlinear = 61.5-550.6 N/mm FEM_linear = 63.0-788.3 N/mm FEM_lowheight = 24-152 N/mm	Bulked soft tissues together (not representing the heterogeneity of the tissue) and used ballistics gel as a soft tissue surrogate Muscle activation at the hip joint was not modelled (since little is known about the muscle activation patterns around the hip during sideways fall impacts)
Galliker et al. (2022)	FE model of generic hip protector models combined with subject-specific FE models for 4 specimens (2 males and 2 females) to represent ex vivo fall simulations	Generic hip protector FE model was designed using dimensions of a low BMI female (BMI = 15.4 kg/m^2) Subject-specific FE models matched the design of FE models described in Fleps et al. (2018) and (2019)	Bone, ligaments, cartilage, femoral capsule & bulk TSTT	Didn't provide much info except: Hip protector stiffness was measured as the tangent slope at specific points within the force-displacement curve (0.5, 1.0, 2.0, and 3.0 kN). Additionally, the overall stiffness up to 4.0 kN, the stored energy up to 4.0 kN, and the absolute and relative dissipated energy were calculated.	Bulked soft tissues together (not representing the heterogeneity of the tissue) and used ballistics gel as a soft tissue surrogate Muscle activation at the hip joint was not modelled (since little is known about the muscle activation patterns around the hip during sideways fall impacts)

2.4 Utilizing Shear Wave Elastography to Quantify the Young's Moduli of Soft Tissues

2.4.1 Introduction to Shear Wave Elastography

Shear wave elastography (SWE) is an ultrasound (US) imaging technique that allows for the quantification of the SWV of tissues throughout the body, which can be used to compute their Young's modulus. The US transducer is used to generate an acoustic radiation force pulse sequence, which generates shear waves away from the region of interest (ROI) within the tissue of interest. The ROI is a

feature within the US system's software that defines the area within the SWE image that will be used to calculate the SWV. The shear waves propagate perpendicular to the primary US wave, producing the acoustic radiation force and generating local stress that causes displacements in the tissue. Fast plane wave excitation is then used to track the displacements in the tissue and SWV within the ROI (Taljanovic et al., 2017). Tissue displacement maps are used to calculate the shear wave velocity, in meters per second (m/s), which is directly related to the shear modulus (G). The shear modulus is calculated using Equation 1.

$$\textbf{\textit{Equation 1}}: G = \rho * SWV^2$$

Where G = shear modulus, SWV = shear wave velocity, and ρ = density of the tissue (assumed to be 1 g/cm^3). The tissue's underlying properties are assumed to be linear, isotropic, incompressible, and homogenous).

Shear modulus is also directly related to Young's modulus (E), as long as the tissue is assumed to be linear, isotropic, incompressible, and homogenous (Shina et al., 2015). Young's modulus (E) is the ratio of tensile stress to tensile strain (Taljanovic et al., 2015) and is calculated in kilopascals (kPa) using Equation 2.

$$\textbf{\textit{Equation 2}}: E = 3G = 3 * \rho * SWV^2$$

For a better understanding, Figure 3 displays the basic operational steps of SWE described by Taljanovic and colleagues (2017).

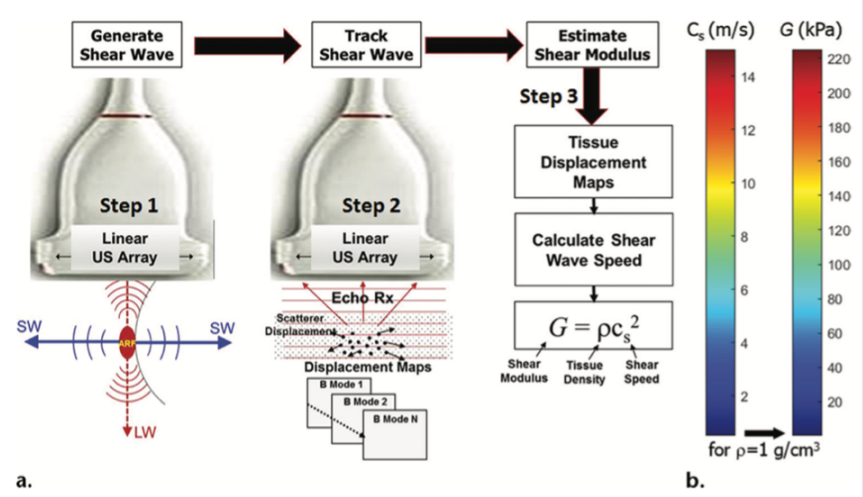

Figure 1. **(a)** Basic physics of SWE. In step 1, shear waves are generated using acoustic radiation force; they propagate perpendicularly to the primary US wave at a lower velocity. In step 2, fast plane wave excitation is used to track displacement and velocity as shear waves propagate, and tissue displacement is calculated using a speckle tracking algorithm. In step 3, tissue displacements are used to calculate shear-wave velocity (c_s) and shear modulus *(G)*. **(b)** Relationship between shear velocity and shear modulus expressed as a color bar, which assumes, in this case, a density equal to that of water (1 g/cm³). Actual density estimates will vary for different types of soft tissue and can also be found using values published in the literature.

Figure 3: *Basic Operational Steps of SWE (Taljanovic et al., 2017)*

Once measurements are taken, the quantitative shear modulus maps are represented by colour-coded elastograms. These elastograms can either display shear wave velocity (m/s) or Young's modulus (kPa). This thesis focuses on extracting the shear wave velocity (SWV) of the tissues that are in the region of interest. Figure 4 is an example of the elastogram obtained when using SWE to quantify the SWV of the soft tissues directly above the GT. Red represents tissues with a higher Young's moduli, while blue represents tissues with a lower Young's moduli. Green and yellow represent regions with intermediate Young's moduli. Additionally, shear waves propagate faster in stiffer and contracted tissues and along the long axis of healthy tendons (Taljanovic et al., 2017). Shear wave velocities decrease when measuring deeper tissues and with the presence of bone below the ROI (Ewertsen et al., 2016).

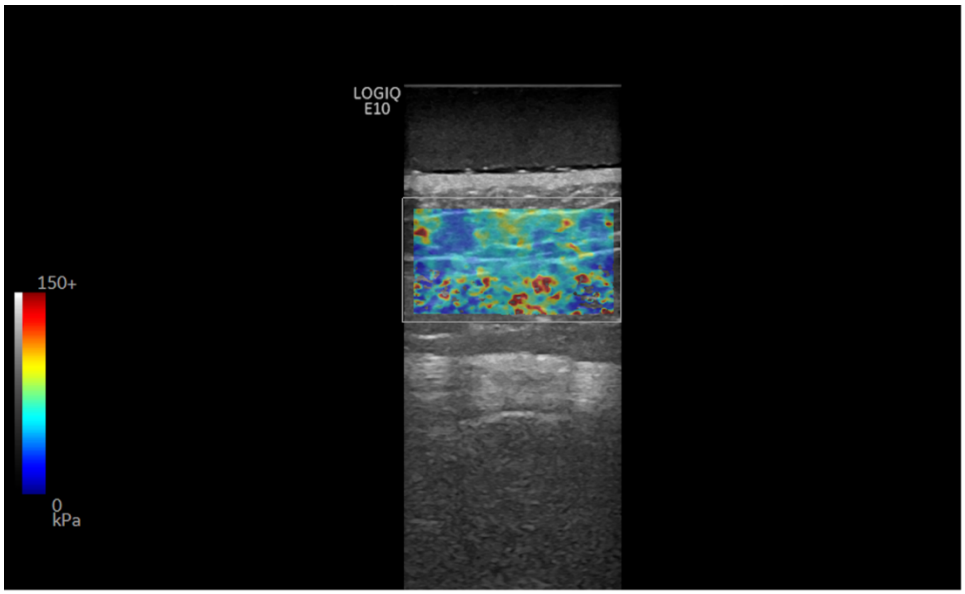

Figure 4: *SWE Image of the Soft Tissues Overlying the Greater Trochanter – The elastogram is used to obtain the SWV of the region of interest. Within the elastogram, red represents stiffer tissues with a harder consistency, while blue represents softer, less stiff tissue. Green and yellow represent regions with intermediate stiffness.*

There are three main types of US transducers that are used for B-mode imaging, including the linear, curvilinear, and phased array. Linear transducers are ideal for imaging superficial structures and operate at a higher frequency. Curvilinear transducers penetrate deeper than linear transducers and operate at lower frequencies which results in a wider field of view, and phased transducers contain a series of elements that are used to generate pulsed waves in the tissue to generate images (Markowitz, 2011). SWE is a feature that can be used with both the linear and curvilinear transducers; however, majority of the literature used the linear transducer (Alfuraih et al., 2019; Baumer et al., 2017; Botanlioglu et al., 2012; Dieterich et al., 2017; Eby et al., 2015; Lin et al., 2015; Matsuda et al., 2019; Nojiri et al., 2021; Quack et al., 2019; Wu et al., 2018; Yun et al., 2019; Zhou et al., 2019). Linear transducers generate US waves in straight lines and have a greater resolution than curvilinear transducers, which have a cone-like field of view and greater depth perception (Chan & Perlas, 2011) (Figure 5). For this thesis, a linear transducer will be used to differentiate and quantify the SWV of the subcutaneous adipose and muscle tissues within the hip region because it has a higher resolution. Additionally, the ultrasound system being used does not support using the curvilinear probe for performing SWE on musculoskeletal tissue. Figure 5 represents a B-mode US image taken with a curvilinear transducer and demonstrates the difficulty of differentiating the soft tissues, especially when compared to the image from the linear probe (Figure 4).

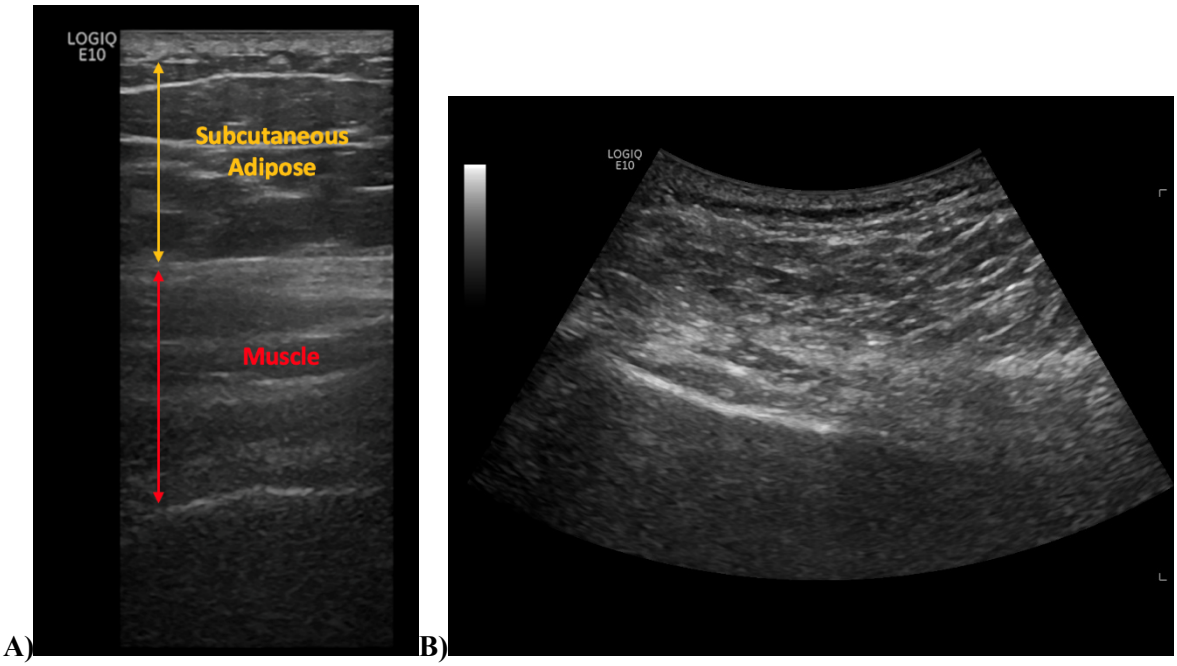

Figure 5: *B-mode US image taken with the Linear (A) vs Curvilinear (B) Probes – The linear probe has a higher resolution than the curvilinear probe, allowing for the differentiation between the different soft tissues in the lateral hip region.*

2.4.2 Benefits and Limitations of SWE

There are several benefits of utilizing SWE to quantify the SWV of tissues within the body, which can be used to quantify Young's moduli. Firstly, it is a non-invasive modality that allows for the direct, real-time assessment of tissue elasticity (Dieterich et al., 2017; Shina et al., 2015). In comparison to other techniques, like compression sonoelastography, SWE is more objective and reproducible, as it is simple to use and does not require manual compression (Taljanovic et al., 2017). Additionally, it has been reported to have moderate to good intra- and inter-reliability ($0.85 < ICC < 0.96$), which is discussed in more depth in section 2.4.4. It also does not expose individuals to harmful radiation (Abramowicz, 2013). However, there are some limitations to this technique. The reliability of SWE measurements of superficial tissues may also be influenced by the pressure exhibited by the transducer onto the skin that can cause high artifactual shear wave speeds (SWS) due to the localized pre-stress. To improve the reliability of the superficial tissues' SWE measurements, the operator should minimize the pressure applied from the probe to the tissue of interest (Bamber et al., 2013). Additionally, gel stand-offs can be used to reduce the occurrence of artifacts generated by pressure from the probe onto the skin (DeJong et al., 2017; DeJong et al., 2020). Another limitation of SWE is that the shape and size of the region of interest (ROI) is limited, resulting in the quantification of SWV/modulus at only certain parts of the tissue of interest, rather than

the entire tissue (Zhou et al., 2019). Although SWE has these limitations, in comparison to other methods that are discussed in more depth in section 2.5, it is a reliable, non-invasive modality. It has been used for the real-time assessment of tissues throughout the body and will allow for the characterization of the mechanical properties of pelvic soft tissues.

2.4.3 The Use of SWE at Diverse Anatomical Regions

As previously mentioned, SWE is a non-invasive method of quantifying the Young's moduli of soft tissue (Dieterich et al., 2017; Matsuda et al., 2019). Table 2 summaries a few of the many studies in which researchers have used SWE to identify pathology (Alfuraih et al., 2019; Botanlioglu et al., 2012; Yun et al., 2019) or tissue state changes associated with aging (Baumer et al., 2017; Eby et al., 2015; Wu et al., 2018; Yun et al., 2019), sex (Botanlioglu et al., 2012; Eby et al., 2015; Wu et al., 2018), posture (Dieterich et al., 2017; Eby et al., 2015), pain (Lin et al., 2015), stretching (Nojiri et al., 2021; Zhou et al., 2019), and surgical interventions (Quack et al., 2019).

The main body regions where SWE has been used to quantify the tissues' Young' moduli include the neck, shoulder, elbow, lower back, leg, and the iliopsoas muscle of the hip. Additionally, it has recently been used to characterize the non-linear mechanical behaviour of the heel pad (Lin et al., 2015; Wu et al., 2018). Specifically, the SWV was quantified with no compression to characterize the initial moduli (i.e. initial shear and Young's moduli) of the tissues, with additional measurements that quantified their non-linear mechanical behaviour by increasing the compressive loads on the tissue (Chatzistergos et al., 2018). SWE has been used across multiple anatomical locations to characterize their soft tissues' mechanical properties, except for in the lateral pelvic-hip region. Addressing this gap in the literature will allow for the computation of more biofidelic hip models and the improvement of engineering-based interventions, such as hip protectors and safety flooring.

Table 2: Summary of SWE Research. *This table provides a summary of the different SWE studies that have been conducted on different body regions, along with details about their SWE settings, main findings, and limitations.*

Body Region	Author/Year	Main Theme/ Purpose	SWE Settings	Main Findings	Limitations
Neck	Dieterich et al. (2017)	Muscle (passive/active) Main neck extensor muscles investigated – multifidus, semispinalis cervicis, semispinalis capitis, splenius capitis, and trapezius Purpose – To examine the influence of the layered organization (muscle depth) of the neck extensors on muscle stiffness in the resting state and during a head lift (active state)	SWE recorded at 1Hz using linear transducer (SL10-2 MHz)	Highest passive and active stiffness values were recorded for the deeper neck extensor muscles During head lift, semispinalis cervicis experienced the greatest increase in active stiffness	Previous studies have reported lower reproducibility of shear modulus measurements for deeper muscles. For current study, they used smaller muscle-specific ROIs
Shoulder	Baumer et al. (2017)	Muscle/tendon (passive/active), aging, rotator cuff tear Supraspinatus tendon and muscle Purposes – assess the association between SWS and age in healthy, asymptomatic subjects, and to compare measures of SWS between patients with a rotator cuff tear and healthy, asymptomatic subjects	9L4 linear probe was used Muscle and tendon SWE images were acquired under both passive and active conditions - active condition involved the subjects lifting their forearm off their thigh and abducting their shoulder in the scapular plane only enough to remove contact with the abduction pillow (not MVC)	Mean shear wave speed (SWS) was of the muscle and tendon increased with age for both passive and active conditions Subjects with rotator cuff tears had lower mean SWS in the muscle and tendon during active condition, but there was no difference during the passive condition	Did not measure intramuscular tendon cross-sectional dimensions, which can influence SWS measurements

Body Region	Author/Year	Main Theme/ Purpose	SWE Settings	Main Findings	Limitations
Shoulder	Yun et al. (2019)	Tendons, idiopathic adhesive capsulitis of the shoulder (ACS) & aging Main muscles – supraspinatus (SST) & infraspinatus (IST) To compare the elasticity of the supraspinatus tendon (SST) and infraspinatus tendon (IST) in patients with idiopathic adhesive capsulitis of the shoulder (ACS) with those in the control groups and to evaluate the relationship between age and tendon elasticity.	Circular region of interest (ROI) of size 0.09 cm^2 was set in the target tendon	SST and IST were stiffer in patients with ACS than those with normal shoulders regardless of age	Specific ROIs within the SST and IST were measured, which may not represent the entire tendon Intra-observer agreement was not evaluated
Elbow/ Biceps	Eby et al. (2015)	Muscle & Aging Purpose – Quantify passive stiffness/ shear modulus of biceps brachii throughout adulthood in flexed and extended elbow positions	Trials lasted approximately 30-60s Used SL15-4 (linear array) transducer with a frequency of 8.5 MHz	Females in the same age group have higher shear modulus than males due to muscle cross-sectional area or other joint structures Shear modulus of the muscle increased with age Age and sex account for 44% of the variation in shear modulus in group of 60 years and older	All personal information was collected using a self-reporting questionnaire Did not obtain info regarding menstrual cycle for premenopausal females Number of male subjects above 30 was lower than women – reducing the statistical power Participants were requested to remain relaxed but

Body Region	Author/Year	Main Theme/ Purpose	SWE Settings	Main Findings	Limitations
Elbow/ Biceps	Eby et al. (2015)			Did not find significant contributions of BMI, arm circumference, or exercise frequency on shear modulus values	did not confirm with EMG
Lower Back	Matsuda et al. (2019)	Muscle (passive) Main muscle investigated – multifidus (MF) Purpose – To investigate the reproducibility of elastic moduli measurements of the MF (superficial and deep) at different trunk angles using SWE	SL10-2 (linear array) transducer with a frequency of 2-10 MHz; SWE penetration depth range: 2.5–45 mm; SWE resolution: 2.0 mm	ICCs revealed that the elastic modulus measurements of the superficial and deep layers of MF under different trunk angles was reliable	Participants were requested to remain relaxed but did not confirm with EMG
Hip	Nojiri et al. (2021)	Muscle & static stretching (SS) Main muscles investigated – iliopsoas muscle consisting of the iliacus and psoas major muscles Purpose – To investigate the time required for hip extension SS to reduce the stiffness of the iliacus muscle	SuperLinear SL 10–2 probe Square (1.5 cm x 1.5 cm) was centered at the iliacus muscle belly and a circle was drawn inside to represent the ROI	Shear elastic moduli decreased with 1 min of SS and continued to decrease as SS continued for 5 min	Only investigated the acute effects of SS and not long-term

Body Region	Author/Year	Main Theme/ Purpose	SWE Settings	Main Findings	Limitations
Leg	Quack et al. (2019)	Total knee arthroplasty (TKA) including the patellar & quadriceps tendons Purposes – to examine the non-invasive sonographic imaging modalities B-mode US, PD-US, and SWE to morphologically and quantitatively evaluate tendon anatomy and stiffness in quadriceps and patellar tendons after TKA and to compare non-operative knees. Also, to find out if there was any correlation between sonographic displayable pathologic changes in the quadriceps and/or patellar tendon and the existence of AKP	High-resolution linear (SuperLinear SL 15-4) 15 MHz transducer Standoff –gel cushion delay block was used: Sonogel, Sonokit Proxon, length 100x100 mm, delay distance 10 mm	Tendons in the operated knee had decreased stiffness compared to the non-operated knee (assessed by SWE). B-US and PD-US also showed significant changes. Tendons improved as the knee healed – SWE is great tool to use during follow-up	Did not investigate inter-rater and intra/-rater reliability
	Alfuraih et al. (2019)	Muscle (passive) & glucocorticoid-induced myopathy (GIM) Main muscles of the proximal leg explored – quadriceps, hamstrings and biceps brachii muscles	SL10-2 (linear array) transducer with a frequency of 2 MHz Muscles were scanned in resting posture	Proximal lower limb muscles of GCA patients can lose on average 15% and up to one-quarter of its stiffness after being exposed to high glucocorticoid dose therapy for 3 and 6 months	Small sample size (half the participants dropped out)

Body Region	Author/Year	Main Theme/ Purpose	SWE Settings	Main Findings	Limitations
Leg	Alfuraih et al. (2019)	Purpose – To investigate the responsiveness of muscle stiffness as measured by SWE and physical strength tests in patients exposed to high doses of glucocorticoid treatment			
	Botanlioglu et al. (2012)	Muscle (passive/active) & Patellofemoral pain syndrome Main muscles investigated – vastus lateralis (VL) and vastus medialis obliquus (VMO) muscles Purpose – to define and compare the mechanical properties of the VMO and VL muscles (in resting and in contraction phases) by the way of quantitative shear-wave elastography in male and female healthy control (HC) subjects, and in female patients with PFPS	4-15 MHz transducer was used Shear modulus determined in kPa by system Resting and MVC trials were performed in neutral and 30° abduction position of the hip	Found differences in VL and VMO elasticity based on sex and posture Found significant VMO weakness in patients with PFPS	Participants were requested to remain relaxed but did not confirm with EMG

Body Region	Author/Year	Main Theme/ Purpose	SWE Settings	Main Findings	Limitations
Leg	Zhou et al. (2019)	Muscle (passive), tendon & static stretching Main muscles and tendons of ankle explored – gastrocnemius-achilles tendon complex Purposes – (1) to investigate the acute effects of static stretching (SS) on the shear modulus of the medial gastrocnemius muscles (MG) and lateral gastrocnemius muscles (LG) and AT for different regions; (2) to examine the differences in range of motion (ROM) before and after SS; and (3) to investigate the change of thickness of AT and fascicle length of MG and LG before and after SS	50-mm linear-array (SL15-4) transducer Used the default standard musculoskeletal (MSK) pre-sets Upper limit (800 kPa) of the system was adopted for measurement of the muscle-tendon Young's modulus Q-box diameter of the MG and LG were set as 5×5 mm, and the size of the ROIs was 10×10-mm	5-minutes of SS significantly decreased stiffness of the MG and LG, while increasing the stiffness of the AT Passive stiffness differs amongst the different regions of the muscle and tendon Significant differences found within the 3 regions of the MG and LG pre-stretching, but not after post-stretching Significant differences found within the 3 regions of AT measured pre- and post-stretching	Participants were requested to remain relaxed but did not confirm with EMG; however, B-mode imaging was used to confirm that the muscle was not contracted

Body Region	Author/Year	Main Theme/ Purpose	SWE Settings	Main Findings	Limitations
Heel pad	Lin et al. (2015)	Heel pad & plantar heel pain Purposes – (1) To investigate the reliability of SWE in measuring stiffness of the heel pad and its microchamber and microchamber layers (2) To compare heel pads with plantar heel pain and normal heel pads with respect to the stiffness of the heel pad and its microchamber and macrochamber layers (3) To understand how changes in heel pad stiffness are related to plantar heel pain	SL15-4 (linear array) transducer with a frequency of 4-15 MHz and frame rate of 20,000 frames/s Transducer placed perpendicular on the plantar heel lightly, without touching the skin and compressing the heel pad	Stiffness of the microchamber layer was higher than the microchamber layer Stiffness of bulk heel pad was a little higher than microchamber Heel pads with plantar pain were stiffer than normal ones, either in the bulk of the heel pad or in its micro- or macrochamber layers Plantar pain may be associated with loss of elasticity of the heel pad	Did not investigate inter-rater reliability nor hour-to-hour or day-to-day reliability; results obtained may be exaggerated Two clinical assessment groups were not matched for age
	Wu et al. (2018)	Heel pad & Aging Purpose – Determine and compare the elasticities of the microchamber and microchamber heel pad layers between young and elderly subjects using SWE	SL15-4 (linear array) transducer with a frequency of 4-15 MHz and frame rate of 20,000 frames/s Shear modulus determined in kPa by system No external compression was applied	Elasticity was similar between males and females Older subjects had a stiffer microchamber layer and softer macrochamber than younger individuals	The shape of the ROI could not be adjusted, preventing them from obtaining whole heel pad elasticity Measurements taken in non-weightbearing condition and not assessed during standing or walking

2.4.3.1 The Use of SWE to Assess the Mechanical Properties of Muscle & Subcutaneous Adipose

As previously mentioned in section 2.2.3, muscle activation is known to influence the impact characteristics by increasing the magnitude and rate of loading of the external loads experienced during lateral falls on the hip (Martel et al., 2018). It is also known to increase the pelvic tissue's stiffness in females (Martel et al., 2018) and may influence the impact force distribution following a lateral fall (Pretty et al., 2017). Although it plays a critical role in fall impact dynamics, the mechanical properties of the muscles in the lateral hip region have not been characterized, nor has the influence of muscle activation on these properties been investigated.

Table 3 demonstrates a few of the studies that have utilized SWE to quantify the elastic moduli of different muscles throughout the body, including the neck, shoulder, elbow, lower back, leg, and the iliopsoas muscle of the hip. These studies were mainly concerned with understanding the tissue state changes associated with aging (Baumer et al., 2017; Eby et al., 2015; Wu et al., 2018; Yun et al., 2019), posture (Dieterich et al., 2017; Eby et al., 2015), stretching (Nojiri et al., 2021; Zhou et al., 2019), and surgical interventions (Quack et al., 2019). They also focused on investigating the influence of certain pathologies, like idiopathic adhesive capsulitis (Yun et al., 2019) and patellofemoral pain syndrome (Botanlioglu et al., 2012), on the muscles and tendons' mechanical properties. The majority of these studies focused on assessing muscles in their resting (passive) state (Alfuraih et al., 2019; Eby et al., 2015; Matsuda et al., 2019; Nojiri et al., 2021; Quack et al., 2019; Yun et al., 2019; Zhou et al., 2019), while a few explored the influence of muscle activation on the tissues' elastic moduli (Baumer et al., 2017; Botanlioglu et al., 2012; Dieterich et al., 2017; Lee et al., 2021). The studies that explored the effects of muscle activation observed an increase in the tissue's elastic modulus as the muscle contracted and experienced an increase in its internal force production. This was regardless of whether the muscle was healthy or pathological. Additionally, Nojiri and colleagues (2021) are the only researchers that have explored the mechanical properties of a muscle (iliopsoas) within the hip region; however, this is not the primary muscle located in the lateral pelvic-hip region that would influence the soft tissues' properties during a lateral fall. Thus, there is a need to characterize the resting and muscle-active mechanical properties of the gluteus maximus since it is in the region where lateral falls are commonly sustained.

Based on Table 2, it is evident that researchers have not utilized SWE to quantify the elastic modulus of the subcutaneous adipose throughout the body. As previously mentioned in section 2.2.3, the soft tissues overlying the hip region influence the impact force attenuation during a fall. Although many studies have focused on the combined effects of muscle and adipose tissues on fall impact dynamics, they have failed to investigate their independent effects. For instance, a higher BMI has been found to act as a protective mechanism against hip fractures (Armstrong et al., 2011) as increased soft tissue will be able to

absorb energy during a fall (Fleps et al., 2018a). However, an individual may have a higher BMI due to increased muscle or adipose mass. Since each of these tissues is different, their effects on force attenuation may also be different. Hence, there is a need to characterize the mechanical properties of these individual tissues within the hip region, which can be incorporated into computational models to better understand their unique roles during lateral falls.

Table 3: Summary of Studies that have Used SWE to Quantity the Mechanical Properties of Muscles.

This table provides a summary of the previously conducted studies that have used SWE to quantify the shear modulus or SWV of muscles throughout the body.

Author/ Year	**Muscle**	**Sample Size**	**Age (years) (Mean ± SD)**	**Mean Shear Modulus (kPa)/ Shear wave speed (SWV) (Mean ± SD)**	**Conversion of results into Shear Wave Velocity (m/s) (Mean ± SD)**
Dieterich et al. (2017)	Neck: main neck extensor muscles investigated – multifidus, semispinalis cervicis, semispinalis capitis, splenius capitis, and trapezius Both resting and contracted states	4 females 7 males	Mean: 21.17 ± 3.2	Resting: Multifidus: 14.9 kPa (IQR 1.4) Semispinalis capitis: 9.5 kPa (IQR 2.5) Semispinalis cervicis: 8.9 kPa (IQR 2.8) Splenius capitis: 6.5 kPa (IQR 2.5) Trapezius: 7.7 kPa (IQR 4.4) Head lift (contracted state): shear modulus increased but explicit values were not shared	Resting: Multifidus: 3.86 (IQR 1.18) Semispinalis capitis: 3.08 (IQR 1.58) Semispinalis cervicis: 2.98 (IQR 1.66) Splenius capitis: 2.55 (IQR 1.58) Trapezius: 2.77 (IQR 2.10)
Baumer et al. (2017)	Shoulder: supraspinatus tendon and muscle Both resting and contracted states	Control: 17 females 2 males Full-thickness rotator cuff tear (RCT): 4 females 7 males	Control: Mean: 42.4 ± 18.9 RCT: Mean: 60.0 ± 6.1	Passive muscle SWS: Control: 2.4 ± 0.4 m/s RCT: 2.4 ± 0.6 m/s Passive tendon SWS: Control: 2.9 ± 0.4 m/s RCT: 3.0 ± 0.9 m/s Active muscle SWS: Control: 4.0 ± 0.4 m/s RCT: 3.3 ± 0.8 m/s	Passive muscle: Control: 2.40 ± 0.40 RCT: 2.40 ± 0.60 Passive tendon: Control: 2.90 ± 0.40 RCT: 3.00 ± 0.90 Active muscle: Control: 4.00 ± 0.40 RCT: 3.30 ± 0.80

Author/ Year	Muscle	Sample Size	Age (years)	Shear Modulus (kPa)/ Shear wave speed (SWV)	Conversion of results into Shear Wave Velocity (m/s)
Baumer et al. (2017)				Active tendon SWS: Control: 6.1 ± 1.4 m/s RCT: 4.5 ± 1.3 m/s	Active tendon: Control: 6.10 ± 1.40 RCT: 4.50 ± 1.30
Yun et al. (2019)	Shoulder: supraspinatus tendon (SST) and infraspinatus tendon (IST) Resting state	Control: 6 females 12 males Idiopathic adhesive capsulitis (ACS): 14 females 6 males	Control: 52.6 ± 10.5 ACS: 53.5 ± 7.9	Control: SST median moduli: 3.24 kPa (IQR 2.08–5.02) IST median moduli: 3.49 kPa (IQR 2.66–5.25) ACS: SST median moduli: 32.55 kPa (IQR 12.14–56.41) IST median moduli: 19.49 kPa (IQR 13.39–65.98)	Control: SST median SWV: 1.04 (IQR 0.83–1.29) IST median SWV: 1.08 (IQR 0.94–1.32) ACS: SST median SWV: 3.29 (IQR 2.01–4.34) IST median SWV: 2.55 (IQR 2.11–4.69)
Eby et al. (2015)	Biceps brachii Resting state at 90 deg elbow flexion and full extension	86 females 47 males	Mean age: 44.3 years (range: 21-94) Divided subjects into subgroups and quantified shear modulus during 90 deg elbow flexion and full extension (ext)	20–29 years: 90 deg shear modulus: 5.23 ± 1.86 kPa Ext shear modulus: 16.13 ± 4.51 kPa 30–39 years: 90 deg shear modulus: 5.44 ± 2.10 kPa Ext shear modulus: 15.48 ± 4.07 kPa 40–49 years: 90 deg shear modulus: 5.75 ± 1.62 kPa Ext shear modulus: 17.76 ± 5.62 kPa 50–59 years: 90 deg shear modulus: 5.78 ± 1.43 kPa Ext shear modulus: 16.33 ± 3.02 kPa	20–29 years: 90 deg SWV: 2.29 ± 1.36 Ext SWV: 4.02 ± 2.12 30–39 years: 90 deg SWV: 2.33 ± 1.45 Ext SWV: 3.93 ± 2.02 40–49 years: 90 deg SWV: 2.40 ± 1.27 Ext SWV: 4.21 ± 2.37 50–59 years: 90 deg SWV: 2.40 ± 1.20 Ext SWV: 4.04 ± 1.74 60–69 years: 90 deg SWV: 2.48 ± 1.61 Ext SWV: 3.91 ± 2.42 70–79 years: 90 deg SWV: 2.48±1.52 Ext SWV: 4.27 ± 2.02

Author/ Year	Muscle	Sample Size	Age (years)	Shear Modulus (kPa)/ Shear wave speed (SWV)	Conversion of results into Shear Wave Velocity (m/s)
Eby et al. (2015)				90 deg shear modulus: 6.15 ± 2.58 kPa Ext shear modulus: 15.31 ± 5.87 kPa <u>70–79 years:</u> 90 deg shear modulus: 6.15 ± 2.32 kPa Ext shear modulus: 18.27 ± 4.10 kPa <u>80–89 years:</u> 90 deg shear modulus: 6.40 ± 3.89 kPa Ext shear modulus: 20.98 ± 8.87 kPa <u>90–99 years:</u> 90 deg shear modulus: 5.06 ± 2.81 kPa Ext shear modulus: 19.82 ± 5.44 kPa	<u>80–89 years:</u> 90 deg SWV: 2.53 ± 1.97 Ext SWV: 4.58 ± 2.98 <u>90–99 years:</u> 90 deg SWV: 2.25 ± 1.68 Ext SWV: 4.45 ± 2.33
Matsuda et al. (2019)	Back muscle: multifidus (MF) Resting state	3 females 8 males	23.0 ± 5.9	Reproducibility study – didn't report values obtained from SWE	
Nojiri et al. (2021)	Hip: iliopsoas muscle consisting of the iliacus and psoas major muscles Resting state before and after 5 min of static stretching (SS)	26 males	23.2 ± 2.9	Before SS: 22.1 ± 3.5 kPa 1 min after SS: 20.5 ± 4.2 kPa 2 min after SS: 20.1 ± 4.4 kPa 3 min after SS: 19.8 ± 3.7 kPa 4 min after SS: 19.4 ± 3.5 kPa 5 min after SS: 18.2 ± 2.4 kPa	Before SS: 4.70 ± 1.87 1 min after SS: 4.54 ± 2.05 2 min after SS: 4.48 ± 2.10 3 min after SS: 4.45 ± 1.92 4 min after SS: 4.40 ± 1.87 5 min after SS: 4.27 ± 1.55

Author/ Year	Muscle	Sample Size	Age (years)	Shear Modulus (kPa)/ Shear wave speed (SWV)	Conversion of results into Shear Wave Velocity (m/s)
Quack et al. (2019)	Total knee arthroplasty (TKA) including the patellar & quadriceps tendons Resting state	35 males 28 females	64 ± 8.44	Non-operated (n=50) shear modulus: Patellar tendon – 60.08 ± 19.13 kPa Quadriceps tendon – 52.65 ± 16.20 kPa TKA (n=76) shear modulus: Patellar tendon – 45.69 ± 14.78 kPa Quadriceps tendon – 36.43 ± 16.51 kPa	Non-operated: Patellar tendon: 7.75 ± 4.37 Quadriceps tendon: 7.26 ± 4.02 TKA: Patellar tendon: 6.76 ± 3.84 Quadriceps tendon: 6.04 ± 4.06
Alfuraih et al. (2019)	Muscle (passive) & glucocorticoid-induced myopathy (GIM) Main muscles of the proximal leg explored – quadriceps, hamstrings and biceps brachii muscles Resting and passively stretched states Passively stretched state was only investigated for a few muscles	10 females 4 males	68.2 ± 4.3	Baseline mean SWS (m/s): Vastus lateralis – 1.62 ± 0.16 Rectus femoris – 1.68 ± 0.11 Vastus medialis – 1.70 ± 0.33 Vastus intermedius – 1.96 ± 0.33 Biceps brachii – 1.83 ± 0.30 Biceps femoris – 1.62 ± 0.17 Semitendinosus – 1.58 ± 0.15 Semimembranosus – 1.59 ± 0.15 Baseline passively stretched mean SWS (m/s): Vastus lateralis – 2.67 ± 0.33 Rectus femoris – 2.28 ± 0.63 Vastus medialis – 2.41 ± 0.28 Vastus intermedius – 2.42 ± 0.22	Baseline: Vastus lateralis – 1.62 ± 0.16 Rectus femoris – 1.68 ± 0.11 Vastus medialis – 1.70 ± 0.33 Vastus intermedius – 1.96 ± 0.33 Biceps brachii – 1.83 ± 0.30 Biceps femoris – 1.62 ± 0.17 Semitendinosus – 1.58 ± 0.15 Semimembranosus – 1.59 ± 0.15 Baseline passively stretched: Vastus lateralis – 2.67 ± 0.33 Rectus femoris – 2.28 ± 0.63 Vastus medialis – 2.41 ± 0.28 Vastus intermedius – 2.42 ± 0.22

Author/ Year	Muscle	Sample Size	Age (years)	Shear Modulus (kPa)/ Shear wave speed (SWV)	Conversion of results into Shear Wave Velocity (m/s)
Alfuraih et al. (2019)				3 months after baseline (1st glucocorticoids treatment) mean SWS (m/s): Vastus lateralis – 1.40 ± 0.10 Rectus femoris – 1.54 ± 0.13 Vastus medialis – 1.36 ± 0.12 Vastus intermedius – 1.62 ± 0.19 Biceps brachii – 1.82 ± 0.18 Biceps femoris – 1.37 ± 0.09 Semitendinosus – 1.36 ± 0.08 Semimembranosus – 1.41 ± 0.11 3 months after baseline (1st glucocorticoids treatment) passively stretched mean SWS: Vastus lateralis – 2.66 ± 0.28 Rectus femoris – 1.99 ± 0.28 Vastus medialis – 2.30 ± 0.22 Vastus intermedius – 2.37 ± 0.34 6 months after baseline (2nd glucocorticoids treatment) mean SWS (m/s): Vastus lateralis – 1.31 ± 0.06 Rectus femoris – 1.41 ± 0.15 Vastus medialis – 1.41 ± 0.15 Vastus intermedius – 1.76 ± 0.22 Biceps brachii – 1.84 ± 0.28	3 months after baseline (1st glucocorticoids treatment): Vastus lateralis – 5.88 ± 0.03 Rectus femoris – 7.11 ± 0.05 Vastus medialis – 5.55 ± 0.04 Vastus intermedius – 7.87 ± 0.11 Biceps brachii – 9.94 ± 0.10 Biceps femoris – 5.63 ± 0.02 Semitendinosus – 5.55 ± 0.02 Semimembranosus – 5.96 ± 0.04 3 months after baseline (1st glucocorticoids treatment): Vastus lateralis – 21.23 ± 0.24 Rectus femoris – 11.88 ± 0.24 Vastus medialis – 15.87 ± 0.15 Vastus intermedius – 16.85 ± 0.35 6 months after baseline (2nd glucocorticoids treatment): Vastus lateralis – 1.31 ± 0.06 Rectus femoris – 1.41 ± 0.15 Vastus medialis – 1.41 ± 0.15 Vastus intermedius – 1.76 ± 0.22 Biceps brachii – 1.84 ± 0.28 Biceps femoris – 1.21 ± 0.10 Semitendinosus – 1.26 ± 0.08

Author/ Year	Muscle	Sample Size	Age (years)	Shear Modulus (kPa)/ Shear wave speed (SWV)	Conversion of results into Shear Wave Velocity (m/s)
Alfuraih et al. (2019)				Biceps femoris – 1.21 ± 0.10 Semitendinosus – 1.26 ± 0.08 Semimembranosus – 1.35 ± 0.10 <u>6 months after baseline (2nd glucocorticoids treatment) passively stretched mean SWS (m/s):</u> Vastus lateralis – 2.50 ± 0.34 Rectus femoris – 2.05 ± 0.11 Vastus medialis – 2.30 ± 0.15 Vastus intermedius – 2.08 ± 0.34	Semimembranosus – 1.35 ± 0.10 <u>6 months after baseline (2nd glucocorticoids treatment) passively stretched mean:</u> Vastus lateralis – 2.50 ± 0.34 Rectus femoris – 2.05 ± 0.11 Vastus medialis – 2.30 ± 0.15 Vastus intermedius – 2.08 ± 0.34
Zhou et al. (2019)	Muscle (passive), tendon & static stretching Main muscles and tendons of ankle explored – medial gastrocnemius muscles (MG) and lateral gastrocnemius muscles (LG) and achilles tendon (AT) Measurements were made at 3 regions along the muscle: proximal (pro), middle (mid) and distal (dis)	15 females 15 males	21.33 ± 2.72	<u>Pre-stretching shear modulus (kPa):</u> MG – Pro: 28.37±15.13 MG – Mid: 18.11±6.94 MG – Dis: 25.67±17.54 LG – Pro: 32.94±13.69 LG – Mid: 23.72±8.69 LG – Dis: 22.18±10.98 AT – Pro: 430.56±53.25 AT – Mid: 400.14±50.49 AT – Dis: 396.81±65.34	<u>Pre-stretching:</u> MG – Pro: 5.33±3.89 MG – Mid: 4.26 ± 2.63 MG – Dis: 5.16 ± 4.19 LG – Pro: 5.74 ± 3.70 LG – Mid: 4.87 ± 2.95 LG – Dis: 4.71 ± 3.31 AT – Pro: 20.75 ± 7.79 AT – Mid: 20.00 ± 7.11 AT – Dis: 19.92 ± 8.08

Author/ Year	Muscle	Sample Size	Age (years)	Shear Modulus (kPa)/ Shear wave speed (SWV)	Conversion of results into Shear Wave Velocity (m/s)
Zhou et al. (2019)				Post-stretching shear modulus (kPa): MG – Pro: 17.22±6.71 MG – Mid: 13.56±3.58 MG – Dis: 16.92±6.98 LG – Pro: 19.46±9.33 LG – Mid: 15.77±5.51 LG – Dis: 16.59±6.98 AT – Pro: 512.15±64.14 AT – Mid: 465.32±56.90 AT – Dis: 487.06±55.50	Post-stretching: MG – Pro: 4.15 ± 2.59 MG – Mid: 3.68 ± 1.89 MG – Dis: 4.11 ± 2.64 LG – Pro: 4.41 ± 3.05 LG – Mid: 3.97 ± 2.35 LG – Dis: 4.07 ± 2.64 AT – Pro: 22.63 ± 8.01 AT – Mid: 21.57 ± 7.54 AT – Dis: 22.07 ± 7.45
Botanlioglu et al. (2012)	Muscle & Patellofemoral pain syndrome Main muscles investigated – vastus lateralis (VL) and vastus medialis obliquus (VMO) muscles Resting and contracted states in neutral (N) and 30 deg abduction (30) of the hip positions	Control group: 11 females 11 males Patellofemoral pain patients (PFPS): 11 subjects	Control group: Females – 28.1 ± 4.0 Males – 28.8 ± 2.0 PFPS: 30.8 ± 8.2	Control males resting mean elastic modulus (kPa): VL (N) right – 16.2 ± 3.7 VL (N) left – 14.9 ± 5.2 VL (30) right – 14.3 ± 3.0 VL (30) left – 15.1 ± 3.5 VMO (N) right – 14.8 ± 5.3 VMO (N) left – 13.4 ± 3.7 VMO (30) right – 12.9 ± 4.1 VMO (30) left – 13.9 ± 4.4 Control males contracted mean elastic modulus (kPa): VL (N) right – 201.8 ± 70.5 VL (N) left – 173.8 ± 43.7 VL (30) right – 152.5 ± 44.1 VL (30) left – 153.6 ± 41.0	Control males resting: VL (N) right – 2.32 ± 1.11 VL (N) left – 2.23 ± 1.32 VL (30) right – 2.18 ± 1.00 VL (30) left – 2.24 ± 1.08 VMO (N) right – 2.22 ± 1.33 VMO (N) left – 2.11 ± 1.11 VMO (30) right – 2.07 ± 1.17 VMO (30) left – 2.15 ± 1.21 Control males contracted: VL (N) right – 8.20 ± 4.85 VL (N) left – 7.61 ± 3.82 VL (30) right – 7.13 ± 3.83 VL (30) left – 7.16 ± 3.70 VMO (N) right – 8.19 ± 4.44 VMO (N) left – 8.42 ± 4.65

Author/ Year	Muscle	Sample Size	Age (years)	Shear Modulus (kPa)/ Shear wave speed (SWV)	Conversion of results into Shear Wave Velocity (m/s)
Botanlioglu et al. (2012)				VMO (N) right – 201.3 ± 59.1 VMO (N) left – 212.7 ± 64.9 VMO (30) right – 204.4 ± 44.3 VMO (30) left – 234.5 ± 73.1 Control females resting mean elastic modulus (kPa): VL (N) right – 16.5 ± 2.6 VL (N) left – 13.9 ± 3.7 VL (30) right – 16.9 ± 4.5 VL (30) left – 14.6 ± 3.8 VMO (N) right – 11.4 ± 3.7 VMO (N) left – 12.1 ± 3.5 VMO (30) right – 12.4 ± 5.1 VMO (30) left – 9.6 ± 2.3 Control females contracted mean elastic modulus (kPa): VL (N) right – 113.7 ± 53.2 VL (N) left – 122.6 ± 58.1 VL (30) right – 125.5 ± 51.6 VL (30) left – 113.7 ± 42.0 VMO (N) right – 139.1 ± 47.6 VMO (N) left – 157.6 ± 31.0 VMO (30) right – 160.6 ± 46.1 VMO (30) left – 168.3 ± 37.3	VMO (30) right – 8.25 ± 3.84 VMO (30) left – 8.84 ± 4.94 Control females resting: VL (N) right – 2.35 ± 0.93 VL (N) left – 2.15 ± 1.11 VL (30) right – 2.37 ± 1.22 VL (30) left – 2.21 ± 1.13 VMO (N) right – 1.95 ± 1.11 VMO (N) left – 2.01 ± 1.08 VMO (30) right – 2.03 ± 1.30 VMO (30) left – 1.79 ± 0.88 Control females contracted: VL (N) right – 6.16 ± 4.21 VL (N) left – 6.39 ± 4.40 VL (30) right – 6.47 ± 4.15 VL (30) left – 6.16 ± 3.74 VMO (N) right – 6.81 ± 3.98 VMO (N) left – 7.25 ± 3.21 VMO (30) right – 7.32 ± 3.92 VMO (30) left – 7.49 ± 3.53 PFPS resting: VL (N) right – 2.14 ± 1.18 VL (N) left – 2.29 ± 1.05 VL (30) right – 2.14 ± 1.43 VL (30) left – 2.11 ± 1.17

Author/ Year	Muscle	Sample Size	Age (years)	Shear Modulus (kPa)/ Shear wave speed (SWV)	Conversion of results into Shear Wave Velocity (m/s)
Botanlioglu et al. (2012)				PFPS resting mean elastic modulus (kPa): VL (N) right – 13.8 ± 4.2 VL (N) left – 15.8 ± 3.3 VL (30) right – 13.7 ± 6.1 VL (30) left – 13.3 ± 4.1 VMO (N) right – 14.2 ± 4.0 VMO (N) left – 13.0 ± 3.3 VMO (30) right – 12.1 ± 3.6 VMO (30) left – 11.6 ± 3.7 PFPS contracted mean elastic modulus (kPa): VL (N) right – 80.6 ± 26.0 VL (N) left – 98.2 ± 34.3 VL (30) right – 98.5 ± 34.6 VL (30) left – 92.2 ± 38.5 VMO (N) right – 116.2 ± 45.2 VMO (N) left – 103.9 ± 39.3 VMO (30) right – 101.8 ± 28.3 VMO (30) left – 102.9 ± 41.1	VMO (N) right – 2.18 ± 1.15 VMO (N) left – 2.08 ± 1.05 VMO (30) right – 2.01 ± 1.10 VMO (30) left – 1.97 ± 1.11 PFPS contracted: VL (N) right – 5.18 ± 2.94 VL (N) left – 5.72 ± 3.38 VL (30) right – 5.73 ± 3.40 VL (30) left – 5.54 ± 3.58 VMO (N) right – 6.22 ± 3.88 VMO (N) left – 5.89 ± 3.62 VMO (30) right – 5.83 ± 3.07 VMO (30) left – 5.86 ± 3.70
Lee et al. (2021)	Lower limb muscles investigated: rectus femoris (RF), tibialis anterior (TA), biceps femoris (BF) & medial gastrocnemius (MG) Both resting and contracted states	20 males & 20 females	22.15 ±2.29	Resting Young's Moduli: RF – 13.99 ± 3.14 TA – 21.10 ± 2.99 BF – 13.13 ± 3.70 MG – 12.29 ± 2.84 Contracted Young's Moduli: RF – 79.76 ± 14.99 TA – 138.97 ± 32.80 BF – 80.45 ± 15.74 MG – 79.68 ± 18.45	Resting SWV: RF – 2.16 ± 1.02 TA – 2.65 ± 1.00 BF – 2.09 ± 1.11 MG – 2.02 ± 0.97 Contracted SWV: RF – 5.16 ± 2.24 TA – 6.81 ± 3.31 BF – 5.18 ± 2.29 MG – 5.15 ± 2.48

2.4.4 The Inter-Rater & Intra-Rater Reliability of SWE

The two types of reliability used to evaluate the consistency of a measurement tool and its users are intra-rater and inter-rater reliability. Intra-rater reliability is used to evaluate the consistency of one rater over several trials of the same measurement, while inter-rater reliability is used to evaluate the consistency of two or more raters when measuring the same measurement on a single subject (Scheel et al., 2018). The intraclass correlation coefficient (ICC) is the reliability index used for the analysis of intra-rater and inter-rater reliability. ICC values less than 0.5, between 0.5 and 0.75, between 0.75 and 0.9, and greater than 0.90 are indicative of poor, moderate, good, and excellent reliability, respectively (Koo & Li, 2016).

A few of the studies that utilized SWE to quantify the tissues' elastic moduli also explored the reliability of this tool and their results are summarized in Table 4. According to the calculated ICCs in these studies, the inter-rater and intra-rater reliability was moderate or higher. Additionally, Lin and colleagues (2015) mentioned that a few conditions must be met during measurements for good repeatability. These include a standardized scanning site, controlling the tilt/orientation of the transducer, the amount and homogeneity of the coupling gel and the stability of the hand holding the transducer. Since no studies have investigated the elastic moduli of tissues in the pelvic-hip region using the SWE, it would be beneficial to explore the intra-rater reliability of this tool in this region.

Table 4: Summary of the Reliability Results from Studies that Utilized SWE. *This table provides a summary of the different SWE studies that have assessed the intra and inter-rater reliability of their trials.*

Author/Year	**Body Region**	**Intra-Rater Reliability Results (ICC (95% confidence interval))**	**Inter-Rater Reliability Results (ICC (95% confidence interval))**
Wu et al. (2018)	Heel pad	• Microchamber: 0.94 (0.79-0.99) • Microchamber: 0.89 (0.53-0.97) • Entire heel pad: 0.96 (0.87-0.99) Classification: Good to excellent	• Microchamber: 0.87 (0.51-0.97) • Microchamber: 0.80 (0.26-0.95) • Entire heel pad: 0.93 (0.72-0.98) Classification: Good to excellent
Lin et al. (2015)	Heel pad	• Microchamber: 0.95 (7.1 6 2.5%) • Microchamber: 0.93 (8.8 ± 3.3%) • Entire heel pad: 0.96 (6.1 ± 2.2%) • Concordance correlation coefficient was used to confirm the repeatability,	Did not explore inter-rater reliability

		a value of >0.9 indicated adequate reliability. Classification: Excellent	
Baumer et al. (2017)	Shoulder – Rotator Cuff	Previously studies by Sahrmann (2002) • Supraspinatus muscle & tendon: > 0.87 Classification: Good	Previously studies by Sahrmann (2002) • Supraspinatus muscle & tendon: > 0.73 Classification: Moderate
Matsuda et al. (2019)	Lower Back - Multifidus	Superficial layer of the multifidus in different positions: • Prone: 0.88 (0.64-0.96) • Flexed prone: 0.95 (0.86-0.98) • Extended prone: 0.85 (0.57-0.95) Classification: Good to excellent Deep layer of the multifidus in different positions: • Prone: 0.88 (0.65-0.96) • Flexed prone: 0.85 (0.57-0.95) • Extended prone: 0.86 (0.59-0.96) Classification: Good	Did not explore inter-rater reliability
Nojiri et al. (2021)	Hip - Iliacus	• Iliacus: 0.85 (0.69-0.93) Classification: Good	Did not explore inter-rater reliability

2.5 Alternative Methods of Quantifying the Mechanical Properties of Soft Tissues

There are several other methods that can be used to quantify the mechanical properties of soft tissues, including myotonometry, strain elastography, and transient elastography.

2.5.1 Myotonometry

Myotonometry allows for the quantification of the physiological properties of muscles, including Young's modulus. A small, non-invasive, handheld myotonometer (Davidson et al., 2017), which is a metal probe consisting of two cylindrical pieces (Kerins et al., 2013) is used. The outer cylinder remains stationary, while the inner cylinder has a force transducer that moves when the myotonometer is pushed into the soft tissue (Kerins et al., 2013). Rather than Young's modulus, the muscle's dynamic modulus is calculated as a ratio of the maximum acceleration of the damped oscillations, that characterize the soft tissue's resistance to the externally applied force, divided by the total displacement of the soft tissue, measured by the movement of the inner cylinder. (Lee et al., 2021). Bizzini and colleagues (2003) found that this is a reliable method for measuring the moduli of muscles, like the rectus femoris, vastus lateralis, biceps femoris, and gastrocnemius. It was also sensitive to changes in the muscles' mechanical properties,

including changes in their lengths. This method has good to excellent intra-rater reliability for quantifying the muscles' moduli during resting and muscle contracted states. When its Young's moduli outputs were compared to SWE, they showed moderate to good correlations during both resting and muscle active states. However, unlike SWE, myotonometry is not suitable for measuring the moduli of muscles that are covered with more than 20 mm of subcutaneous adipose (Lee et al., 2021). A few additional limitations are that the probe's rate of compression is not standardized (Kerins et al., 2013), which would result in an increased reported moduli of muscles that are compressed faster (van Loocke et al., 2008) than those that are compressed at a slower rate. The probe must also be perpendicular to the tissues being measured, increasing the likelihood of error with the slightest changes in the probes' orientation (Kerins et al., 2013).

2.5.2 Strain Elastography (SE)

Strain elastography (SE), also known as compression sonoelastography, is another mode available on the US machine, similar to SWE. The examiner applies rhythmic and regular compression to the area of interest to quantify the axial strain of the tissue. Physiologic changes in pressure, from heartbeats and respiratory movements, can also be used to evaluate strain (Carlsen et al., 2015; Prado-Costa et al., 2018). The US machine provides a visualization of the differences in the tissue's strain by comparing the US images throughout the compression period (Taljanovic et al., 2017). Strain is related to the structural stiffness and Young's modulus of the tissue (Shina et al., 2015), where softer tissues will have a larger strain than stiffer tissues (Prado-Costa et al., 2018). Strain ratios (SR) are calculated in which the strain of the region of interest (ROI) is compared to its surrounding tissue's strain and a ratio above one signifies that the ROI is stiffer than the surrounding tissue (Carlsen et al., 2015). This technique is influenced by the depth of the ROI, probe positioning (Prado-Costa et al., 2018), and is operator-dependent (Ozturk et al., 2018). Thus, Young's moduli values obtained from SWE have better repeatability than SE because it is difficult to ensure consistent compression and there is limited consistency in selecting the reference surrounding tissue that is required for the quantification of SR (Carlsen et al., 2015; Sowa et al., 2016).

2.5.3 Transient Elastography (TE)

Similar to SWE, transient elastography (TE) utilizes low-frequency shear waves to quantify the Young's moduli of tissues that are assumed to be homogeneous. However, these shear waves are generated using controlled external vibration and their motion is tracked using the US (Ozturk et al.,

2018; Prado-Costa et al., 2018). The mean of the SWV within the ROI is measured and used to compute Young's modulus (Shina et al., 2015). The Young's modulus of the regional tissue that can be quantified is limited by its depth (Taljanovic et al., 2017), unlike SWE, which can measure the Young's moduli of deeper tissues using push beams (Prado-Costa et al., 2018). This limitation specifically decreases the reliability of TE measurements in obese individuals (Ozturk et al., 2018).

2.6 Key Gaps in Literature

The key gaps in the literature that this thesis aimed to address are:

1. There is no previous research that focused on characterizing the mechanical properties, specifically the SWV, of the muscle (gluteus maximus) and subcutaneous adipose tissues in the lateral hip region.
2. There is scarce research on the influence of muscle contraction on the mechanical properties of the soft tissues in the lateral hip region.

It is important to consider the individual mechanical properties of the tissues in this area to better understand how they contribute to the energy absorption and impact dynamics of lateral falls. This information can be used to improve the biofidelity of hip models and the design of engineering-based interventions, like hip protectors and compliant flooring.

2.7 Thesis Objectives and Hypothesis

2.7.1 Primary Analysis

There were two main objectives of this thesis. The first objective was to evaluate the intra-rater reliability of the SWE protocol that was used to characterize the SWV of the soft tissues (subcutaneous adipose and muscle) in the lateral-hip region. Along with determining whether muscle contraction influenced the protocol's intra-rater reliability. The second objective was to assess the influence of muscle contraction on the soft tissues' SWV.

Specifically, the **main questions** that were investigated are:

1. What is the intra-rater reliability of the subcutaneous adipose and muscles' SWV measurements and is it influenced by muscle contraction?
2. Does muscle contraction influence the SWVs of the subcutaneous adipose and muscle tissues in the lateral hip region?

The **hypotheses**, related to the main questions were:

1. The intra-rater reliability of the subcutaneous adipose and muscle SWV measurements:
    a. Would range from good to excellent (ICC > 0.75), based on the findings of previously conducted SWE studies; and
    b. Would not be influenced by the contraction state.
2. There would be an interaction effect of muscle contraction on the SWV magnitudes of the soft tissues. It is expected that:
    a. The muscle SWV magnitude would be greater during the muscle contracted state compared to the resting state.
    b. The subcutaneous adipose SWV magnitude would not change during the resting and muscle contracted states.

2.7.2 Secondary Analysis

A secondary analysis was conducted to explore differences in SWV based on sex and BMI and explore the influence of muscle contraction on soft tissue thicknesses. The main questions that were being investigated were:

1. Does sex influence the SWVs of the subcutaneous adipose and muscle during resting and contracted states?
2. Does BMI influence the SWVs of the soft tissues during resting and contracted states?
3. Does muscle contraction influence the subcutaneous adipose, muscle, and total soft tissue's thickness in a location in the lateral hip region?

Chapter 3
Research Experiment

3.1 Introduction

As previously mentioned, the pelvic soft tissues influence the total force distribution during an impact and the effectiveness of fall intervention devices, such as hip protectors and compliant flooring. However, studies have not explored the individual characteristics of these tissues, such as the properties of the subcutaneous adipose and muscle, during relaxed and muscle contracted states. Thus, this proposed thesis aimed to address these gaps by exploring the objectives and research questions listed in section 2.7.

3.2 Methodology

3.2.1 Participants

Twenty participants between the ages of 19-35 years old were recruited for this study. Table 5 summarizes their age and anthropometric characteristics.

Table 5: Mean (SD) Participant Anthropometric Characteristics

	Participants	
Sex	Male	Female
N	10	10
Age (years)	23.8 (4.0)	23.8 (3.5)
Height (m)	1.78 (0.09)	1.69 (0.08)
Mass (kg)	75.0 (14.0)	61.0 (13.0)
BMI (kg/m^2)	23.3 (3.0)	21.4 (3.7)

Prior to the data collection, power calculations were conducted to compute the appropriate sample size for this study (Table 6). These sample size calculations used the results from a previously conducted study by Botanlioglu and colleagues (2012) that quantified the SWV of the vastus medialis obliquus (VMO) and vastus lateralis (VL) of the right (R) and left (L) sides during resting and contracted states. These muscles are in close proximity to the gluteus maximus, which is the muscle of interest in this thesis, and contraction state was one of the primary factors being explored in this thesis. According to the literature review, there was no available data that quantified the SWV of the subcutaneous adipose; thus, the sample size was computed using the muscle SWV values. All calculations were conducted using G*Power 3.1 (Universität Düsseldorf, Düsseldorf, Germany) to achieve an 80% power for identifying differences in each of the independent variables, along with an α-value of 0.05.

Based on the SWV of the muscles collected by Botanlioglu and colleagues (2012), the predicted sample size for observing differences in SWV based on muscle contraction ranged from 5-7 participants. Overall, the sample size calculations presented in Table 6 were used to justify the sample size of 20 participants for this thesis. The sample size was increased from 5-7 participants to 20 participants to maximize the probability of achieving adequate statistical power. Although sex-based differences were not primarily being explored in this thesis, both sexes were equally represented by recruiting 10 male and 10 female participants. Finally, additional sample size calculations were conducted based on the SWV results of other studies that focused on muscles in different body regions, and a range of theoretical effect sizes (Appendix A) – overall, these data also aligned with the sample size selected.

Table 6: Sample Size Calculations to Identify Differences in SWV Based on the Muscle Contraction Results from Botanlioglu et al. (2012). *They focused on the vastus lateralis (VL) and vastus medialis obliquus (VMO) muscles on both sides of the body.*

Independent Variable	Group Comparison from Literature	Resting Mean SWV (m/s)	Muscle Contracted Mean SWV (m/s)	Resting SWV SD (m/s)	Muscle Contracted SWV SD (m/s)	Effect Size	Predicted Sample Size (N)	Predicted Sample Size averaged across sexes and sides
Muscle Contraction (Botanlioglu et al., 2012)	VL males' right side	2.32	8.20	1.11	4.85	1.335981	6	7
	VL males' left side	2.23	7.61	1.32	3.82	1.600992	5	
	VL females' right side	2.35	6.16	0.93	4.21	0.994615	8	
	VL females' left side	2.15	6.39	1.11	4.40	1.069804	7	
	VMO males' right side	2.22	8.19	1.33	4.44	1.512614	5	5
	VMO males' left side	2.11	8.42	1.11	4.65	1.500125	5	
	VMO females' right side	1.95	6.81	1.11	3.98	1.366188	5	
	VMO females' left side	2.01	7.25	1.08	3.21	1.852191	4	

3.2.1.2 Eligibility/Exclusion Criteria

Participants were recruited based on sex to obtain a representative distribution from both sexes. They were excluded from this study if they:

- Were not between the ages of 18-35 years.
- Had allergies to ultrasound gel, rubbing alcohol, tapes, or other adhesives that may have been used during data collection.
- Had chronic or recently acquired hip or pelvis injuries.
- Lost or gained twenty-five or more pounds in the last year.
- Had recent injections of gaseous contrast media to the hip or pelvic area.
- Suspected or known pregnancy.
- Had a BMI > 24.9 kg/m^2.

Participants with chronic or recent hip or pelvis injuries, including hip replacement(s) were excluded from the study because they may have confounded the typical relationship between soft tissues and body composition, pelvic location, and muscle contraction. Similarly, sudden weight loss or gain affects soft tissue characteristics and may also have confounded the typical relationship between soft tissues and age, body composition, pelvic location, and muscle contraction. Participants who had recent injections of gaseous contrast media and a suspected or known pregnancy could not participate because the increased temperatures resulting from the ultrasound exposure for longer than five minutes could have been harmful to the individual or fetus, respectively.

Additionally, individuals with a higher BMI were excluded from this thesis because it was difficult to obtain high-resolution images of their muscle tissue. Higher-resolution images were required to differentiate between the subcutaneous adipose and muscle tissues when obtaining the tissue-specific SWV values. It was particularly difficult to differentiate between the soft tissues directly overlying the greater trochanter (Figure 6). Thus, the linear ultrasound probe which results in higher resolution images compared to the curvilinear probe (Figure 7), was used (Chan & Perlas, 2011; Mandal et al., 2015). The penetration depth of the linear probe was 14 cm, making it difficult to image and clearly differentiate tissues in higher BMI individuals. According to Table 2, majority of the SWE literature has utilized the linear probe (Eby et al., 2015; Dieterich et al., 2017; Nojiri et al., 2021; Zhou et al., 2019; Botanlioglu et al., 2012; Alfuraih et al., 2019; Yun et al., 2019; Wu et al., 2018; Baumer et al., 2017; Quack et al., 2019; Lin et al., 2015; Matsuda et al., 2019). As an initial step towards utilizing SWE in the lateral hip region to quantify the tissue specific SWV values, low and normal BMI individuals were recruited for this thesis to ensure that there was a clear distinction between the soft tissues being quantified.

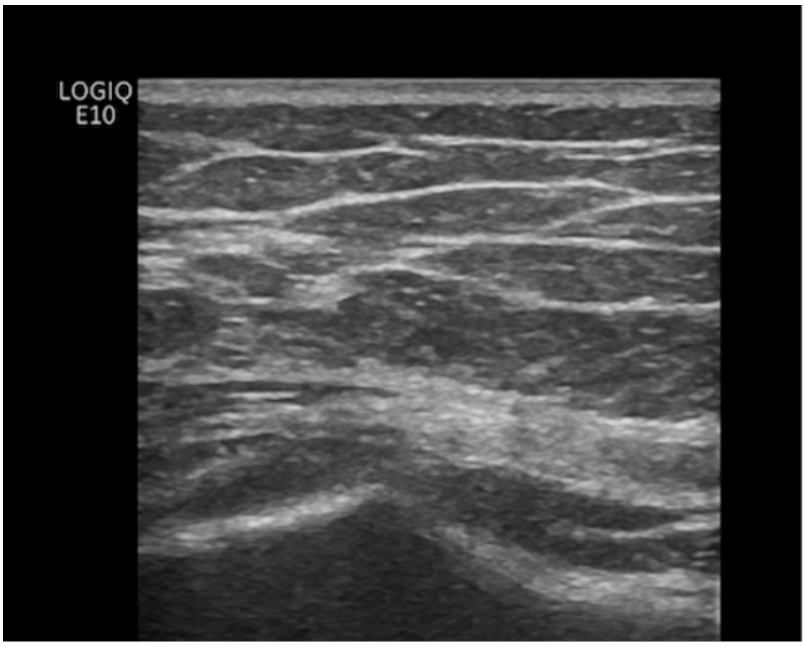

Figure 6*: B-mode US Image of the Greater Trochanter – This image of the soft tissues over the greater trochanter in a normal BMI individual demonstrates the difficulty in identifying the different soft tissues at this location.*

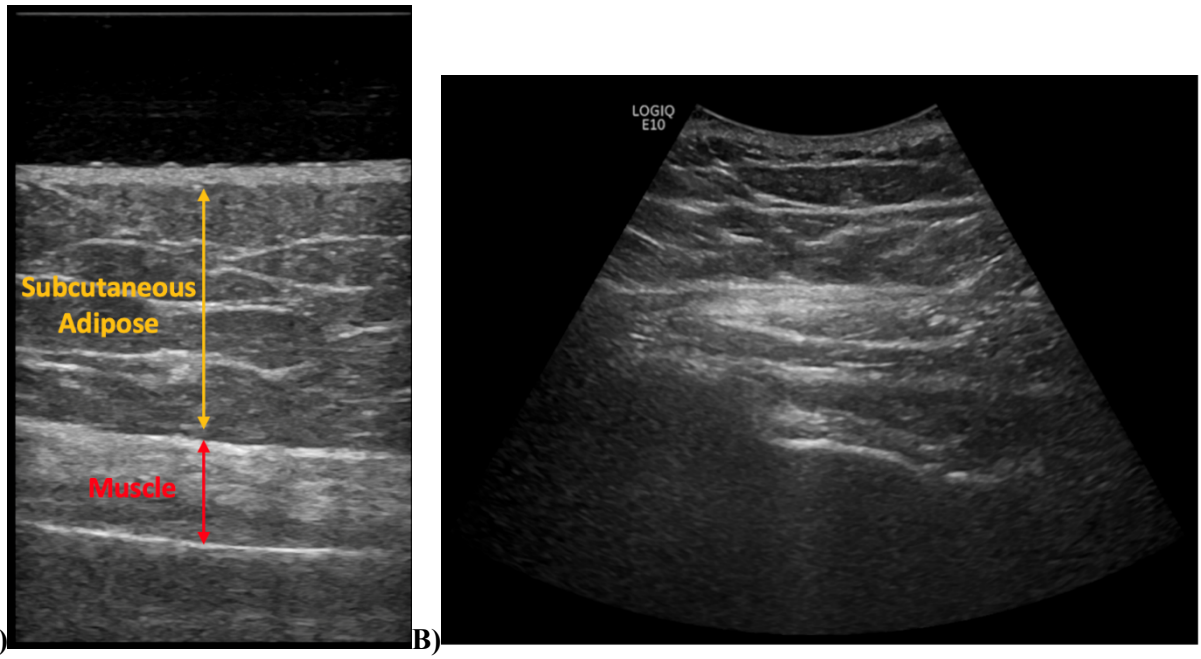

A) **B)**

Figure 7: *Image Resolution Differences between the Linear (A) & Curvilinear (B) Probes – The linear probe has a higher resolution than the curvilinear probe, allowing for the improved differentiation between the different soft tissues in the lateral hip region.*

3.2.2 Instrumentation

The elastography setting on a GE LOGIQ E10 commercial ultrasound machine (Figure 8-A; GE Healthcare Canada, ON, Canada), an L2-9VN-D linear array ultrasound probe (Figure 8-B; GE Healthcare Canada, ON, Canada), and AquaFlex gel pad stand-off (Figure 9) were used to obtain the SWV measurements of the subcutaneous adipose and muscle tissues at the location of interest. The linear probe was used because it allowed for higher resolution imaging, compared to the curvilinear probe (Chan & Perlas, 2011; Mandal et al., 2015) and a clearer differentiation of the soft tissues (adipose and muscle) in this region (Figure 7). Additionally, the curvilinear probe on the GE LOGIQ E10 system does not support the use of SWE for musculoskeletal tissue, thus the linear probe was used.

For all SWE measurements, the general musculoskeletal imaging setting (MSK Gen) and the largest region of interest (ROI) of 2 x 4 cm were used. Once all the SWE images were collected, the systems' built-in measurement software was used to extract the SWV of the ROI in meters per second (m/s), which is described in greater detail in section 3.4.

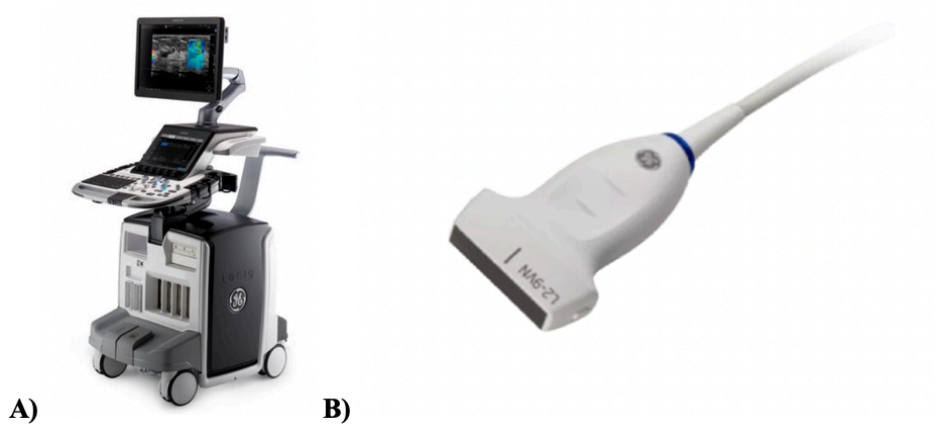

Figure 8: A) *GE LOGIQ E10 Commercial Ultrasound Machine (https://www.logiqclub.net/emea/logiq-e10) and* ***B)*** *the L2-9VN-D Linear Array Ultrasound Probe (https://theultrasoundsource.com/ge-l2-9vn-d-linear-probe/)*

(https://www.civco.com/catalog/accessories/aquaflex-standoff-pads/)

***Figure 9**: AquaFlex Gel Stand-off Pads*

A force transducer (HG Schaevitz: model FTA-IT-500, Pickering, Ontario, Canada) with a rated force capacity of 500 lbs and a LVDT amplifier (Daytronic: model 3230, Miamisburg, Ohio, United States) were also utilized during the muscle contracted trials to collect the functional output of the muscle during its contracted state. It was also used to provide visual biofeedback to participants ensuring that they met the force exertion criteria of this thesis. One side of the force transducer was connected to a customized metal mount that was hooked onto the ultrasound table, while the other side was attached to the participant's left thigh (Figure 10). The participants were asked to externally rotate and extend their left hip to activate their gluteus maximus muscle, which was the muscle located within the region of interest (Figure 11). Their force output was displayed on custom software (NIAD 3.0, University of Waterloo, Waterloo, Ontario, Canada) using a laptop that was placed in front of them.

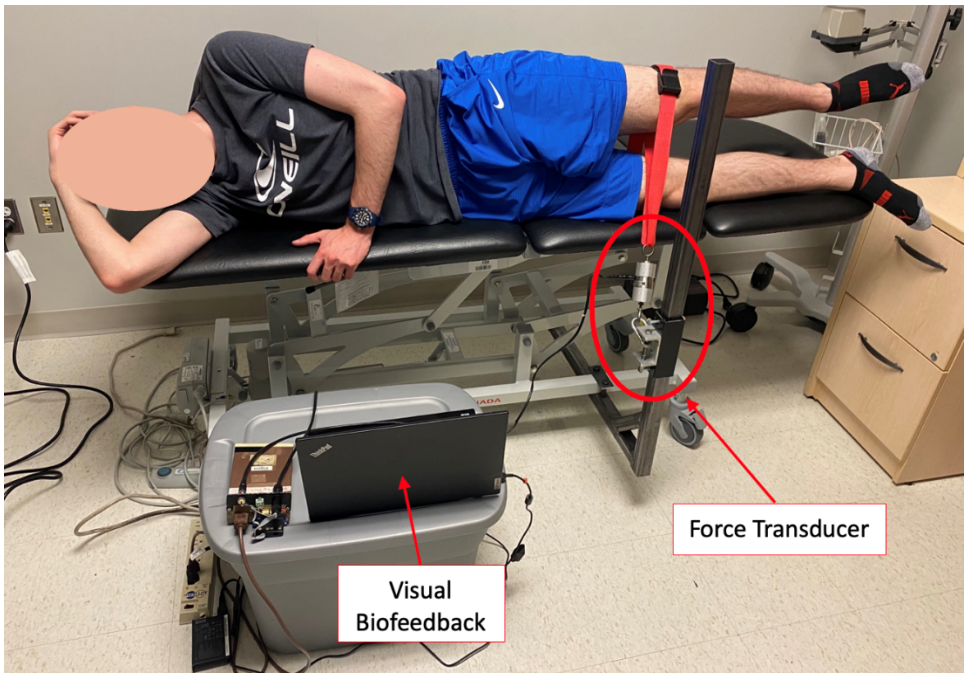

Figure 10: *Force Transducer Visual Biofeedback Set Up – Live biofeedback from the force transducer was set up in front of the participants on a laptop. This updated the participant on the amount of force they exerted during the muscle contracted state trials.*

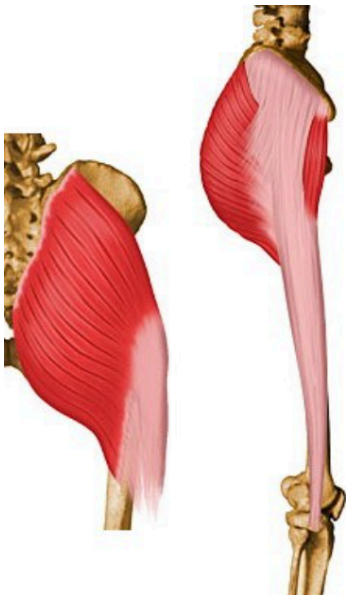

Figure 11: *Gluteus Maximus (University of Washington, 2023) – This was the muscle located in the region of interest which was 6 cm distal and 3 cm posterior to the greater trochanter.*

Electromyography (EMG) (Bortec Biomedical, Calgary, Alberta, Canada) was used to confirm that this force transducer set-up was activating the gluteus maximus. This EMG collection was conducted on one participant prior to the actual data collection of this protocol. Two electrodes were placed between their sacral vertebrae and the greater trochanter, which corresponded to the center of the muscle's belly

based on the Seniam (2023) recommendations, and a reference electrode was placed on the participant's wrist. Custom software (NIAD 3.0) was used to collect data from both the force transducer and the EMG system. The participant was first asked to perform 3 maximum voluntary contractions (MVC) and the average of the maximum forces exerted during these trials was used to calculate the 10%, 20%, 30%, 40%, 50%, 60%, 70%, 80%, and 90% of their MVC. These acted as targets for the participant to hold for 10 seconds during the next 9 trials. The visual biofeedback system set-up (Figure 10) was used to display the participant's force exertion targets on a laptop in front of them. They were instructed to maintain these targets by externally rotating and extending their hip. Upon completion of the trials, the EMG data was full wave rectified, linear enveloped, and normalized to the participant's MVC trial's EMG data in MATLAB (R2022b). The force transducer data was also normalized to the MVC trial's force transducer output. Figure 12 presents both the normalized EMG and force transducer data, where it was evident that as the participant exerted a greater percentage of force, their muscle activation also increased proportionally. This supported using the force transducer and visual biofeedback set-up as an accurate method for controlling muscle activation during the muscle contracted trials.

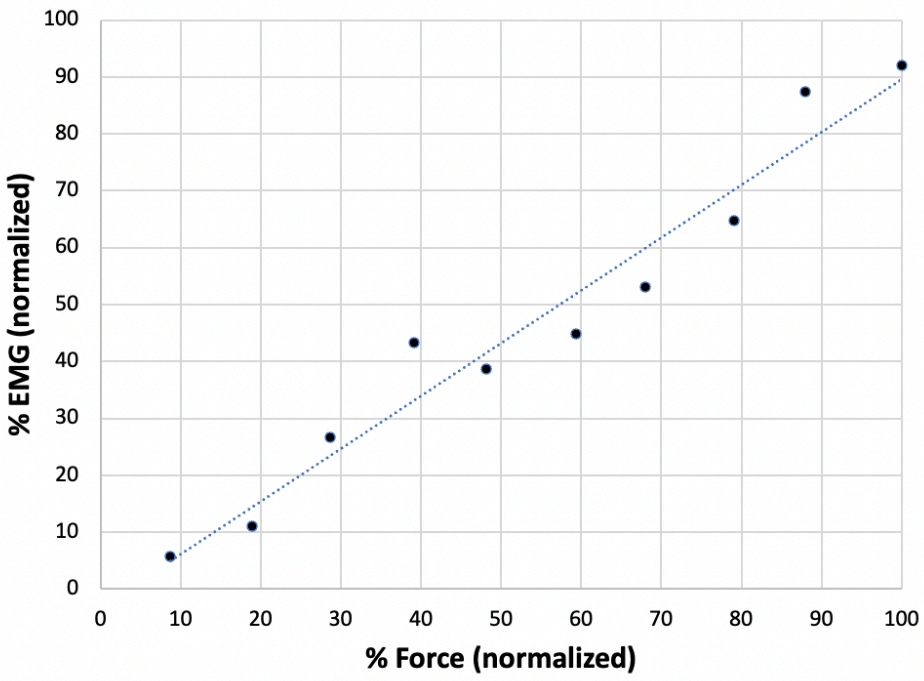

Figure 12: *Normalized EMG and Force Transducer Data during Different Force Exertion Percentages of an MVC – As the participant exerted a greater percentage of force, their muscle activation also proportionally increased. This supported using the force transducer to control muscle activation during the muscle contracted trials.*

3.2.3 Experimental Protocol

The data collection was broken down into the set-up, introductory, resting trials, muscle contracted trials, and clean-up stages which are broken down in Table 7. Two researchers were required for this data collection: the primary and secondary researchers. The primary researcher was responsible for landmarking and controlling the ultrasound probe. They were also responsible for instructing the secondary researcher to position the ROI, initiate the force collections during the muscle contracted trials, and save the SWE images. The secondary researcher was mainly responsible for controlling the US based on the primary researcher's instructions.

After the collection set-up was completed and the participant arrived, they were asked to provide verbal and written informed consent. They were then instructed to change into a loose comfortable t-shirt and loose-fitting shorts before their height and weight were measured to confirm that their BMI was within the inclusion criteria.

Participants were then instructed to lie on their right side with their knees and hips straight (no flexion) during the landmarking and imaging procedures, to simulate a lateral fall configuration. Visual cues were used to correct the participants' posture and ensure that this posture was maintained throughout the collection. This position was standardized for all participants to prevent the effects of postural changes from influencing the SWE measurements.

The location of interest (P1) was marked on the participants using a grid centered over the greater trochanter (Figure 13). This grid had a total of 3 locations with two over the lateral aspect of the femur (L1-L2) and one over the posterolateral aspect of the femur (P1). Point L1 was centered over the greater trochanter, while L2 aligned with the diaphysis of the femur to ensure that the grid was placed consistently across all subjects. The main P1 location was chosen in accordance with the peak center of pressure during a lateral impact, which is posterior and distal to the GT (Pretty et al., 2021a; Pretty et al., 2021b). The distance between L1 and L2 was 6 cm and P1 was 3 cm posterior to L2 (Figure 13). A permanent marker was used to mark these locations on the participants' left side through the holes in the grid.

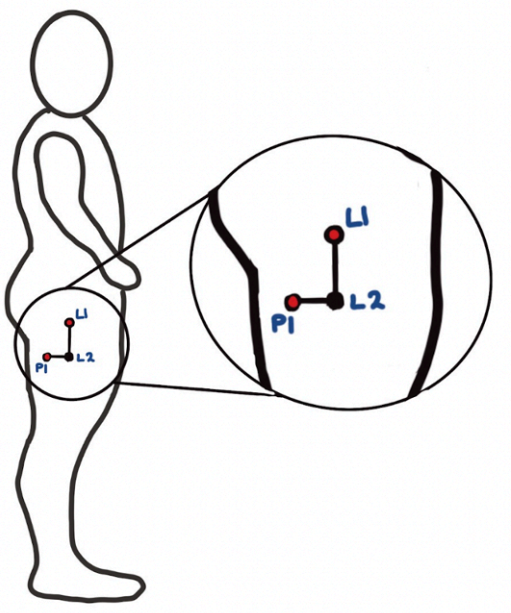

Figure 13: *Landmarking the Measurement Location – Black circles indicate the 3 locations that were marked on the participant, while the red circles indicate the 2 locations (L1 and P1) from which the SWE modulus measurements were taken. Point L2 is the point over the GT, while L2 is aligned with the femur's diaphysis. The distance from L1 to L2 was 6 cm, while P1 was positioned 3 cm posterior to L2.*

Once the measurement location was landmarked, the data collection process began. The data collection was divided into the resting and muscle contracted states. During the resting state, participants were asked to keep their entire body relaxed with their knees and hips straight (no flexion) and stacked on top of one another (Figure 14). The primary researcher controlled the probe placement, applying minimal to no compression, and instructed the secondary researcher to collect and save the SWE images. Visual cues from the ultrasound images were used to ensure that the tissues at the P1 location were not being compressed. Figure 15-A represents an US image of the tissues when compression is applied, while Figure 15-B represents an image where no compression is applied. The tissues and gel standoff compress together when compression is applied which becomes very evident on the US screen, and this was avoided during the collection. Additionally, the gel standoff is very soft and dents when compression is applied, which is another cue that was used to ensure that tissues were not being compressed throughout the collection. A total of 6 SWE measurements were collected, resulting in 3 SWE images for the subcutaneous adipose and 3 for muscle. The tissue order (muscle versus adipose) was randomized for each of the 3 trials, however, both subcutaneous and muscle measurements for a specific trial were completed before initiating the next trial.

Figure 14: *Participant Positioning during the Landmarking and Resting State Trials – Participants laid on their right side with their bodies relaxed and their hips and knees straight (no flexion). SWV measurements were taken from the left side.*

A) 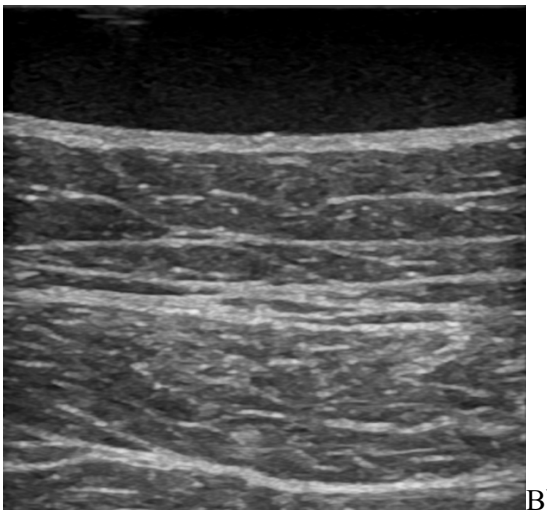 B) 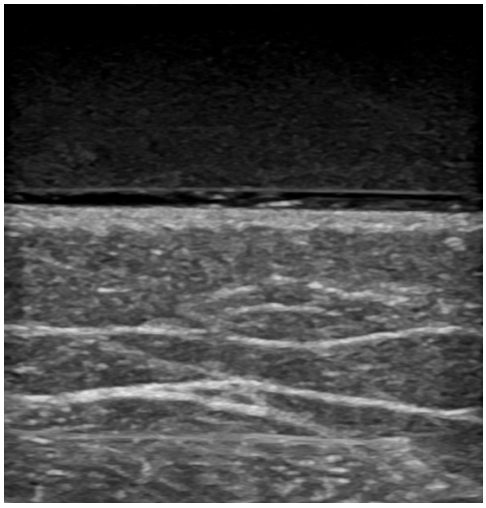

Figure 15: *Visual Cues Used to Ensure Minimal to No Compression was Applied from the Probe onto the Tissue – A) When compression is applied, the tissues and standoff compress together which is visually evident on the US screen, whereas B) when no compression is applied, there is no compression of the tissues and standoff.*

Prior to collecting the muscle contraction trials, the participant performed 3 MVC trials that targeted the gluteus maximus, which was the muscle underlying P1. This was accomplished by having them externally rotate and extend their hip and the force transducer was used to collect their maximum exerted force during these MVCs (Figure 16). The MVCs were averaged and for the muscle contracted trials, participants were asked to maintain 40-60% of the force exerted during their MVC for approximately 10-20 seconds, with a two-to-four-minute break between each of the trials. They performed contractions using the force transducer and visual biofeedback system mentioned in section 3.2.3. Forty to sixty percent of their maximum exertion was chosen as a desired exertion level because Martel and colleagues (2018) found that muscle activation of 20-30% MVC led to increased pelvic

stiffness in females. However, their muscle activation target was based on upper limb impact data and this thesis's protocol aimed to capture the SWV of tissues during increased muscle contraction levels. This is because there is currently a gap in the literature regarding the level of muscle contraction maintained during a lateral fall. Thus, the highest-level possible force exertion (60% MVC) was used to explore the influence of muscle contraction on the soft tissues' SWV. Initially, the aim of this thesis was to obtain the SWV of the tissues during a 100% MVC contraction, however, the SWE system slows down when obtaining images of contracted and deeper tissues, like the muscle. Thus, participants would be expected to maintain their MVC from 40-50 seconds, which would not be realistic for them to maintain for multiple trials without the onset of fatigue. During the piloting trials for this protocol, 60% MVC was the highest force exertion output that most of the participants could maintain for the entire trial. Some participants struggled to maintain this force exertion target; therefore, a minimum target of 40% MVC was implemented to provide them with a force exertion range. Similar to the resting state, a total of 6 SWE measurements were collected, resulting in 3 SWE images for the subcutaneous adipose and 3 for muscle, with the tissue order being randomized during each trial.

Figure 16: *Participant Positioning during the Contracted State Trials – Participants laid on their right side. During the SWE measurements, they performed an external rotation and extension of their left hip, while keeping their leg straight to activate the gluteus maximus. This pulled on the force transducer and updated the force that the participant was exerting on the biofeedback system set-up in front of them.*

During both stages, the AquaFlex gel stand-off (Figure 9) was placed over the measurement location while the L2-9VN-D linear probe was positioned above it longitudinally to obtain the SWE images. The center of the probe was positioned directly above the marked location and compression to the probe was not applied since SWE does not require manual compression as it influences the SWV values (Taljanovic et al., 2017). Before taking the images, clear visualization of the standoff, skin, adipose, muscle and femur was ensured by using a water-soluble ultrasound gel, adjusting the gain setting of the ultrasound, and the penetration depth of the probe. The maximum size of the ROI (2 cm by 4 cm) was

used and positioned over the tissue of interest when capturing the SWE images. To obtain the SWV for the muscle, the ROI was positioned between the outer edge of the femur to the inner edge of the muscle fascia (Figure 17-C). Whereas it was positioned between the outer edge of the muscle fascia to the inner edge of the skin to obtain the SWV for the subcutaneous adipose (Figure 17-B). If the ROI overlapped between both tissues, the ultrasound's lasso tool was used to extract the SWV of the tissue of interest during the data analysis stage (Figure 18). Until then, the SWE images containing the elastogram within the ROI were saved on the ultrasound system.

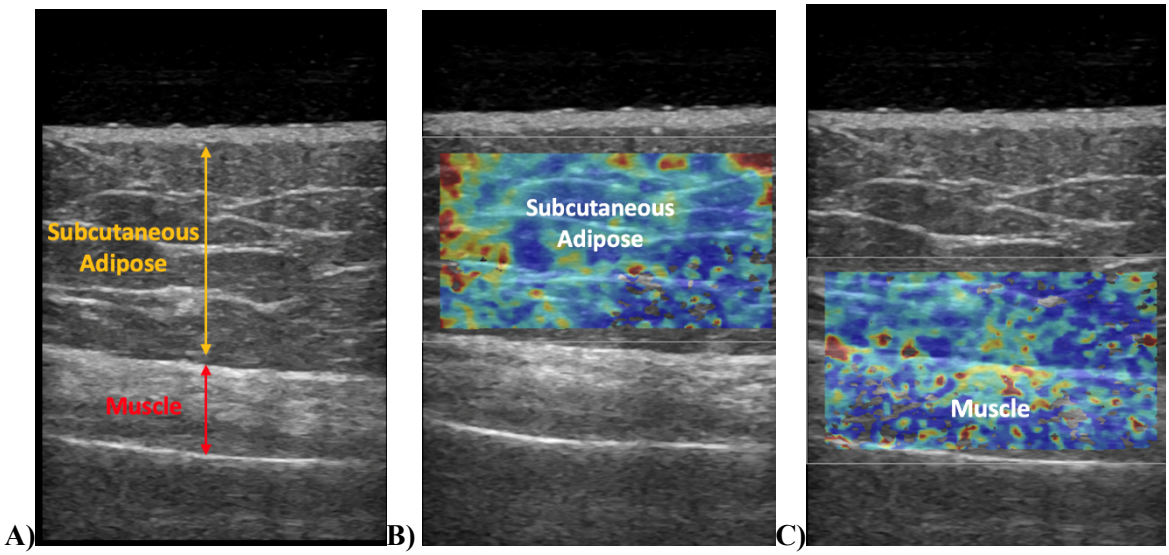

Figure 17: *ROI for Subcutaneous Adipose and Muscle Tissues – B)* ***Subcutaneous adipose –*** *ROI was positioned between the inner edge of the skin to the outer edge of the muscle fascia. C)* ***Muscle –*** *ROI was positioned between the inner edge of the muscle fascia to the outer edge of the bone. However, the elastogram often included the adipose tissue above the muscle because the maximum ROI (2 cm by 4 cm) was used for all measurements. The SWV of the muscle was extracted using the lasso tool to ensure that the adipose did not influence this measurement.*

A total of 12 SWE images were taken during the collection, 3 for the subcutaneous adipose and 3 for muscle during the resting and muscle contracted states. The resting state was completed first with the tissue order being randomized using a random number generator, which prevented the imaging order from influencing the results. Subsequently, the muscle contracted state was collected using the random number generator as well. Once all the muscle contracted trial SWE images were saved, the collection was terminated, and the researchers cleaned up.

Table 7: Data Collection Breakdown

Stage	Description	Time

Set-up	• Set-up the participants' file on the US
	• Gathered materials for collection:
	  o Consent forms
	  o Laptop
	  o Permanent marker
	  o Landmarking grid
	  o Force transducer, amplifier, and breakout box
	• Set-up the force transducer set up and connected it to the mount
		30 minutes

Introduction	• Provided a breakdown of the collection • Consent forms • Asked participant to change into loose-fitting shorts • Obtained the height and weight measurements • Calculated BMI	10 – 15 minutes
Landmarking	• Landmarked the greater trochanter while the participant was standing • Asked participant to lie on their right hip with their knees and hips straight • Used visual cues to correct their posture • As a practice for the muscle contracted trials, asked participants to externally rotate and extend their left leg to activate their gluteus maximus o Pointed out the differences they should feel during a resting versus muscle contracted state • Used the ultrasound to confirm the greater trochanter location and the femoral shaft • Used the grid to mark the L1 (GT), L2 (femoral shaft) locations, and P1 locations (Figure 13)	10 minutes

Resting State	• Instructed participant to remain relaxed throughout the collection (Figure 14)
	• Used visual cues to ensure they maintained the correct posture
	• Collected 3 subcutaneous adipose and 3 muscle images at the P1 location using the following steps:
	  o Primary researcher positioned the probe over the P1 location and asked the secondary researcher (responsible for controlling the US) to move the ROI over the tissue of interest
	  o Collected 3 images for each trial
	  o Primary researcher went through the images and saved the best one
		20 – 25 minutes

Muscle Contracted State	• Connected the force transducer to the participants' left thigh and instructed them to activate their gluteus maximus (Figure 16)
	  o Used visual cues to correct their posture to ensure that their knees and hips remained straight to prevent them from using other muscle groups to compensate during the muscle contraction
	• After they performed some practice trials, 3 MVC trials were collected with 2 – 4 minutes of rest in-between
	• Calculated their 40-60% MVC force exertions and marked them on the laptop screen
	• Instructed the participant to maintain this force exertion during the muscle contracted trials
	• Once the participant was in this contraction range, their force output was collected along with the 6 SWE images. The specific breakdown of these steps is:
	  o Participant began contraction and met their 40-60% MVC force exertion
	  o Probe was positioned at the P1 location and the ROI was focused on the tissue of interest
	  o Secondary research began the force collection on the laptop
	  o Primary researcher the secondary researcher to begin collecting the SWE images when they were ready
	  o Once three images were collection (for one trial), the trial was terminated
	  o Participant rested for 2-4 minutes
	  o Primary researcher selected the best image from the trial to save
		30 – 45 minutes

Clean-up	• Saved all the images on the US and shut down the system • Cleaned all the equipment and stored it away	10 – 20 minutes

3.3 Data Analysis

During the data analysis process, the ultrasound's built-in software (General Electric Company, version R1, revision 5.2, software part number 5821700-8) was used to obtain the SWV of the subcutaneous adipose and muscle tissues from the saved SWE images. The lasso and circle cut-out tools (Figure 18) were used to outline the tissue of interest within the ROI that contained the elastogram to extract the SWV in meters per second (m/s). The red in the elastogram represented stiffer tissue with a harder consistency, while the blue represented softer, less stiff tissue. This SWV can be used to compute the Young's moduli of the tissues using Equation 2. Once the SWV values were extracted from each of the trials, they were saved for the statistical analysis process.

$$\textbf{\textit{Equation 2}}: E = 3G = 3 * \rho * SWE^2$$

Where G = shear modulus, SWV = shear wave velocity, and ρ = density of the tissue (assumed to be 1 g/cm^3). The tissue's underlying properties are assumed to be linear, isotropic, incompressible, and homogenous).

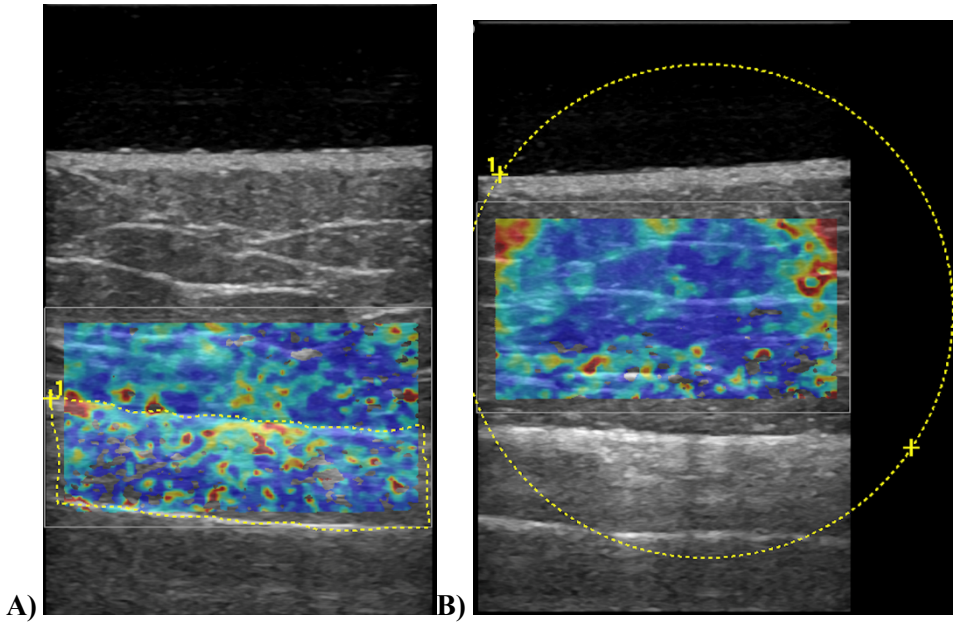

Figure 18: *Tools Used to Extract SWV Measurements from the Elastograms –* ***A) Lasso tool*** *was used to outline around the tissue of interest to extract its SWV measurements, while the* ***B) Circle cut-out tool*** *was used to extract the SWV of tissues where the elastogram fell within the tissue's boundaries.*

3.4 Statistical Analysis

3.4.1 Primary Statistical Analysis

A summary of the statistical analysis for hypotheses 1 and 2 is provided in Table 8 and it was conducted in RStudio (2022.07.2+576).

For hypothesis 1, a two-way mixed effects absolute agreement intraclass correlation (ICC) model was used to assess the intra-rater reliability of this protocol. Specifically, the intra-rater reliability of multiple factors of this collection's protocol and data analysis processes were assessed. During the data collection process positioning and orienting the probe above the landmarked location, along with the participants' positioning, postural changes, movement of the underlying tissues, changes in muscle activation, fatigue, and selecting the best image from each trial could influence the intra-rater reliability. Additionally, potential changes in the contact pressure applied to the standoff while taking measurements

throughout the data collection could have also affected the intra-rater reliability. During the image analysis process, identifying and selecting the tissue of interest with the lasso tool could influence the intra-rater reliability. A total of 2 ICC values were calculated for each tissue during the resting and contracted states (Figure 19). These ICC values were compared to Koo and Li's (2016) ICC classifications where an ICC < 0.5, between 0.5 – 0.75, 0.75 – 0.9, or ICC > 0.9 are classified as poor, moderate, good, or excellent, respectively. The 95th percentile confidence interval was also computed and compared across the different trial conditions to identify whether the intra-rater reliability between the conditions was significantly different (significant differences being signified if the confidence intervals did not overlap).

For hypothesis 2, a two-way repeated measures analysis of variation (ANOVA) statistical model was used to assess the effects of tissue type (adipose and muscle) and tissue state (resting and contracted) on SWV values. For each participant, the SWV measurements from the three repeated trials for each condition were averaged prior to performing this analysis. The two repeated measures factors were tissue type and contraction state. The main effects of tissue type and contraction state were examined, along with the two-way interaction between these two factors. If a significant two-way interaction was observed, it was decomposed using paired samples t-tests to test the effect of contraction state within each tissue type.

Table 8: Summary of the Statistical Tests for the Primary Analysis

Hypothesis	**Statistical Test**
Hypothesis 1: The intra-rater reliability of the subcutaneous adipose and muscle SWV measurements will be good to excellent (ICC > 0.75) and will not be influenced by muscle contraction.	Two-way mixed effects absolute agreement intraclass correlation (ICC) model The lower and upper bounds of the 95th percent confidence intervals were compared to identify whether the ICCs for each condition are significantly different.
Hypothesis 2: There will be an interaction effect of muscle contraction on the SWV magnitudes of the soft tissues. It is expected that: 1. The muscle SWV magnitude will be greater during the muscle contracted trials compared to the resting trials. 2. The subcutaneous adipose SWV magnitude will not change between the resting and muscle contracted trials.	Two-way repeated measures ANOVA • Factors: Contraction state and Tissue type • Dependent Variable: SWV • Interaction effect of contraction state was examined for the muscle and subcutaneous adipose tissues • If interaction was present, paired samples t-tests were used to test the effect of contraction state within each tissue type

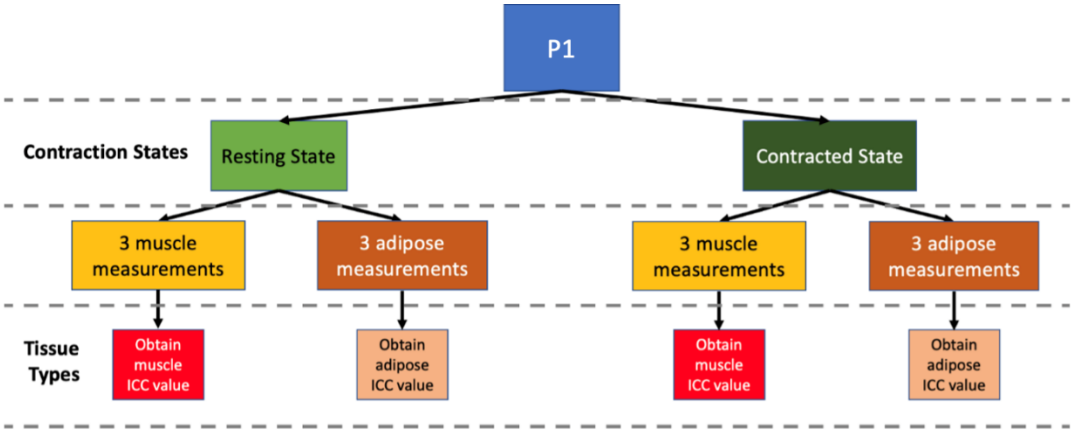

Figure 19: *Breakdown of the Collection Protocol Demonstrating the Four Different Conditions that the Intraclass Correlation (ICC) Model was Conducted For – The ICC values were calculated individually for each condition resulting in two ICC values being collected for both tissues during the resting and muscle contracted states.*

3.4.2 Secondary Statistical Analysis

Although exploring sex and BMI-related differences was not the primary goal of this thesis, a secondary analysis was performed to explore whether these differences existed across the SWV values of the soft tissues. The influence of muscle contraction on the subcutaneous adipose, muscle, and total soft tissue thicknesses was also explored during the secondary analysis. Table 9 summarizes the statistical tests that were conducted for each of these additional analyses.

The dataset was divided among males and females prior to conducting the statistical analysis to explore the influence of sex on the SWV of the tissues during the resting and muscle contracted states. A three-way mixed effects ANOVA was conducted where the main factors were sex (between-subjects), tissue type (repeated measures), and contraction state (repeated measures). The main effect of sex was examined, along with the three-way interaction between sex, tissue type, and contraction state. Pairwise comparisons and post-hoc tests were performed when significant main effects and interactions were found.

Similarly, when investigating the influence of BMI on the SWV of the soft tissues during resting and muscle contracted states, the data set was divided based on the median BMI. This divided the participants into low BMI and high BMI groups. A three-way mixed effects ANOVA was conducted using BMI (between-subjects), tissue type (repeated measure), and contraction state (repeated measure) as its three factors. The main effect of BMI was examined, along with the three-way interaction between

BMI, tissue type, and contraction state. Pairwise comparisons and post-hoc tests were performed when significant main effects and interactions were observed.

A two-way repeated measures ANOVA was conducted to investigate the influence of muscle contraction on the thicknesses of the subcutaneous adipose, muscle, and total soft tissues. The two repeated measures factors were the type of soft tissue thickness and contraction state. Pairwise comparisons and post-hoc tests were performed when significant main effects and interactions were found.

Table 9: Summary of the Statistical Tests for the Secondary Analysis

Purpose	**Statistical Test**
Investigate the influence of sex on the SWV of the tissues during resting and muscle contracted states	Three-way mixed measures ANOVA • Between-subjects factor: sex • Repeated measures factors: tissue type and contraction state • Dependent variable: SWV
Investigate the influence of BMI on the SWV of the tissues during resting and muscle contracted states	Three-way mixed measures ANOVA • Between-subjects factor: BMI • Repeated measures factors: tissue type and contraction state • Dependent variable: SWV
Investigate the influence of muscle contraction on the adipose, muscle and total soft tissues' thicknesses	Two-way repeated measures ANOVA • Repeated measures factors: type of soft tissue thickness and contraction state • Dependent Variable: soft tissue thickness

Chapter 4
Results

4.1 Results for the Primary Analysis

A two-way mixed effects absolute agreement intraclass correlation (ICC) model was conducted to assess the intra-rater reliability of the adipose and muscle SWV measurements during the resting and contracted states (Table 10). The intra-rater reliability for the adipose SWV measurements during the resting state was 0.93, with a 95% confidence interval of 0.86-0.97, and it increased to 0.95, with a 95% confidence interval of 0.90-0.96, during the contracted state. Based on Koo and Li's (2016) ICC classifications, the intra-rater reliability was classified as excellent during both these conditions. The intra-rater reliability for the muscle SWV measurements during the resting state was 0.91, with a confidence interval of 0.81-0.96, and it decreased to 0.81, with a confidence interval of 0.60-0.92, during the contracted state (Table 10). The resting muscle intra-rater reliability was classified as excellent and dropped to good during the muscle contracted trials (Koo & Li, 2016). Since all the confidence intervals overlapped, there was no significant difference between the intra-rater reliability of the different trial conditions (Figure 20).

Table 10: Intra-rater reliability ICC classification and the lower & upper bounds of the 95% CI for the SWV trial conditions using Koo & Li's Classifications (2016)

Condition	ICC Value	Lower Bound of 95% CI	Upper Bound of 95% CI	Classification
Subcutaneous Adipose – Resting	0.93	0.86	0.97	Excellent
Subcutaneous Adipose – Contracted	0.95	0.90	0.98	Excellent
Muscle – Resting	0.91	0.81	0.96	Excellent
Muscle – Contracted	0.81	0.60	0.92	Good

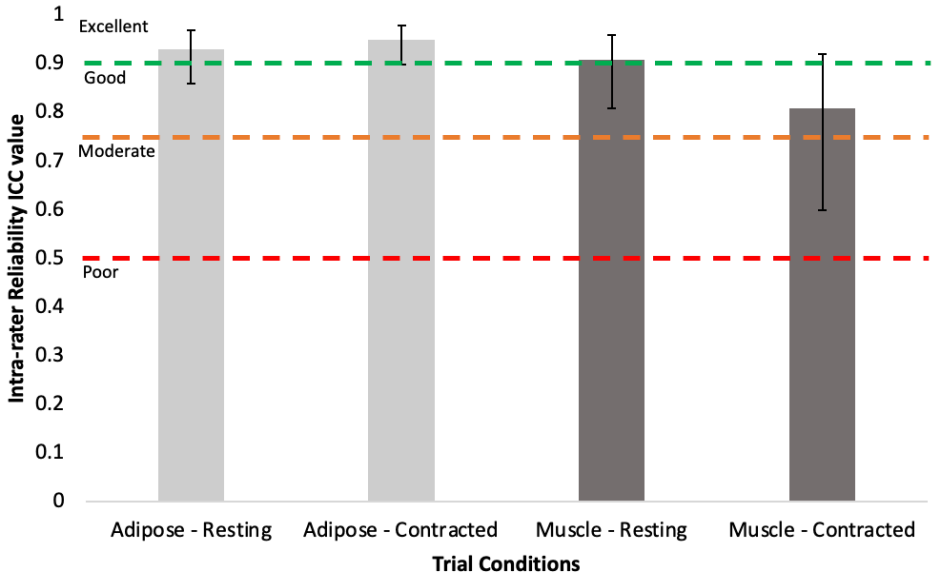

Figure 20: *Intra-Rater Reliability (ICC values and 95% CI represented by the error bars) for the SWV Trial Conditions using the Koo & Li's Classifications (2016) – The area below the red line represents poor reliability (ICC < 0.50) and the area between the orange and red lines represent moderate reliability (0.50 < ICC < 0.75). The area between the green and orange lines represents good reliability (0.75 < ICC < 0.90), while the area above the green line represents excellent reliability (ICC > 0.90).*

A two-way repeated measures ANOVA was conducted to assess the influence of tissue type (subcutaneous adipose and muscle) and contraction state (resting and muscle contracted) on SWV measurements. SWV was influenced by a significant tissue type-contraction state interaction ($F_{1,19}$ = 19.42, $p < 0.001$, $\eta^2 = 0.054$), as well as a main effect of tissue type ($F_{1,19} = 42.98$, $p < 0.001$, $\eta^2 = 0.182$) and contraction state ($F_{1,19} = 10.87$, $p < 0.05$, $\eta^2 = 0.065$) (Figure 21). Decomposition of the interaction using paired samples t-tests revealed that the SWV of muscle during its resting state was significantly lower than its SWV during its contracted state ($p < 0.001$). Whereas the SWV of the subcutaneous adipose showed no change ($p = 0.825$) during the resting (mean (SD) = 2.45 (0.16) m/s) and contracted (mean (SD) = 2.47 (0.17) m/s) states. Therefore, the interaction between tissue type and contraction state was driven by the 25% increase in the muscle tissues' SWV from resting (mean (SD) = 2.64 (0.19) m/s) to contracted (mean (SD) = 3.05 (0.27) m/s) state.

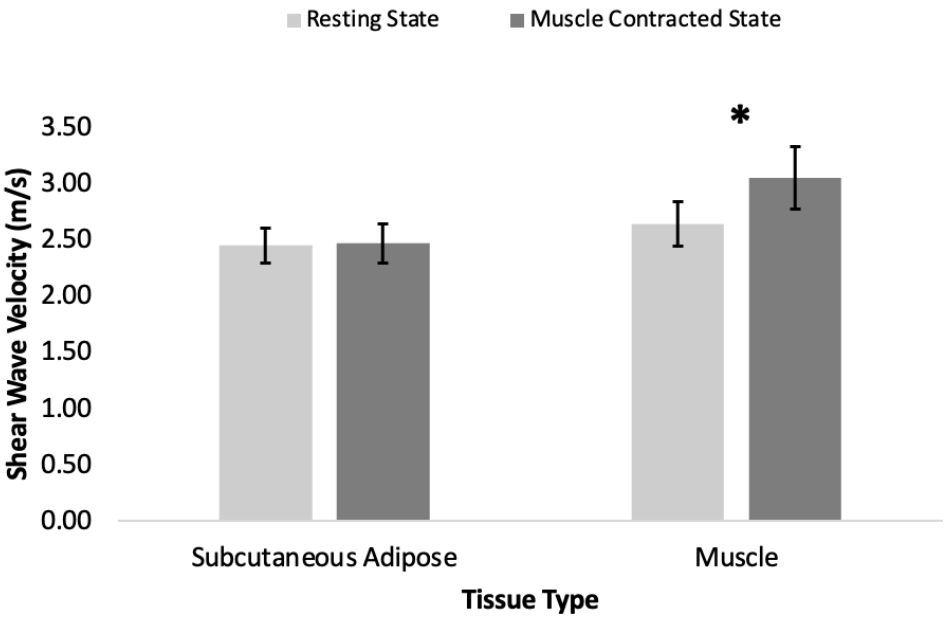

Figure 21: *Shear Wave Velocity of the Subcutaneous Adipose and Muscle Tissues during the Resting and Muscle Contracted States (SD is represented by the error bars) – A significant tissue type-contraction state interaction was observed, along with the main effects of tissue type and contraction state. (* indicated significant differences between the muscle SWV during resting and contracted states based on the post hoc paired samples t-tests α = 0.05).*

4.2 Results for the Secondary Analysis

A secondary analysis was completed to analyze the influence of sex and BMI, along with tissue type and contraction state, on SWV. Additionally, the influence of the contraction state on the subcutaneous adipose, muscle, and total soft tissue thicknesses was also investigated.

A three-way mixed measures ANOVA was conducted to assess the effects of sex (between-subjects), tissue type (repeated measures), and contraction state (repeated measures) on SWV. The ANOVA did not reveal a significant interaction between sex, tissue type, and contraction state ($F_{1,18}$ = 0.278, p = 0.604, η^2 = 0.001). However, it did reveal a significant tissue type-contraction state interaction ($F_{1,18}$ = 18.69, $p < 0.001$, η^2 = 0.086), as well as main effects of sex ($F_{1,18}$ = 19.873, $p < 0.001$, η^2 = 0.384), tissue type ($F_{1,18}$ = 41.22, $p < 0.001$, η^2 = 0.267), and contraction state ($F_{1,18}$ = 10.94, $p < 0.05$, η^2 = 0.102) (Figure 22). Decomposition of the interaction using pairwise comparisons revealed that the muscles' SWV was significantly greater during its contracted state compared to its resting state ($F_{1,19}$ = 34.70, $p <$ 0.001, η^2 = 215). Females experienced a 13% increase in the SWV of their muscle tissue from resting (mean (SD) = 2.40 (0.19) m/s) to contracted (mean (SD) = 2.76 (0.27) m/s) state, while males

experienced a 14% increase from resting (mean (SD) = 2.88 (0.43) m/s) to contracted (mean (SD) = 3.34 (0.27) m/s) state. However, there was no significant difference between the resting and muscle contracted SWV of the subcutaneous adipose tissue ($F_{1,19} = 0.05$, $p = 0.825$, $\eta^2 = 0.0005$). The resting state mean SWV of the subcutaneous adipose in females was 2.26 (SD = 0.17) m/s, while the contracted state mean SWV was 2.19 (SD = 0.32) m/s. The resting and contracted state means for the males' subcutaneous adipose were 2.64 (SD = 0.43) m/s and 2.75 (SD = 0.46) m/s, respectively. Additionally, the main effect of sex indicated that males have significantly greater SWV measures than females.

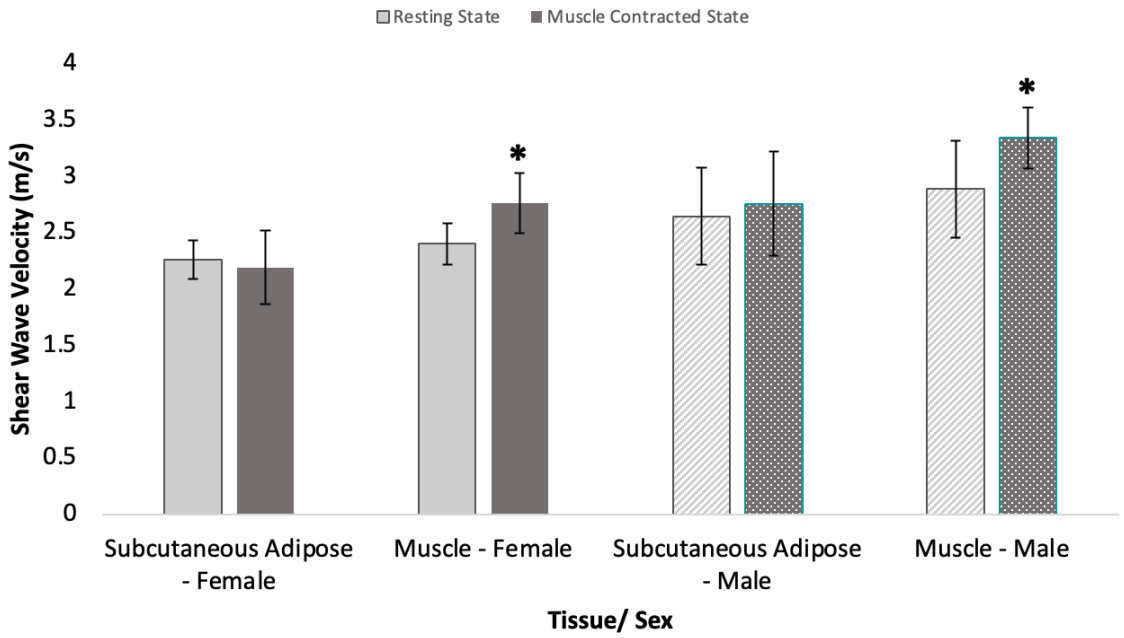

Figure 22: *Shear Wave Velocity of the Subcutaneous Adipose and Muscle Tissues during Resting and Contracted States Divided by Sex (SD is represented by the error bars) – A significant tissue type-contraction state interaction was observed, along with main effects of sex, tissue type, and contraction state. (* indicated significant differences between the muscle SWV during resting and contracted states, in both sexes, based on the post hoc pairwise comparison tests α = 0.05).*

A three-way mixed measures ANOVA was conducted to assess the effect of BMI, tissue type, and contraction state on SWV. BMI was treated as a between-subjects factor, while tissue type and contraction state were repeated measures factors. The ANOVA did not reveal a significant interaction between BMI, tissue type, and contraction state ($F_{1,18} = 0.185$, $p = 0.672$, $\eta^2 = 0.0006$). However, the ANOVA did reveal a significant tissue type-contraction state interaction ($F_{1,18} = 18.59$, $p < 0.001$, $\eta^2 = 0.057$), as well as a main effect of tissue type ($F_{1,18} = 41.66$, $p < 0.001$, $\eta^2 = 0.190$) and contraction state ($F_{1,18} = 10.43$, $p = 0.005$, $\eta^2 = 0.068$) (Figure 23). Decomposition of the interaction using pairwise

comparisons revealed that the muscle SWV was significantly greater during its contracted state compared to its resting state ($F_{1,19} = 34.70$, $p < 0.001$, $\eta^2 = 215$). Low BMI individuals experienced a 14% increase in the SWV of their muscle tissue from resting (mean (SD) = 2.70 (0.40) m/s) to contracted (mean (SD) = 3.13 (0.33) m/s) state, while high BMI individuals experienced a 13% increase from resting (mean (SD) = 2.58 (0.43) m/s) to contracted (mean (SD) = 2.97 (0.46) m/s) state. However, there was no significant difference between the resting and muscle contracted SWV of the subcutaneous adipose tissue ($F_{1,19} = 0.05$, $p = 0.825$, $\eta^2 = 0.0005$). The resting state mean SWV of the subcutaneous adipose in low BMI individuals was 2.53 (SD = 0.43) m/s, while the contracted state mean SWV was 2.60 (SD = 0.54) m/s. The resting and contracted state means for high BMI individuals' subcutaneous adipose were 2.37 (SD = 0.31) m/s and 2.34 (SD = 0.41) m/s, respectively. Therefore, although BMI does not influence SWV, tissue type and contraction state do have an influence on SWV.

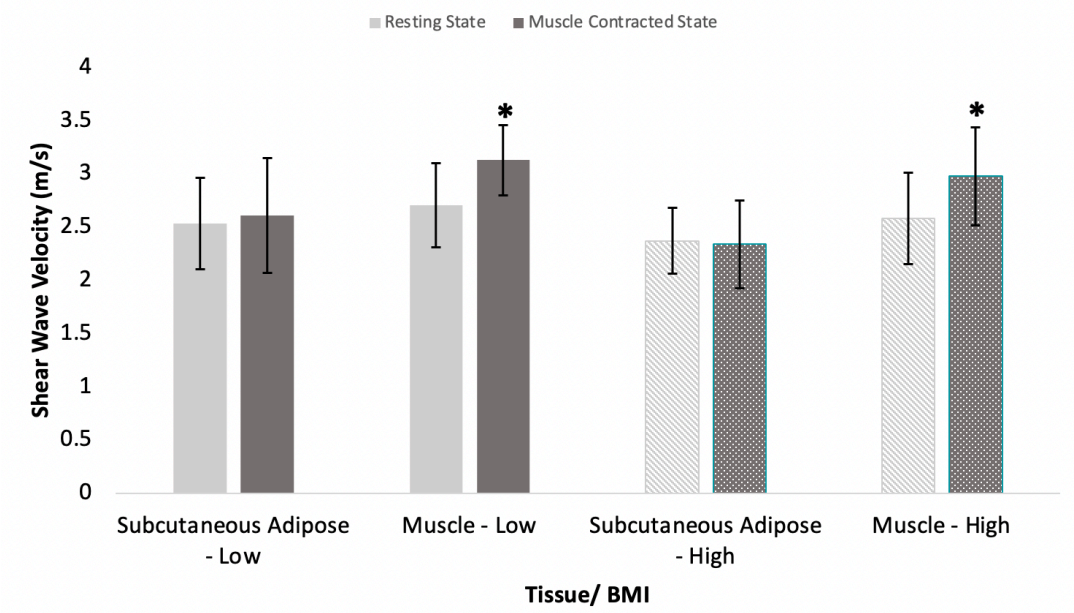

Figure 23: *Shear Wave Velocity of the Subcutaneous Adipose and Muscle Tissues during the Resting and Contracted States divided by BMI (SD is represented by the error bars) – A significant tissue type-contraction state interaction was observed, along with main effects of tissue type and contraction state. (* indicated significant differences between the muscle SWV during resting and contracted states, in both BMI groups, based on the post hoc pairwise comparison tests α = 0.05).*

A two-way repeated measures ANOVA was conducted to assess the influence of soft tissue thickness type (subcutaneous adipose, muscle, and total thicknesses) and contraction state (resting and muscle contracted) on thickness measurements. The ANOVA revealed a significant interaction between soft tissue thicknesses and contraction state ($F_{2,28} = 4.62$, $p = 0.01$, $\eta^2 = 0.006$), as well as a main effect of

tissue type thicknesses ($F_{2,38} = 85.76$, $p < 0.001$, $\eta^2 = 0.629$) (Figure 24). Decomposition of the interaction using pairwise comparisons revealed that the interaction was being driven by a significant increase in the muscle's thickness from resting to contracted state ($p = 0.039$), while adipose ($p = 0.110$) and total tissue ($p = 0.424$) thicknesses were not significantly different during these states. The muscle thickness increased by 12% from resting (mean (SD) = 14.54 (1.24) mm) to contracted (mean (SD) = 16.44 (0.87) mm) state. While the adipose thickness did not change during resting (mean (SD) = 25.32 (0.95) mm) and contracted states (mean (SD) = 24.09 (0.97) mm). Similarly, the total tissue thickness also did not change during resting (mean (SD) = 41.99 (0.88) mm) and contracted states (mean (SD) = 42.67 (1.47) mm).

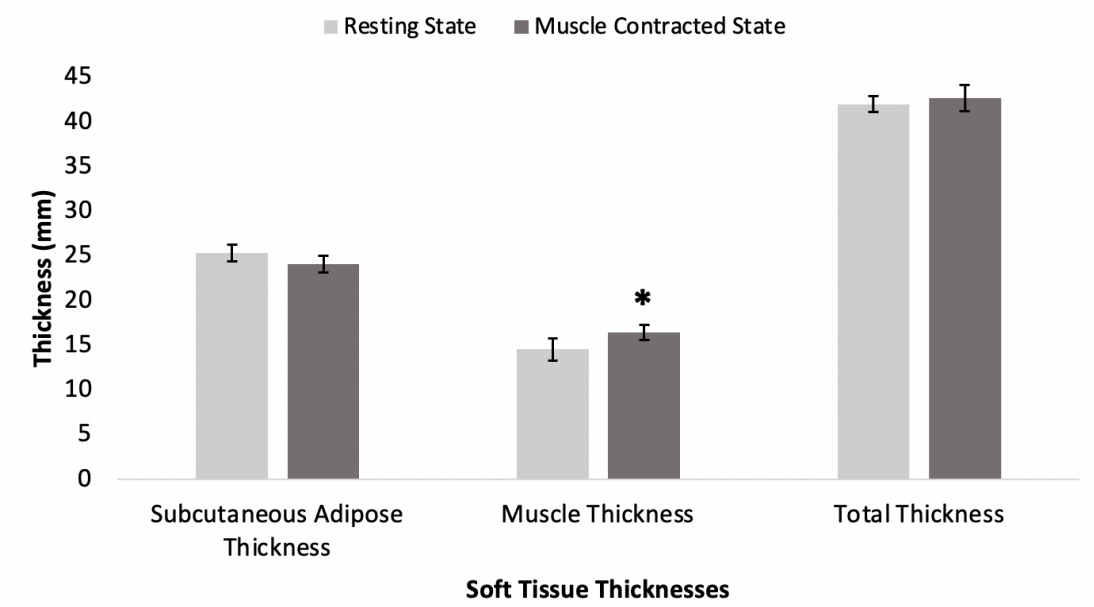

Figure 24: *Subcutaneous Adipose, Muscle & Total Soft Tissue Thickness during the Resting and Muscle Contracted States (SD is represented by the error bars) – A significant soft tissue thicknesses-contraction state interaction was observed, along with main effect of soft tissue thicknesses. (* indicated significant differences between the muscle's thickness during resting and contracted states, based on the post hoc pairwise comparison tests α = 0.05)*

Chapter 5
Discussion & Conclusion

The primary objectives of this thesis were to evaluate the intra-rater reliability of the SWE protocol used to characterize the SWV of the soft tissues in the lateral-hip region, determine whether contracted state influenced the intra-rater reliability, and assess the influence of muscle contraction on the SWV of the soft tissues. In support of the first hypothesis, the intra-rater reliability of the subcutaneous adipose and muscle SWV measurements obtained from this protocol ranged from good to excellent (ICC > 0.75) during the resting and muscle contracted trials. Intra-rater reliability also was not influenced by the contraction state. Similarly, in support of the second hypothesis, a tissue type-contraction state interaction existed. The muscle SWV was significantly greater during the muscle contracted state compared to the resting state, while the SWV of the subcutaneous adipose did not change.

5.1 Intra-Rater Reliability

The intra-rater reliability of the subcutaneous adipose and muscle SWV measurements obtained using this protocol ranged from good to excellent (ICC > 0.75) during both the resting and muscle contracted trials. This aligns with the results of previous studies that used SWE to quantify the SWV or Young's moduli of different tissues across the body. Wu et al. (2018) and Lin et al. (2015) quantified the shear moduli and Young's moduli, respectively, and reported good (0.75 < ICC < 0.90) to excellent (ICC > 0.90) intra-rater reliability of the entire heel pad and it's microchamber and microchambers. Baumer et al. (2017) reported good intra-rater reliability of the SWE measurements taken of the supraspinatus muscle and tendon, while Matsuda et al. (2019) found the SWE measurements of the superficial and deep layers of the multifidus to range from good to excellent. The SWE measurements of the iliacus, a muscle within the pelvic region, were found to have good intra-rater reliability (Nojiri et al., 2021). Lin and colleagues (2015) also mentioned a few conditions that must be met to ensure good repeatability that were considered during our collections. These included controlling the tilt/orientation of the transducer, the amount of ultrasound gel used, and hand stability throughout the collections.

While considering the conditions mentioned by Lin and colleagues (2015), the intra-rater reliability explored in this thesis was influenced by many factors of its collection protocol and data analysis processes. During the data collection process, controlling the positioning and orientation of the probe, participants' positioning, postural changes, movement of the underlying tissues, changes in muscle activation, fatigue, and selecting the best image from each trial could have influenced the intra-rater

reliability results. Potential changes in the contact pressure applied to the standoff while taking measurements throughout the data collection could have also affected the intra-rater reliability. While, during the data analysis process, identifying and selecting the tissue of interest with the lasso tool are factors that could have also influenced this reliability. Although this thesis investigated the combined influence of multiple factors on the protocol's intra-rater reliability, it would be beneficial to break these factors apart and explore their individual influence on the intra-rater reliability in future studies.

Additionally, although the intra-rater reliability between the different conditions was not statistically different, the intra-rater reliability of the muscle's measurements decreased from excellent (ICC = 0.91) to good (ICC = 0.81) during the muscle contracted trials compared to the resting trials based on Koo & Li's ICC classification approach (2016). In addition to the factors mentioned above, there are potential explanations for this. For example, participants were asked to contract their left gluteus maximus by externally rotating and extending their left hip, which resulted in their left leg being suspended in the air during the contracted trials. In contrast, this leg rested on the right leg during the resting trials. While their leg was suspended, during the contraction, it tended to slightly move or twitch, which may have influenced the SWV measurements during these trials. In the future, it may be beneficial to add an extension to the mount or another type of touch point target for the contracted leg to help stabilize it while it contracts. This would allow the participant to maintain a similar posture to the one in this thesis while keeping their leg stabilized for the researcher to acquire the SWE images more repeatably.

The previously conducted studies that utilized SWE and investigated the intra-rater reliability of their protocol took measurements from different regions in the body, while this thesis was one of the first to focus on the lateral hip region. It is important to quantify the mechanical properties of the soft tissues within this region as it is the primary contact site during the majority of lateral falls. Currently, there is literature regarding the morphological properties of these tissues, like thickness, and their influence on fall impact dynamics (Choi et al., 2010; Pretty et al., 2017; Levine et al., 2013; Pretty et al., 2021b). However, studies have not explored the influence of their Young's moduli on fall impact dynamics. As the protocol in this thesis has been found to have good to excellent intra-rater reliability, potential next steps could involve exploring its inter-rater reliability before using it to investigate the SWV of additional locations in the hip region and the influence of sex, BMI, and age on SWV.

5.2 The Influence of Muscle Contraction on the Subcutaneous Adipose & Muscle SWVs

The SWV of the gluteus maximus increased by 25% during the muscle contracted state, while the SWV of the subcutaneous adipose did not change during both the resting and muscle contracted states. As

previously mentioned, SWV can be used to compute the Young's moduli of these soft tissues. The changes in the muscle's SWV support the findings of previously conducted studies that have reported an increase of up to 40-75% in the SWV of their muscles during muscle contracted trials. The muscles studied include the vastus lateralis, vastus medialis obliquus (Botanlioglu et al., 2012), supraspinatus (Baumer et al., 2017), neck extensor muscles (Dieterich et al., 2017), rectus femoris, tibialis anterior, biceps femoris, and medial gastrocnemius (Lee et al., 2021).

A major limitation of the previously conducted studies was that they did not quantify the functional output of the muscles' contraction nor reported the contraction level of their muscle contracted trials. Hence, their participants may have been contracting closer to 100% of their MVC, which may help to explain the larger differences between their resting and muscle contracted muscle SWV measurements, compared to those observed in this thesis. It is difficult to use electromyography (EMG) to quantify the muscles' activity during the SWV muscle contracted trials because electrodes would be located above the measurement location, making it challenging to orient the ultrasound probe to obtain the SWE images. However, in this thesis, the functional output of the gluteus maximus was quantified using a force transducer and the visual biofeedback set-up ensured that all participants were exerting 40-60% of their MVC forces. Additionally, the mechanical properties of subcutaneous adipose have not been previously investigated and this thesis is the first to quantify them. Altogether, this thesis addressed many of the key limitations of previous SWE studies and its findings have many implications.

Muscle quality refers to the force generated by each volumetric unit of muscle tissue (Chiles Shaffer et al., 2017) and is often quantified using measures of muscular strength or intramuscular fat content (Koo, 2022). In healthy muscles, stiffness increases during active muscle contraction. These increases in stiffness are influenced by the muscle's intrinsic factors, including the mechanical properties of its cycling cross-bridges that form between its myofilaments and the level of motor unit recruitment. Cross-bridges have spring-like properties that contribute to changes in the stiffness of muscle fibres. As more motor units are recruited, intrinsic muscle force and stiffness increase disproportionately, such that stiffness increases to a lesser degree than force (Nichols & Huyghues-Despointes, 2009). A decline in muscle quality, specifically in the hip region, can occur due to various muscle dysfunctions, such as myosteatosis and sarcopenia. Myosteatosis is the decline in muscle quality caused by excessive fat infiltration in a muscle (Koo, 2022) and is a characteristic of many other muscle conditions, including sarcopenia. Sarcopenia is the age-related decline in muscle mass, strength, and quality (Walston, 2012). Currently, there is no consensus in the literature on the link between age-related decline in muscle quality and changes in passive muscle stiffness or Young's modulus. Passive muscle stiffness may increase (Brandenburg et al., 2014; Eby et al., 2015) or decrease (Alfuraih et al., 2019) with an age-related decline

in muscle quality. Additionally, changes between the resting and contracted states of a muscle have not been evaluated. SWE can potentially be used to quantify the muscle's SWV and Young's modulus, allowing for the characterization of muscle quality, as mechanical properties are associated with the muscle's force production (Koo et al., 2013; Phan et al., 2019). As ultrasonography is currently an established method to assess muscle quality by quantifying muscle thickness and echo intensity (Lv et al., 2022), SWE may be another avenue to explore and assess changes in muscles in the clinical setting.

Shear wave elastography can also be used to improve the biofidelity of physical and computational FE models. There is currently a gap in the literature regarding the mechanical properties of the subcutaneous adipose and muscle in the pelvic region, preventing these characteristics from being included in hip models. Most of the FE models incorporate these soft tissues (Fleps et al., 2018; Fleps et al., 2019; Galliker et al., 2022; Majumder et al., 2007; Majumder et al., 2008) by simplifying their properties. Their morphological and mechanical properties, if considered, are bulked together, rather than the models considering their unique properties. They also fail to consider the influence of muscle activation during lateral falls, although it is known to affect total impact forces, soft tissue stiffness (Martel et al., 2018), and tissue level stresses (Choi et al., 2015). Similarly, physical models, also known as test systems, of the femur consider soft tissues in this region by bulking them together (Yahaya et al., 2020). Different types of gels and foams, such as silicone elastomer (Derler et al., 2005), poly-ethylene foam, soft flexible foam (Yahaya et al., 2020) and others, are used to represent the subcutaneous adipose and muscle around the femur. Both computational and physical models are used to understand the impact dynamics of lateral falls and improve the effectiveness of hip injury prevention technologies, including hip protectors and compliant floorings. Studies that have used these models have reported that the effectiveness of hip protectors and compliant floors is affected by the underlying soft tissue thickness (Bhan et al., 2013; Choi et al., 2010; Galliker et al., 2022; Laing et al., 2008a; van Schoor et al., 2006). However, the influence of the mechanical properties of the subcutaneous adipose and muscle on the effectiveness of these preventative technologies is currently unknown. SWE can be utilized to quantify the SWV and the Young's moduli of these tissues, which can be incorporated into both computational and physical models to improve their biofidelity and bridge this gap in the literature.

The secondary analysis conducted in this thesis revealed that the soft tissues in males have significantly greater SWV than females and this can be further supported by exploring this in future studies using a larger sample size. BMI was found to not influence the soft tissues' SWV, however, the BMI cut-off for this thesis was 24.9 kg/m^2 due to the ultrasound probe's depth perception capabilities. Thus, the sample size of this thesis fell within the underweight to normal BMI range. However, replicating this protocol using an ultrasound transducer with a greater depth perception on a sample size

with a larger BMI range will allow for further investigation of the effect of BMI on SWV. This thesis also focused on collecting from young individuals, however, collecting on different age groups will be beneficial in identifying the effects of aging on these tissues. Ideally, exploring the sex, BMI, and age-related changes will aid our understanding of the mechanical properties of the soft tissues in the hip region.

5.3 Limitations

The SWE system's capabilities did present some limitations to this protocol. Firstly, the system tends to slow down when collecting the SWV of muscle at higher percentages of the MVC contraction and this limited the muscle contracted trials' force exertion range to 40-60% MVC. There is currently a gap in the literature regarding the level and pattern of muscle activation during a lateral fall, which could be addressed in the future using computational modelling, as it is difficult to use EMG to collect this data during a falling scenario. The muscle activation data obtained should be considered in a future SWE protocol to better understand the SWV of the tissues during a lateral fall. Additionally, the linear ultrasound probe used has a depth perception of 14 cm. It was also noted that the GE LOGIQ E10 system slows down when taking measurements of contracted muscle and deeper tissues. Thus, the strict BMI criteria only allowed low to normal-BMI individuals to participate. It would be beneficial to extend this work to incorporate higher BMI individuals with varying body compositions to better understand the mechanical properties of their tissues, in contrast to the participants that were recruited for the current thesis. Thirdly, there were some postural differences associated with the resting and muscle contracted trials that may have influenced the SWV results. As the posture changed, different regions of the soft tissues may have been measured due to the tissues shifting underneath the landmarked location of interest. In future collections, it would be valuable to position a pillow between the participants' legs during the resting trials to prevent the left hip from adducting. This change would also improve the resemblance of the hip and knee's postures between the resting and muscle contracted trials.

There are also limitations associated to the study's recruitment criteria and data analysis process. Firstly, young, healthy participants were recruited to infer soft tissue characteristics of older adults who are at a greater risk for hip fractures. There are several age-related changes that influence the composition and functioning of the soft tissues, such as the loss of skeletal muscle mass and function, redistribution of adipose tissue, and physiologic changes that also occur at the cellular level (De Carvalho et al., 2019). These age-related tissue-state changes could ultimately influence the subcutaneous adipose and muscle's SWV. Thus, it would be beneficial to conduct this protocol on a wider age range in future collections. Secondly, there is some subjectivity involved when saving the best SWE image during each trial. The best

SWE image is chosen from the 3 images collected during each trial based on image clarity and the patchiness of the elastogram. Additionally, there is some subjectivity involved when differentiating the soft tissues during the data analysis process to obtain their SWV. Exploring the inter-rater reliability of this protocol in future studies would help to address these limitations. Lastly, the SWE system applies specific assumptions regarding the properties of the soft tissues when computing their SWV and converting it into their Young's moduli. These assumptions include the tissues being linear, isotropic, incompressible, and homogenous when they are non-linear, anisotropic, compressible, and heterogenous.

5.4 Conclusion

Overall, this thesis is unique as it is the first to quantify the SWV of the soft tissues in the lateral hip region during both resting and contracted states and is the first to quantify the functional output of the muscle contractions during the contracted state. The intra-rater reliability of this protocol ranged from good to excellent; a next step would be to explore its inter-rater reliability. Future applications of the protocol could involve investigating the SWV of additional locations in the hip region and the influence of sex, BMI, and age on SWV. As other modes of ultrasonography, specifically echo intensity, are already being used to assess muscle quality, SWE is another prospective avenue that can be used. SWE allows for the characterization of the muscles' mechanical properties during their resting and contracted states and could potentially be used to augment clinical research on muscular disorders. The findings from this thesis also help to address gaps in the literature regarding physical and computational models and aid in increasing their biofidelity. Bridging these gaps will improve our understanding of fall impact dynamics and the design of hip injury prevention technologies. Ultimately, SWE is a non-invasive modality that allows for the direct, real-time quantification of the tissues' mechanical properties and has the potential to help address many gaps within the literature.

Chapter 6
Thesis Synthesis & Significance

Overall, this thesis had two primary objectives. The first objective was to evaluate the intra-rater reliability of the SWE ultrasound system when characterizing the SWV of the soft tissues (subcutaneous adipose and muscle) in the lateral-hip region and determine whether muscle contraction influenced it. The second objective was to assess whether the SWV of the soft tissues is influenced by muscle contraction.

6.1 Significance

Shear wave elastography is a new technology that previous studies have used to quantify the mechanical properties of different muscles throughout the body. Some body regions where it has been used include the neck, back, shoulders and leg. Yet, it has never been used in the lateral hip region which is the primary contact site during lateral falls. This thesis is the first to quantify the mechanical properties of the subcutaneous adipose and muscle within this region. Additionally, previous studies have investigated the effect of muscle contraction on the muscles' mechanical properties; however, they did not quantify the force output during their muscle contraction trials. This thesis was the first to use a force transducer set-up to quantify the force output during the muscle contraction trials to determine and confirm the level of muscle contraction. The influence of muscle contraction was also investigated for both the subcutaneous adipose and muscle tissues, and the results indicate that these tissues have unique Young's moduli and react differently during the muscle contracted state. The findings from this thesis and its protocol add valuable insight into the literature and their implications will be discussed in the following sections.

6.2 Future Research

6.2.1 Enhancing the Protocol

The intra-rater reliability of the subcutaneous adipose and muscle SWV during both the resting and muscle contracted states was investigated in this thesis. Based on Koo and Li's (2016) ICC classifications, it ranged from good to excellent during both these conditions, deeming this protocol to be reliable. The next step would be to explore the inter-rater reliability to ensure that different raters are also obtaining reliable measurements with this protocol before it continues to be used. Eventually, the goal would be to use this protocol on a wider BMI and age range to understand the effect of these factors on the mechanical properties of the soft tissues within this region, as this thesis only collected from a small range. Ideally, this protocol can also be used to characterize the mechanical properties of the soft tissues

in additional locations in the lateral-hip region, rather than focusing on a single location. This would add interesting input to the literature as it would characterize the mechanical properties of tissues throughout the hip region, increasing our understanding of their properties.

6.2.2 Quantifying Changes in the Tissues' Mechanical Properties due to Myostestosis & Sarcopenia

The mechanical properties of the soft tissues in the hip being affected by muscle dysfunctions, including sarcopenia and myostestosis, can also be explored using the protocol used in this thesis. Sarcopenia is the age-related decline in muscle mass, strength, and quality (Pahor et al., 2009). Myostestosis is the deposition of adipose in a muscle which declines the muscle's quality (Koo, 2022). It is a characteristic of several diseases, such as sarcopenia and solid cancers (Cespiati et al., 2022). Both these muscle dysfunctions result in a decline in muscle quality, prohibiting the muscle from functioning regularly. Currently, the literature has reported that these conditions influence passive muscle stiffness (Alfuraih et al., 2019; Brandenburg et al., 2014; Eby et al., 2015), however, their influence on active muscle stiffness has not yet been evaluated. The protocol used in this thesis can potentially be used to bridge this gap by quantifying the SWV and Young's moduli of muscles in individuals with these conditions. Since ultrasonography techniques, such as muscle thickness and echo intensity (Lv et al., 2022), are already being used in clinical settings to assess muscle quality, SWE is another avenue that can be explored.

6.2.3 Model & Hip Injury Prevention Devices

The majority of the physical test systems and computational models that represent the hip simplify the characteristics of the soft tissues in this region by bulking them together and not considering their unique morphological and mechanical properties (Fleps et al., 2018; Fleps et al., 2019; Galliker et al., 2022; Majumder et al., 2007; Majumder et al., 2008). This can be attributed to an existing void in the literature regarding the mechanical properties of the subcutaneous adipose and muscle within this region. This thesis allows us to characterize and understand the role of muscle contraction on these mechanical properties, which can potentially be incorporated into models to improve their biofidelity. These models are currently being applied to understand the impact dynamics of lateral falls that cannot be tested in-vivo and improve the effectiveness of hip injury prevention technologies. They have allowed for the understanding of the role that the morphology of these soft tissues has on the effectiveness of injury prevention technologies. However, the influence that the mechanical properties of these soft tissues has not been previously explored. SWE can be used to characterize these mechanical properties that can

further be incorporated into models to bridge the existing gap in the literature. Overall, this would increase the biofidelity of hip models, enhance our understanding of lateral-fall impact dynamics, and improve the design of injury prevention technologies.

Currently, there is also a gap in the literature regarding the level of muscle activation and pattern during lateral falls. It is difficult to address this gap in vivo with fall simulations because EMG cannot be used on the leg which would impact the floor as it would influence the data collected. However, modelling is a potential avenue that can be used to bridge this gap in future studies. Ultimately, implementing these findings, specifically the level of activation of the gluteus maximus, could be incorporated into the current SWE protocol to better understand the mechanical properties of the muscle during a lateral fall.

6.2.4 Conclusion

Overall, this thesis has presented the first reliable SWE protocol used in the lateral hip region and has characterized the mechanical properties of the soft tissues in this region during resting and muscle contracted states. The findings from this thesis, along with its protocol can be used to bridge many of the existing gaps in literature regarding the mechanical properties of these tissues and the influence they have on fall impact dynamics and injury prevention technologies. The next step is to explore the inter-rater reliability of this protocol and use it to characterize the mechanical properties of additional sites within the hip region in a wider BMI and age-range. Ideally, the long-term goals would be to potentially use SWE to understand the effects of different muscle dysfunctions on the Young's moduli of the soft tissues within this region, allowing this technology to be used in clinical research. An alternative goal involves potentially using these findings to improve the biofidelity of hip models and the design of hip injury prevention technologies. Altogether, the knowledge gained from this thesis aids the older adult population, as it provides a greater understanding of the tissues in the hip region that are susceptible to injury during lateral falls.

References

Abramowicz J. S. (2013). Benefits and risks of ultrasound in pregnancy. *Seminars in perinatology*, *37*(5), 295–300. https://doi.org/10.1053/j.semperi.2013.06.004

Aldrich J. E. (2007). Basic physics of ultrasound imaging. *Critical care medicine, 35*(5 Suppl), S131–S137. https://doi.org/10.1097/01.CCM.0000260624.99430.22

Alfuraih, A. M., Tan, A. L., O'Connor, P., Emery, P., Mackie, S., & Wakefield, R. J. (2019). Reduction in stiffness of proximal leg muscles during the first 6 months of glucocorticoid therapy for giant cell arteritis: A pilot study using shear wave elastography. *International Journal of Rheumatic Diseases*, *22*(10), 1891–1899. https://doi.org/10.1111/1756-185X.13667

Alfuraih, A. M., Tan, A. L., O'Connor, P., Emery, P., & Wakefield, R. J. (2019). The effect of ageing on shear wave elastography muscle stiffness in adults. A*ging clinical and experimental research, 31*(12), 1755–1763. https://doi.org/10.1007/s40520-019-01139-0

Aristizabal, S., Amador Carrascal, C., Nenadic, I. Z., Greenleaf, J. F., & Urban, M. W. (2018). Application of Acoustoelasticity to Evaluate Nonlinear Modulus in Ex Vivo Kidneys. *IEEE Transactions on Ultrasonics, Ferroelectrics, and Frequency Control*, *65*(2), 188–200. https://doi.org/10.1109/TUFFC.2017.2781654

Armstrong, M. E., Spencer, E. A., Cairns, B. J., Banks, E., Pirie, K., Green, J., Wright, F. L., Reeves, G. K., Beral, V., & Million Women Study Collaborators (2011). Body mass index and physical activity in relation to the incidence of hip fracture in postmenopausal women. *Journal of bone and mineral research: the official journal of the American Society for Bone and Mineral Research*, *26*(6), 1330–1338. https://doi.org/10.1002/jbmr.315

Auais, M., French, S. D., Beaupre, L., Giangregorio, L., & Magaziner, J. (2018). Identifying research priorities around psycho-cognitive and social factors for recovery from hip fractures: An international decision-making process. *Injury*, *49*(8), 1466–1472. https://doi.org/10.1016/j.injury.2018.04.017

Balasubramanian, A., Zhang, J., Chen, L., Wenkert, D., Daigle, S. G., Grauer, A., & Curtis, J. R. (2019). Risk of subsequent fracture after prior fracture among older women. *Osteoporosis International*, *30*(1), 79–92. https://doi.org/10.1007/s00198-018-4732-1

Bamber, J., Cosgrove, D., Dietrich, C. F., Fromageau, J., Bojunga, J., Calliada, F., Cantisani, V., Correas, J. M., D'Onofrio, M., Drakonaki, E. E., Fink, M., Friedrich-Rust, M., Gilja, O. H., Havre, R. F.,

Jenssen, C., Klauser, A. S., Ohlinger, R., Saftoiu, A., Schaefer, F., Sporea, I., … Piscaglia, F. (2013). EFSUMB guidelines and recommendations on the clinical use of ultrasound elastography. Part 1: Basic principles and technology. *Ultraschall in der Medizin (Stuttgart, Germany: 1980), 34*(2), 169–184. https://doi.org/10.1055/s-0033-1335205

Baumer, T. G., Dischler, J., Davis, L., Labyed, Y., Siegal, D. S., van Holsbeeck, M., Moutzouros, V., & Bey, M. J. (2018). Effects of age and pathology on shear wave speed of the human rotator cuff. *Journal of Orthopaedic Research*, *36*(1), 282–288. https://doi.org/10.1002/jor.23641

Beaupre, L. A., Cinats, J. G., Jones, C. A., Scharfenberger, A. V., William C Johnston, D., Senthilselvan, A., & Saunders, L. D. (2007). Does functional recovery in elderly hip fracture patients differ between patients admitted from long-term care and the community?. *The journals of gerontology. Series A, Biological sciences and medical sciences*, *62*(10), 1127–1133. https://doi.org/10.1093/gerona/62.10.1127

Berry, S. D., Samelson, E. J., Hannan, M. T., McLean, R. R., Lu, M., Adrienne Cupples, L., Shaffer, M. L., Beiser, A. L., Kelly-Hayes, M., & Kiel, D. P. (n.d.). *Second Hip Fracture in Older Men and Women The Framingham Study*. https://jamanetwork.com/

Bhan, S., Levine, I., & Laing, A. C. (2013). The Influence of Body Mass Index and Gender on the Impact Attenuation Properties of Flooring Systems. In *Journal of Applied Biomechanics* (Vol. 29). www.JAB-Journal.com

Bizzini, M., & Mannion, A. F. (2003). Reliability of a new, hand-held device for assessing skeletal muscle stiffness. *Clinical biomechanics (Bristol, Avon)*, *18*(5), 459–461. https://doi.org/10.1016/s0268-0033(03)00042-1

Botanlioglu, H., Kantarci, F., Kaynak, G., Unal, Y., Ertan, S., Aydingoz, O., Erginer, R., Unlu, M. C., Mihmanli, I., & Babacan, M. (2013). Shear wave elastography properties of vastus lateralis and vastus medialis obliquus muscles in normal subjects and female patients with patellofemoral pain syndrome. *Skeletal Radiology*, *42*(5), 659–666. https://doi.org/10.1007/s00256-012-1520-4

Bower, E. S., Wetherell, J. L., Petkus, A. J., Rawson, K. S., & Lenze, E. J. (2016). Fear of Falling after Hip Fracture: Prevalence, Course, and Relationship with One-Year Functional Recovery. *American Journal of Geriatric Psychiatry*, *24*(12), 1228–1236. https://doi.org/10.1016/j.jagp.2016.08.006

Brandenburg, J. E., Eby, S. F., Song, P., Zhao, H., Brault, J. S., Chen, S., & An, K. N. (2014). Ultrasound elastography: the new frontier in direct measurement of muscle stiffness. *Archives of physical medicine and rehabilitation*, *95*(11), 2207–2219. https://doi.org/10.1016/j.apmr.2014.07.007

Carlsen, J. F., Pedersen, M. R., Ewertsen, C., Săftoiu, A., Lönn, L., Rafaelsen, S. R., & Nielsen, M. B. (2015). A comparative study of strain and shear-wave elastography in an elasticity phantom. *AJR. American journal of roentgenology*, *204*(3), W236–W242. https://doi.org/10.2214/AJR.14.13076

Centers for Disease Control and Prevention. (2017). STEADI—Older adult fall prevention. Retrieved from https://www.cdc.gov/steadi/about.html

Cespiati, A., Meroni, M., Lombardi, R., Oberti, G., Dongiovanni, P., & Fracanzani, A. L. (2022). Impact of Sarcopenia and Myosteatosis in Non-Cirrhotic Stages of Liver Diseases: Similarities and Differences across Aetiologies and Possible Therapeutic Strategies. *Biomedicines*, *10*(1), 182. https://doi.org/10.3390/biomedicines10010182

Chan, V., & Perlas, A. (2011). Basics of ultrasound imaging. *Atlas of ultrasound-guided procedures in interventional pain management* (pp. 13-19). Springer.

Chiles Shaffer, N., Fabbri, E., Ferrucci, L., Shardell, M., Simonsick, E. M., & Studenski, S. (2017). Muscle Quality, Strength, and Lower Extremity Physical Performance in the Baltimore Longitudinal Study of Aging. The Journal of frailty & aging, 6(4), 183–187. https://doi.org/10.14283/jfa.2017.24

Choi, W. J., Cripton, P. A., & Robinovitch, S. N. (2015). Effects of hip abductor muscle forces and knee boundary conditions on femoral neck stresses during simulated falls. *Osteoporosis International*, *26*(1), 291–301. https://doi.org/10.1007/s00198-014-2812-4

Choi, W. J., Hoffer, J. A., & Robinovitch, S. N. (2010). Effect of hip protectors, falling angle and body mass index on pressure distribution over the hip during simulated falls. *Clinical Biomechanics*, *25*(1), 63–69. https://doi.org/10.1016/j.clinbiomech.2009.08.009

Choi, W. J., Wakeling, J. M., & Robinovitch, S. N. (2015). Kinematic analysis of video-captured falls experienced by older adults in long-term care. *Journal of Biomechanics*, *48*(6), 911–920. https://doi.org/10.1016/j.jbiomech.2015.02.025

Colón-Emeric, C., Kuchibhatla, M., Pieper, C., Hawkes, W., Fredman, L., Magaziner, J., Zimmerman, S., & Lyles, K. W. (2003). The contribution of hip fracture to risk of subsequent fractures: Data from two longitudinal studies. *Osteoporosis International*, *14*(11), 879–883. https://doi.org/10.1007/s00198-003-1460-x

Davidson, M. J., Bryant, A. L., Bower, W. F., & Frawley, H. C. (2017). Myotonometry Reliably Measures Muscle Stiffness in the Thenar and Perineal Muscles. *Physiotherapy Canada. Physiotherapie Canada*, *69*(2), 104–112. https://doi.org/10.3138/ptc.2015-85

De Carvalho, F. G., Justice, J. N., Freitas, E. C., Kershaw, E. E., & Sparks, L. M. (2019). Adipose Tissue Quality in Aging: How Structural and Functional Aspects of Adipose Tissue Impact Skeletal Muscle Quality. *Nutrients*, *11*(11), 2553. https://doi.org/10.3390/nu11112553

De Laet, C., Kanis, J. A., Odén, A., Johanson, H., Johnell, O., Delmas, P., Eisman, J. A., Kroger, H., Fujiwara, S., Garnero, P., McCloskey, E. V., Mellstrom, D., Melton, L. J., 3rd, Meunier, P. J., Pols, H. A., Reeve, J., Silman, A., & Tenenhouse, A. (2005). Body mass index as a predictor of fracture risk: a meta-analysis. *Osteoporosis international: a journal established as result of cooperation between the European Foundation for Osteoporosis and the National Osteoporosis Foundation of the USA*, *16*(11), 1330–1338. https://doi.org/10.1007/s00198-005-1863-y

DeJong, H. M., Abbott, S., Zelesco, M., Kennedy, B. F., Ziman, M. R., & Wood, F. M. (2017). The validity and reliability of using ultrasound elastography to measure cutaneous stiffness, a systematic review. *International journal of burns and trauma*, *7*(7), 124–141.

DeJong, H., Abbott, S., Zelesco, M., Spilsbury, K., Martin, L., Sanderson, R., Ziman, M., Kennedy, B. F., & Wood, F. M. (2020). A Novel, Reliable Protocol to Objectively Assess Scar Stiffness Using Shear Wave Elastography. *Ultrasound in Medicine and Biology*, *46*(7), 1614–1629. https://doi.org/10.1016/j.ultrasmedbio.2020.03.003

Derler, S., Spierings, A. B., & Schmitt, K. U. (2005). Anatomical hip model for the mechanical testing of hip protectors. *Medical engineering & physics, 27*(6), 475–485. https://doi.org/10.1016/j.medengphy.2005.02.001

Dieterich, A. v., Andrade, R. J., le Sant, G., Falla, D., Petzke, F., Hug, F., & Nordez, A. (2017). Shear wave elastography reveals different degrees of passive and active stiffness of the neck extensor muscles. *European Journal of Applied Physiology*, *117*(1), 171–178. https://doi.org/10.1007/s00421-016-3509-5

Dragomir-Daescu, D., Rossman, T. L., Rezaei, A., Carlson, K. D., Kallmes, D. F., Skinner, J. A., Khosla, S., & Amin, S. (2018). Factors associated with proximal femur fracture determined in a large cadaveric cohort. *Bone*, *116*, 196–202. https://doi.org/10.1016/j.bone.2018.08.005

Drahota, A., Felix, L. M., Raftery, J., Keenan, B. E., Lachance, C. C., Mackey, D. C., Markham, C., & Laing, A. C. (2022). The SAFEST review: a mixed methods systematic review of shock-absorbing flooring for fall-related injury prevention. *BMC Geriatrics*, *22*(1). https://doi.org/10.1186/s12877-021-02670-4

Drakonaki, E. E., Allen, G. M., & Wilson, D. J. (2009). Real-time ultrasound elastography of the normal Achilles tendon: reproducibility and pattern description. *Clinical Radiology*, *64*(12), 1196–1202. https://doi.org/10.1016/j.crad.2009.08.006

Dyer, S. M., Crotty, M., Fairhall, N., Magaziner, J., Beaupre, L. A., Cameron, I. D., Sherrington, C., & Fragility Fracture Network (FFN) Rehabilitation Research Special Interest Group (2016). A critical review of the long-term disability outcomes following hip fracture. *BMC geriatrics, 16*(1), 158. https://doi.org/10.1186/s12877-016-0332-0

Eby, S. F., Cloud, B. A., Brandenburg, J. E., Giambini, H., Song, P., Chen, S., LeBrasseur, N. K., & An, K. N. (2015). *Shear wave elastography of passive skeletal muscle stiffness: influences of sex and age throughout adulthood. Clinical biomechanics (Bristol, Avon), 30*(1), 22–27. https://doi.org/10.1016/j.clinbiomech.2014.11.011

Ewertsen, C., Carlsen, J. F., Christiansen, I. R., Jensen, J. A., & Nielsen, M. B. (2016). Evaluation of healthy muscle tissue by strain and shear wave elastography - Dependency on depth and ROI position in relation to underlying bone. *Ultrasonics*, *71*, 127–133. https://doi.org/10.1016/j.ultras.2016.06.007

Fleps, I., Enns-Bray, W. S., Guy, P., Ferguson, S. J., Cripton, P. A., & Helgason, B. (2018). On the internal reaction forces, energy absorption, and fracture in the hip during simulated sideways fall impact. *PLoS ONE*, *13*(8). https://doi.org/10.1371/journal.pone.0200952

Fleps, I., Fung, A., Guy, P., Ferguson, S. J., Helgason, B., & Cripton, P. A. (2019). Subject-specific ex vivo simulations for hip fracture risk assessment in sideways falls. *Bone*, *125*, 36–45. https://doi.org/10.1016/j.bone.2019.05.004

Fleps, I., Guy, P., Ferguson, S. J., Cripton, P. A., & Helgason, B. (2019). Explicit Finite Element Models Accurately Predict Subject-Specific and Velocity-Dependent Kinetics of Sideways Fall Impact. *Journal of Bone and Mineral Research*, *34*(10), 1837–1850. https://doi.org/10.1002/jbmr.3804

Fleps, I., Vuille, M., Melnyk, A., Ferguson, S. J., Guy, P., Helgason, B., & Cripton, P. A. (2018). A novel sideways fall simulator to study hip fractures ex vivo. *PLoS ONE*, *13*(7). https://doi.org/10.1371/journal.pone.0201096

Galliker, E. S., Laing, A. C., Ferguson, S. J., Helgason, B., & Fleps, I. (2022). The Influence of Fall Direction and Hip Protector on Fracture Risk: FE Model Predictions Driven by Experimental Data. *Annals of Biomedical Engineering*, *50*(3), 278–290. https://doi.org/10.1007/s10439-022-02917-0

Gonnelli, S., Caffarelli, C., & Nuti, R. (2014). Obesity and fracture risk. *Clinical cases in mineral and bone metabolism: the official journal of the Italian Society of Osteoporosis, Mineral Metabolism, and Skeletal Diseases*, *11*(1), 9–14. https://doi.org/10.11138/ccmbm/2014.11.1.009

Government of Canada. (2021). "*Seniors' Falls in Canada – Infographic*." Government of Canada. https://www.canada.ca/en/public-health/services/health-promotion/aging-seniors/publications/publications-general-public/seniors-falls-canada-second-report/seniors-falls-canada-infographic.html

Government of Canada. (2022). "*Surveillance report on falls among older adults in Canada*." Government of Canada. https://www.canada.ca/en/public-health/services/publications/healthy-living/surveillance-report-falls-older-adults-canada.html

Greenspan, S. L., Myers, E. R., Kiel, D. P., Parker, R. A., Hayes, W. C., & Resnick, N. M. (1998). Fall Direction, Bone Mineral Density, and Function: Risk Factors for Hip Fracture in Frail Nursing Home Elderly. In *Am J Med* (Vol. 104).

Hayes, W. C., Myers, E. R., Morris, J. N., Gerhart, T. N., Yett, H. S., & Lipsitz, L. A. (1993). Impact near the hip dominates fracture risk in elderly nursing home residents who fall. *Calcified tissue international, 52*(3), 192–198. https://doi.org/10.1007/BF00298717

Hollerieth, K., Gaßmann, B., Wagenpfeil, S., Kemmner, S., Heemann, U., & Stock, K. F. (2018). Does standoff material affect acoustic radiation force impulse elastography? A preclinical study of a modified elastography phantom. *Ultrasonography*, *37*(2), 140–148. https://doi.org/10.14366/usg.17002

Hunt, C., Bourke, A., Hospital, C. G., Dass, J., Corica, T., Hardwick, S., Jacques, A., Busch, G., & Dejong, H. (2021). Ultra-sound Shear Wave Elastography Tissue Stiffness and Thickness Assessment After Adjuvant Radiotherapy for Breast Cancer Treatment; An Exploratory Study. https://doi.org/10.21203/rs.3.rs-975254/v1

Jaglal, S. B., Sherry, P. G., & Schatzker, J. (1996). The impact and consequences of hip fracture in Ontario. *Canadian journal of surgery. Journal canadien de chirurgie*, *39*(2), 105–111.

Kerins, C. M., Moore, S. D., Butterfield, T. A., McKeon, P. O., & Uhl, T. L. (2013). Reliability of the myotonometer for assessment of posterior shoulder tightness. *International journal of sports physical therapy*, *8*(3), 248–255.

Keyak J. H. (2001). Improved prediction of proximal femoral fracture load using nonlinear finite element models. *Medical engineering & physics*, *23*(3), 165–173. https://doi.org/10.1016/s1350-4533(01)00045-5

Klauser, A. S., De-Koekkoek, F., Schwabl, C., Fink, C., Friede, M., & Csapo, R. (2022). Intraobserver Assessment of Shear Wave Elastography in Tensor Fasciae Latae and Gluteus Maximus Muscle: The Importance of the Hip Abductor Muscles in Runners Knee Compared to Healthy Controls. *Journal of Clinical Medicine*, *11*(13). https://doi.org/10.3390/jcm11133605

Koo B. K. (2022). Assessment of Muscle Quantity, Quality and Function. *Journal of obesity & metabolic syndrome, 31*(1), 9–16. https://doi.org/10.7570/jomes22025

Koo, T. K., & Li, M. Y. (2016). A Guideline of Selecting and Reporting Intraclass Correlation Coefficients for Reliability Research. *Journal of chiropractic medicine*, *15*(2), 155–163. https://doi.org/10.1016/j.jcm.2016.02.012

Korall, A. M. B., Feldman, F., Yang, Y., Cameron, I. D., Leung, P. M., Sims-Gould, J., & Robinovitch, S. N. (2019). Effectiveness of Hip Protectors to Reduce Risk for Hip Fracture from Falls in Long-Term Care. *Journal of the American Medical Directors Association*, *20*(11), 1397–1403.e1. https://doi.org/10.1016/j.jamda.2019.07.010

Laing, A. C., & Robinovitch, S. N. (2008a). Effect of soft shell hip protectors on pressure distribution to the hip during sideways falls. *Osteoporosis International*, *19*(7), 1067–1075. https://doi.org/10.1007/s00198-008-0571-9

Laing, A. C., & Robinovitch, S. N. (2008b). The force attenuation provided by hip protectors depends on impact velocity, pelvic size, and soft tissue stiffness. *Journal of Biomechanical Engineering*, *130*(6). https://doi.org/10.1115/1.2979867

Laing, A. C., & Robinovitch, S. N. (2009). Low stiffness floors can attenuate fall-related femoral impact forces by up to 50% without substantially impairing balance in older women. *Accident Analysis and Prevention*, *41*(3), 642–650. https://doi.org/10.1016/j.aap.2009.03.001

Laing, A. C., Tootoonchi, I., Hulme, P. A., & Robinovitch, S. N. (2006). Effect of compliant flooring on impact force during falls on the hip. *Journal of Orthopaedic Research*, *24*(7), 1405–1411. https://doi.org/10.1002/jor.20172

Lee, Y., Kim, M., & Lee, H. (2021). The Measurement of Stiffness for Major Muscles with Shear Wave Elastography and Myoton: A Quantitative Analysis Study. *Diagnostics (Basel, Switzerland)*, *11*(3), 524. https://doi.org/10.3390/diagnostics11030524

Levine, I. C., Bhan, S., & Laing, A. C. (2013). The effects of body mass index and sex on impact force and effective pelvic stiffness during simulated lateral falls. *Clinical Biomechanics*, *28*(9–10), 1026–1033. https://doi.org/10.1016/j.clinbiomech.2013.10.002

Levine, I. C., Minty, L. E., & Laing, A. C. (2015). Factors that influence soft tissue thickness over the greater trochanter: Application to understanding hip fractures. *Clinical Anatomy*, *28*(2), 253–261. https://doi.org/10.1002/ca.22499

Lin, C. Y., Lin, C. C., Chou, Y. C., Chen, P. Y., & Wang, C. L. (2015). Heel pad stiffness in plantar heel pain by shear wave elastography. *Ultrasound in Medicine and Biology*, *41*(11), 2890–2898. https://doi.org/10.1016/j.ultrasmedbio.2015.07.004

Lönnroos, E., Kautiainen, H., Karppi, P., Hartikainen, S., Kiviranta, I., & Sulkava, R. (2007). Incidence of second hip fractures. A population-based study. *Osteoporosis international : a journal established as result of cooperation between the European Foundation for Osteoporosis and the National Osteoporosis Foundation of the USA*, *18*(9), 1279–1285. https://doi.org/10.1007/s00198-007-0375-3

Lv, S., Ling, L., Shi, H., Chen, X., Chen, S., Zhu, S., Lin, W., Lv, R., & Ding, G. (2022). Application of Muscle Thickness and Quality Measured by Ultrasound in Frailty Assessment in China. *Frontiers in medicine, 9*, 859555. https://doi.org/10.3389/fmed.2022.859555

Magaziner, J., Hawkes, W., Hebel, J. R., Zimmerman, S. I., Fox, K. M., Dolan, M., Felsenthal, G., & Kenzora, J. (2000). Recovery from hip fracture in eight areas of function. *The journals of gerontology. Series A, Biological sciences and medical sciences*, *55*(9), M498–M507. https://doi.org/10.1093/gerona/55.9.m498

Maitland, L.A., E.R. Myers, J.A. Hipp, W.C. Hayes, & S.L. Greenspan. (1993). Read my hips: measuring trochanteric soft tissue thickness. *Calcified Tissue International, 52*, 85–89.

Majumder, S., Roychowdhury, A., & Pal, S. (2007). Simulation of hip fracture in sideways fall using a 3D finite element model of pelvis-femur-soft tissue complex with simplified representation of whole body. *Medical Engineering and Physics*, *29*(10), 1167–1178. https://doi.org/10.1016/j.medengphy.2006.11.001

Majumder, S., Roychowdhury, A., & Pal, S. (2008a). Three-dimensional finite element simulation of pelvic fracture during side impact with pelvis-femur-soft tissue complex. *International Journal of Crashworthiness*, *13*(3), 313–329. https://doi.org/10.1080/13691450801940309

Majumder, S., Roychowdhury, A., & Pal, S. (2008b). Effects of trochanteric soft tissue thickness and hip impact velocity on hip fracture in sideways fall through 3D finite element simulations. *Journal of Biomechanics*, *41*(13), 2834–2842. https://doi.org/10.1016/j.jbiomech.2008.07.001

Markowitz J (2011). Chapter 4. probe selection, machine controls, and equipment. Carmody K.A., & Moore C.L., & Feller-Kopman D(Eds.), *Handbook of Critical Care and Emergency Ultrasound*. McGraw Hill. https://accessanesthesiology.mhmedical.com/content.aspx?bookid=517&sectionid=41066790

Martel, D. R., Levine, I. C., Pretty, S. P., & Laing, A. C. (2018). The influence of muscle activation on impact dynamics during lateral falls on the hip. *Journal of biomechanics*, *66*, 111–118. https://doi.org/10.1016/j.jbiomech.2017.11.002

Matsuda R, Kumamoto T, Seko T, Miura S, Hamamoto T. Reproducibility of elastic modulus measurement of the multifidus using the shear wave elastography function of an ultrasound diagnostic device. J Phys Ther Sci. 2019 Aug;31(8):617-620. doi: 10.1589/jpts.31.617. Epub 2019 Aug 19. PMID: 31527996; PMCID: PMC6698464.

Minns, R. J., Marsh, A. M., Chuck, A., & Todd, J. (2007). Are hip protectors correctly positioned in use? *Age and Ageing*, *36*(2), 140–144. https://doi.org/10.1093/ageing/afl186

Nabhani, F., & Bamford, J. S. (2004). Impact properties of floor coverings and their role during simulated hip fractures. *Journal of Materials Processing Technology*, *153–154*(1–3), 139–144. https://doi.org/10.1016/j.jmatprotec.2004.04.211

Neuman, M. D., Silber, J. H., Magaziner, J. S., Passarella, M. A., Mehta, S., & Werner, R. M. (2014). Survival and functional outcomes after hip fracture among nursing home residents. *JAMA internal medicine*, *174*(8), 1273–1280. https://doi.org/10.1001/jamainternmed.2014.2362

Nichols, T.R., Huyghues-Despointes, C.M.J.I. (2009). Muscular Stiffness. In: Binder, M.D., Hirokawa, N., Windhorst, U. (eds) Encyclopedia of Neuroscience. Springer, Berlin, Heidelberg. https://doi.org/10.1007/978-3-540-29678-2_3687

Nikitovic, M., Wodchis, W. P., Krahn, M. D., & Cadarette, S. M. (2013). Direct health-care costs attributed to hip fractures among seniors: A matched cohort study. *Osteoporosis International*, *24*(2), 659–669. https://doi.org/10.1007/s00198-012-2034-6

Nojiri, S., Yagi, M., Mizukami, Y., & Ichihashi, N. (2021). Static stretching time required to reduce iliacus muscle stiffness. *Sports Biomechanics*, *20*(7), 901–910. https://doi.org/10.1080/14763141.2019.162032

Norton, R., Campbell, A. J., Lee-Joe, T., Robinson, E., & Butler, M. (1997). Circumstances of falls resulting in hip fractures among older people. *Journal of the American Geriatrics Society*, *45*(9), 1108–1112. https://doi.org/10.1111/j.1532-5415.1997.tb05975.x

Ozkan, M. B., Bilgici, M. C., Eren, E., & Caltepe, G. (2018). The role of linear and convex probes to determine the normal range of splenic and liver stiffness in healthy children assessed by point shear wave elastography. *Iranian Journal of Radiology*, *15*(2). https://doi.org/10.5812/iranjradiol.14267

Ozturk, A., Grajo, J. R., Dhyani, M., Anthony, B. W., & Samir, A. E. (2018). Principles of ultrasound elastography. *Abdominal radiology (New York)*, *43*(4), 773–785. https://doi.org/10.1007/s00261-018-1475-6

Palanca, M., Perilli, E., & Martelli, S. (2021). Body Anthropometry and Bone Strength Conjointly Determine the Risk of Hip Fracture in a Sideways Fall. *Annals of Biomedical Engineering*, *49*(5), 1380–1390. https://doi.org/10.1007/s10439-020-02682-y

Phan, A., Lee, J., & Gao, J. (2019). Ultrasound shear wave elastography in assessment of skeletal muscle stiffness in senior volunteers. *Clinical imaging, 58*, 22–26. https://doi.org/10.1016/j.clinimag.2019.06.006

Papaioannou, A., Kennedy, C. C., Ioannidis, G., Sawka, A., Hopman, W. M., Pickard, L., Brown, J. P., Josse, R. G., Kaiser, S., Anastassiades, T., Goltzman, D., Papadimitropoulos, M., Tenenhouse, A., Prior, J. C., Olszynski, W. P., & Adachi, J. D. (2009). The impact of incident fractures on health-related quality of life: 5 years of data from the Canadian Multicentre Osteoporosis Study. *Osteoporosis International*, *20*(5), 703–714. https://doi.org/10.1007/s00198-008-0743-7

Pinilla, T. P., Boardman, K. C., Bouxsein, M. L., Myers, E. R., & Hayes, W. C. (1996). Impact Direction from a Fall Influences the Failure Load of the Proximal Femur as Much as Age-Related Bone Loss. In *Calcif Tissue Int* (Vol. 58).

Prado-Costa, R., Rebelo, J., Monteiro-Barroso, J., & Preto, A. S. (2018). Ultrasound elastography: compression elastography and shear-wave elastography in the assessment of tendon injury. *Insights into imaging*, *9*(5), 791–814. https://doi.org/10.1007/s13244-018-0642-1

Pretty, S. P., Levine, I. C., & Laing, A. C. (2021a). Anatomically Aligned Loading During Falls: Influence of Fall Protocol, Sex and Trochanteric Soft Tissue Thickness. *Annals of Biomedical Engineering*, *49*(12), 3267–3279. https://doi.org/10.1007/s10439-021-02852-6

Pretty, S. P., Levine, I. C., & Laing, A. C. (2021b). Factors that influence the distribution of impact force relative to the proximal femur during lateral falls. *Journal of Biomechanics*, *127*. https://doi.org/10.1016/j.jbiomech.2021.110679

Pretty, S. P., Martel, D. R., & Laing, A. C. (2017). The Influence of Body Mass Index, Sex, & Muscle Activation on Pressure Distribution During Lateral Falls on the Hip. *Annals of Biomedical Engineering*, *45*(12), 2775–2783. https://doi.org/10.1007/s10439-017-1928-z

Quack, V., Betsch, M., Hellmann, J., Eschweiler, J., Schrading, S., Gatz, M., Rath, B., Tingart, M., Laubach, M., Kuhl, C. K., & Dirrichs, T. (2020). Evaluation of Postoperative Changes in Patellar and Quadriceps Tendons after Total Knee Arthroplasty–A Comprehensive Analysis by Shear Wave Elastography, Power Doppler and B-mode Ultrasound. *Academic Radiology*, *27*(6), 148–157. https://doi.org/10.1016/j.acra.2019.08.015

Robinovitch, S. N., Hayes, W. C., & McMahon, T. A. (1995). Energy-shunting hip padding system attenuates femoral impact force in a simulated fall. *Journal of biomechanical engineering*, *117*(4), 409–413. https://doi.org/10.1115/1.2794200

Robinovitch, S.N., Hayes, W.C., McMahon, T.A. (1995). Force Attenuation in Trochanteric Soft Tissues During Impact from a Fall. *Journal of Orthopaedic Research, 13*(6), 956-962.

Scheel, C., Mecham, J., Zuccarello, V., & Mattes, R. (2018). An evaluation of the inter-rater and intra-rater reliability of OccuPro's functional capacity evaluation. *Work (Reading, Mass.)*, *60*(3), 465–473. https://doi.org/10.3233/WOR-182754

Schneider, E. L., & Guralnik, J. M. (1990). The aging of America. Impact on health care costs. *JAMA*, *263*(17), 2335–2340.

Scott, V., Wagar, L., & Elliott, S. (2010). Falls & Related Injuries among Older Canadians: Fall Trelated Hospitalizations & Intervention Initiatives. Prepared on behalf of the Public Health Agency of Canada, Division of Aging and Seniors. Victoria BC: Victoria Scott Consulting.

Seniam. (2023). *Recommendations for sensor locations in hip or upper leg muscles.* Sensor locations - Gluteus Maximus. http://seniam.org/gluteusmaximus.html

Shina, T., Nightingale, K. R., Palmeri, M. L., Hall, T. J., Bamber, J. C., Barr, R. G., Castera, L., Choi, B. I., Chou, Y. H., Cosgrove, D., Dietrich, C. F., Ding, H., Amy, D., Farrokh, A., Ferraioli, G., Filice, C., Friedrich-Rust, M., Nakashima, K., Schafer, F., … Kudo, M. (2015). WFUMB guidelines and recommendations for clinical use of ultrasound elastography: Part 1: Basic principles and terminology. *Ultrasound in Medicine and Biology*, *41*(5), 1126–1147. https://doi.org/10.1016/j.ultrasmedbio.2015.03.009

Siracusa, J., Charlot, K., Malgoyre, A., Conort, S., Tardo-Dino, P. E., Bourrilhon, C., & Garcia-Vicencio, S. (2019). Resting Muscle Shear Modulus Measured with Ultrasound Shear-Wave Elastography as an Alternative Tool to Assess Muscle Fatigue in Humans. *Frontiers in physiology, 10*, 626. https://doi.org/10.3389/fphys.2019.00626

Sowa, Y., Numajiri, T., & Nishino, K. (2015). Ultrasound Shear-Wave Elastography for Follow-Up Fat Induration after Breast Reconstruction with an Autologous Flap. *Plastic and reconstructive surgery. Global open, 3*(9), 518. https://doi.org/10.1097/GOX.0000000000000493

Statistics Canada. A portrait of the population aged 85 and older in 2016 in Canada. Ottawa (ON): Statistics Canada; 2017. Available from: www12.statcan.gc.ca/census- recensement/2016/as-sa/98-200-x/2016004/98-200-x2016004-eng.cfm.

Taljanovic, M. S., Gimber, L. H., Becker, G. W., Latt, L. D., Klauser, A. S., Melville, D. M., Gao, L., & Witte, R. S. (2017). Shear-wave elastography: Basic physics and musculoskeletal applications. *Radiographics*, *37*(3), 855–870. https://doi.org/10.1148/rg.2017160116

Taljanovic, M. S., Melville, D. M., Klauser, A. S., Latt, L. D., Arif-Tiwari, H., Gao, L., & Witte, R. S. (2015). Advances in Lower Extremity Ultrasound. *Current Radiology Reports, 3*(6), 1-12. https://doi.org/10.1007/s40134-015-0100-5

University of Washington. (2023). *Gluteus maximus*. UW Radiology. https://rad.washington.edu/muscle-atlas/gluteus-maximus/

Vachutka, J., Sedlackova, Z., Furst, T., Herman, M., Herman, J., Salzman, R., & Dolezal, L. (2018). Evaluation of the Effect of Tissue Compression on the Results of Shear Wave Elastography Measurements. *Ultrasonic Imaging*, *40*(6), 380–393. https://doi.org/10.1177/0161734618793837

van der Zijden, A. M., Janssen, D., Verdonschot, N., Groen, B. E., Nienhuis, B., Weerdesteyn, V., & Tanck, E. (2015). Incorporating in vivo fall assessments in the simulation of femoral fractures with finite element models. *Medical Engineering and Physics*, *37*(6), 593–598. https://doi.org/10.1016/j.medengphy.2015.03.006

van Schoor, N. M., van der Veen, A. J., Schaap, L. A., Smit, T. H., & Lips, P. (2006). Biomechanical comparison of hard and soft hip protectors, and the influence of soft tissue. *Bone*, *39*(2), 401–407. https://doi.org/10.1016/j.bone.2006.01.156

Walston J. D. (2012). Sarcopenia in older adults. *Current opinion in rheumatology, 24*(6), 623–627. https://doi.org/10.1097/BOR.0b013e328358d59b

Wang, X., Hu, Y., Zhu, J., Gao, J., Chen, S., Liu, F., Li, W., Liu, Y., & Ariun, B. (2020). Effect of acquisition depth and precompression from probe and couplant on shear wave elastography in soft tissue: An in vitro and in vivo study. *Quantitative Imaging in Medicine and Surgery*, *10*(3), 754–765. https://doi.org/10.21037/QIMS.2020.01.15

Wiktorowicz, M. E., Goeree, R., Papaioannou, A., Adachi, J. D., & Papadimitropoulos, E. (2001). Economic implications of hip fracture: health service use, institutional care and cost in Canada. *Osteoporos Int, 12*(4), 271–278. https://doi.org/10.1007/s001980170116

Wolinsky, F. D., Fitzgerald, J. F., & Stump, T. E. (1997). The effect of hip fracture on mortality, hospitalization, and functional status: a prospective study. *American journal of public health*, *87*(3), 398–403. https://doi.org/10.2105/ajph.87.3.398

World Health Organization. (2007). WHO global report on falls prevention in older age. Retrieved from http://www.who.int/ageing/publications/Falls_prevention-7March.pdf

Wu, C. H., Lin, C. Y., Hsiao, M. Y., Cheng, Y. H., Chen, W. S., & Wang, T. G. (2018). Altered stiffness of microchamber and macrochamber layers in the aged heel pad: Shear wave ultrasound elastography evaluation. *Journal of the Formosan Medical Association*, *117*(5), 434–439. https://doi.org/10.1016/j.jfma.2017.05.006

Yahaya, S. A., Ripin, Z. M., & Ridzwan, M. I. Z. (2020). Test systems for the biomechanical evaluation of hip protectors: a systematic review. *Osteoporos Int, 31*(1), 43–58. https://doi.org/10.1007/s00198-019-05128-x

Yang, Y., Komisar, V., Shishov, N., Lo, B., Korall, A. M. B., Feldman, F., & Robinovitch, S. N. (2020). The Effect of Fall Biomechanics on Risk for Hip Fracture in Older Adults: A Cohort Study of

Video-Captured Falls in Long-Term Care. *Journal of Bone and Mineral Research*, *35*(10), 1914–1922. https://doi.org/10.1002/jbmr.4048

Yang, Y., Mackey, D. C., Liu-Ambrose, T., Feldman, F., & Robinovitch, S. N. (2016). Risk factors for hip impact during real-life falls captured on video in long-term care. *Osteoporosis International*, *27*(2), 537–547. https://doi.org/10.1007/s00198-015-3268-x

Yun, S. J., Jin, W., Cho, N. S., Ryu, K. N., Yoon, Y. C., Cha, J. G., Park, J. S., Park, S. Y., & Choi, N. Y. (2019). Shear-wave and strain ultrasound elastography of the supraspinatus and infraspinatus tendons in patients with idiopathic adhesive capsulitis of the shoulder: A prospective case-control study. *Korean Journal of Radiology*, *20*(7), 1176–1185. https://doi.org/10.3348/kjr.2018.0918

Zhou, J., Liu, C., & Zhang, Z. (2019). uniform Stiffness within Gastrocnemius-Achilles tendon Complex Observed after Static Stretching. In ©*Journal of Sports Science and Medicine* (Vol. 18). http://www.jssm.org

Appendix A

Table A.1 represents the additional sample size calculations that were conducted based on the SWV results of additional studies and effect sizes.

Table A.1: Sample Size Calculations to Identify Differences in SWV Based on Muscle Contraction and Effect Size

Independent Variable	Group Comparison from Literature	Resting Mean SWV (m/s)	Muscle Contracted Mean SWV (m/s)	Resting SWV SD (m/s)	Muscle Contracted SWV SD (m/s)	Effect Size dz	Predicted Sample Size (N)
Muscle Contraction (values from Botanlioglu et al., 2012)	VL males' right side	2.32	8.20	1.11	4.85	1.335981	6
	VL males' left side	2.23	7.61	1.32	3.82	1.600992	5
	VMO males' right side	2.22	8.19	1.33	4.44	1.512614	5
	VMO males' left side	2.11	8.42	1.11	4.65	1.500125	5
	VL females' right side	2.35	6.16	0.93	4.21	0.994615	8
	VL females' left side	2.15	6.39	1.11	4.40	1.069804	7
	VMO females' right side	1.95	6.81	1.11	3.98	1.366188	5
	VMO females' left side	2.01	7.25	1.08	3.21	1.852191	4
Muscle Contraction (Baumer et al., 2017)	Supraspinatus muscle	2.4	4.0	0.4	0.4	4	3
Muscle Contraction (Lee et al., 2021)	Rectus Femoris	2.16	5.16	1.02	2.24	1.544423	5
	Tibialis Anterior	2.65	6.81	1.00	3.31	1.414761	5
	Biceps femoris	2.09	5.18	1.11	2.29	1.557847	5
	Medial gastrocnemius	2.02	5.15	0.97	2.48	1.445963	5
Sample size based on effect size	Small effect	-	-	-	-	0.2	156
	Moderate effect	-	-	-	-	0.5	27
	Large effect	-	-	-	-	0.8	12

Appendix B

A two-way mixed effects model was conducted to assess the intra-rater reliability of the SWE protocol used to characterize the mechanical properties of the soft tissues in the hip region. There are two types of tests that can be computed which are "single measurement" and "mean of k measurements." The type of test is determined based on the future intended use of the protocol. Thus, if the protocol is intended to only be used to only take a single measurement for a given condition, the "single" type is used. However, if the intended use is to take multiple measurements for a given condition and then average them, then the "mean of k measurements" type is used (Koo & Li, 2016). Given the exploratory nature of the protocol developed in this thesis, the "mean of k measurements" type was used during the statistical analysis. Currently, this protocol will not be used in a clinical setting for which the "single" type of test would have been ideal. As this protocol will be further developed in future studies, the "mean of k measurements" type of test was used. However, Figure A.1 represents the results for a "single" type of two-way mixed effects model that was conducted using the dataset. The reliability is lower than the other test because it is computing the reliability based on the actual application being a single measurement, rather than multiple measurements being averaged together. Since the condition of the protocol changes from containing multiple measurements to a single measurement, this decreases its intra-rater reliability.

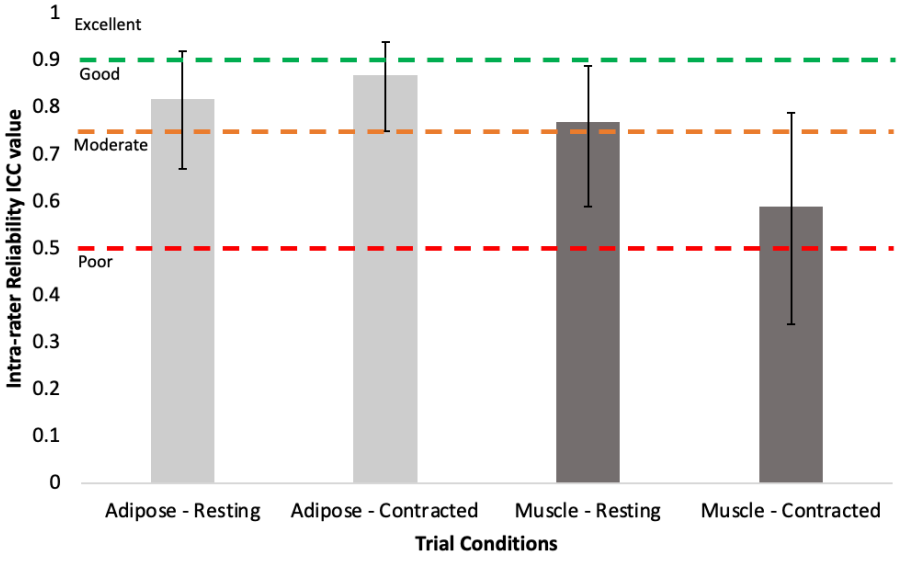

Figure B.1: *Intra-rater reliability (ICC values and 95% CI represented by the error bars) for the SWV trial conditions using Koo & Li's Classifications (2016) – The area below the red line represents poor reliability (ICC < 0.50) and the area between the orange and red lines represents moderate reliability (0.50 < ICC < 0.75). The area between the green and orange lines represents good reliability (0.75 < ICC < 0.90), while the area above the green line represents excellent reliability (ICC > 0.90).*

Appendix C

Figures C.1.A, C.1.B, and C.1.C below were from a pilot SWE collection that was conducted on an individual with a high BMI (30 kg/m^2). It was extremely difficult to capture their femur in the image and obtain elastograms of their muscle tissue at the P1 location.

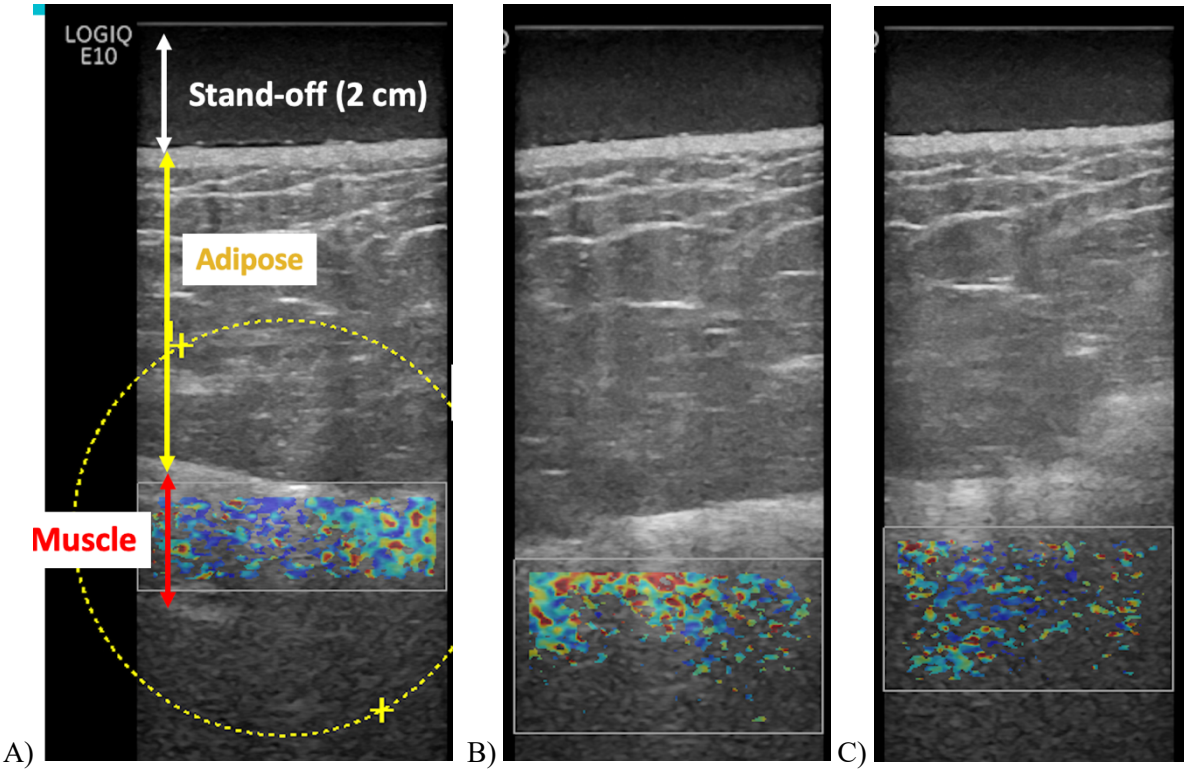

Figure C.1: *SWE images collected at the P1 location in a high BMI individual – It was difficult to capture an image with the femur and obtain elastograms of the muscle tissue.*